

Universidade do Minho

Escola de Engenharia

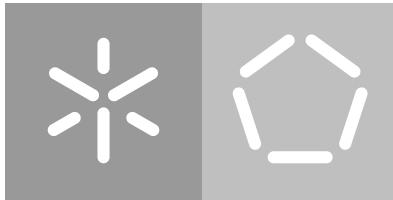
Departamento de Informática

José Diogo da Costa Guimarães

Simulation of Quantum Biology

Quantum simulation of photosynthesis

June 2020



Universidade do Minho

Escola de Engenharia

Departamento de Informática

José Diogo da Costa Guimarães

Simulation of Quantum Biology

Quantum simulation of photosynthesis

Master dissertation

Master Degree in Physics Engineering

Dissertation supervised by

Luís Soares Barbosa

Carlos Tavares

June 2020

ACKNOWLEDGEMENTS

I want to thank my supervisor Luís Soares Barbosa for the helpful discussions along the year and to my co-supervisor Carlos Tavares for his guidance.

Special thanks to Professor Mikhail Vasilevskiy for the time taken to be able to help me.

At last, I want to thank my parents and Francisca, for the incredible support received. To my friends from the group "Jubardisse", a big thank you, for having to listen to me talking about physics, which I know it can be hard sometimes. I also want to thank my colleagues and friends from the course, for the amazing journey in the past 5 years.

ABSTRACT

As quantum computation becomes increasingly powerful, both in hardware and software, the number of real-world applications is also growing. The work of this dissertation, explores the possible application of quantum computation in the field of quantum biology. In particular, the development of a quantum algorithm to simulate the evolution of the energy transport in photosynthesis has been done, where quantum effects have been considered.

Multiple quantum algorithms have been analyzed. The chosen one is able to simulate both the isolated and the open quantum systems in a scalable framework, composed by light-harvesting molecules. The former was implemented in a real quantum computer, an IBM Q machine, while the later was employed in a quantum simulator where, artificial dephase, tunable in its defining parameters, was injected in the system, as random energy fluctuations. The source of dephase is a fluctuator bath at very high temperatures in a weak system-bath interaction. Parameters such as the switching rate and the fluctuation strength controlled the injection of dephase and, consequently, the transport regime of energy in the system. A full coherent evolution of the system, in the form of quantum beating, was observed in the isolated system, while in the open quantum system, dephase suppressed the beating, turning it diffusive. Comparisons between the quantum algorithm and the classical algorithms, such as the Bloch-Redfield equation and the Haken-Ströbl model, have been performed. Similar results for both classical and quantum algorithms were obtained, although the Bloch-Redfield equation failed to provide correct results at some regimes, for the particular chosen environment. Nevertheless, this allowed a fundamental description of the quantum mechanisms in system-bath interactions.

Finally, the required computational resources of the quantum algorithm have been evaluated, such as the qubit resources, the quantum gate complexity and the query complexity.

Keywords: Photosynthesis, Energy transport, Quantum simulation, Computational Physics, Open quantum systems

RESUMO

À medida que a computação quântica se torna cada vez mais desenvolvida, tanto no hardware como no software, o número de aplicações no mundo-real também cresce. O trabalho desta dissertação explora a possível aplicação da computação quântica ao campo da biologia quântica. Em particular, é desenvolvido um algoritmo quântico para simular a evolução do transporte de energia na fotossíntese, onde os efeitos quânticos foram considerados.

Vários algoritmos quânticos foram analisados. O escolhido simula o sistema quântico, tanto isolado como aberto, numa estrutura escalável, composto por moléculas captadoras de luz. O primeiro foi implementado num computador quântico real, na máquina IBM Q, enquanto o último foi implementado num simulador quântico onde, *dephase* artificial, com os seus parâmetros controláveis, foi injetado no sistema, como flutuações aleatórias nas energias. A origem de *dephase* é um banho de flutuadores a elevadas temperaturas, numa interação sistema-banho fraca. Parâmetros tais como a taxa de flutuação e a força da flutuação controlaram a injeção de *dephase* e, conseqüentemente, o regime de transporte de energia no sistema. Uma evolução totalmente coerente, na forma de batimentos quânticos, foi observada no sistema isolado, enquanto no sistema aberto, *dephase* suprimiu os batimentos, tornando-a difusiva. Comparações entre o algoritmo quântico e algoritmos clássicos, tais como a equação de *Bloch-Redfield* e o modelo de *Haken-Ströbl*, foram efetuadas. Resultados similares entre os algoritmos clássicos e quânticos foram obtidos, embora a equação de *Bloch-Redfield* falhou em demonstrar resultados corretos em alguns regimes, para o ambiente especificamente implementado. No entanto, este permitiu uma descrição fundamental dos mecanismos microscópicos nas interações sistema-banho.

Finalmente, os recursos computacionais necessários do algoritmo quântico foram avaliados, tais como os recursos de qubits, a complexidade das portas quânticas e a complexidade de consulta.

Palavras-chave: Fotossíntese, Transporte de energia, Simulação quântica, Física computacional, Sistemas quânticos abertos

CONTENTS

1	INTRODUCTION	1
1.1	Context	1
1.2	Motivation	2
1.3	Objectives	2
1.4	Outline	2
2	STATE OF THE ART	4
2.1	Structure of a photosynthetic system	4
2.1.1	Photosynthesis in bacteria	5
2.1.2	Photosynthesis in plants	8
2.2	Open quantum systems theory	9
2.2.1	Kraus operators	10
2.2.2	Decoherence	11
2.2.3	Redfield equations	12
2.2.4	Lindblad quantum master equation	15
2.2.5	Quantum beating	15
2.2.6	Spectral density	16
2.3	Description of the energy transport dynamics	17
2.3.1	Förster Theory	18
2.3.2	Coherent EET	21
2.3.3	Differences between Förster theory and coherent EET	24
2.3.4	Other approaches to the energy transport	26
2.3.5	The role of decoherence in coherent EET	27
2.4	Quantum simulation	29
2.4.1	Isolated quantum systems simulation	30
2.4.2	Open quantum systems simulation	32
2.5	Summary	34
3	DEVELOPMENT	35
3.1	Decisions	35
3.1.1	Quantum circuit synthesis	35
3.1.2	Artificial decoherence simulation methods	36
3.1.3	The system's qubit model	38
3.2	Implementation	39
3.2.1	Isolated system (no decoherence)	39
3.2.2	Artificial decoherence injection	41

3.3	Computational resources	47
3.4	Quantum circuit optimizations	50
3.4.1	Simple optimizations	50
3.4.2	Basis transformation matrix decomposition	50
3.4.3	Query complexity optimization	51
3.5	Summary	51
4	APPLICATION	52
4.1	Computational setup	52
4.1.1	One qubit system	52
4.1.2	Two qubit system	53
4.2	Results and discussion	58
4.2.1	Isolated system results	58
4.2.2	Results for the system with decoherence	61
4.2.3	Comparisons of the classical algorithms and the quantum algorithm	66
4.2.4	Final considerations	70
4.3	Summary	71
5	CONCLUSION	72
5.1	Conclusions	72
5.2	Future work	73
A	ROTATION DECOMPOSITION OF THE BASIS TRANSFORMATION MATRICES	78
B	A DIFFERENT APPROACH TO THE ARTIFICIAL DECOHERENCE INJECTION	83
B.1	Qubit model of the bath	83
B.2	The model	84
B.3	Quantum circuit implementation	85
B.4	Measurement	87
B.5	Computational resources	89
B.5.1	Qubit resources	89
B.5.2	Quantum gate resources	89
C	THEORETICAL EVOLUTION OF THE TWO MOLECULE SYSTEM	91
D	OPTIMIZED QUANTUM CIRCUITS (TWO MOLECULE SYSTEM)	93
E	CALCULATION OF THE QUANTUM BEATING FREQUENCY	94

LIST OF FIGURES

- Figure 1 Structure of the chloroplast (a) and its thylakoid (b) in plants. In chloroplasts, first stage of photosynthesis occur at the thylakoyd membrane, while the second stage occurs outside the thylakoid [5]. Image taken from [6]. 5
- Figure 2 *Rhodobacter (Rba.)* spheroides: chromatophore. (a) The structure of the chromatophore shown in 3 different colours: blue for RC, green for LH-II and red for LH-I. (b) Here only BChl are shown (without carotenoids). It is worth noticing that plant's photosystems do not exhibit such symmetric shapes as bacteria [3]. Image and legends adapted from [3]. 7
- Figure 3 Summary of photosynthesis in plants. Image taken from [10]. 9
- Figure 4 Molecular states' dynamics with two dissipative vibrational normal modes w_1 and w_2 (two dimensional coordinate system). (I) is the vertical Franck-Condon transition followed by the reorganization dynamics (II), which dissipate the reorganization energy λ ($\hbar = 1$). $\epsilon + \lambda$ is the site energy of the molecule. d_j is the equilibrium displacement for each normal mode j and q_j is the coordinate of each normal mode j . The model of the bath as a set of displaced harmonic oscillators induces a potential energy, in function of the displacement, in the form of a parabola. Image taken from [24]. 24
- Figure 5 Summary of the approaches to the energy transport in photosynthesis. Image taken from [4]. 27
- Figure 6 The molecule excited states $|1\rangle$ and $|2\rangle$ fluctuate, eventually having their energy gap $\Delta = 0$. The lineshape functions, in light-blue and light-red, establish the type of fluctuations present in each molecule. Image taken from [3]. 29
- Figure 7 Implementation of the diagonal Hamiltonian evolution operator. $|1\rangle_{anc}$ is the ancilla qubit initialized at $|1\rangle$. $|q_i\rangle$ is the system's qubit state *in the energy eigenbasis*. 41
- Figure 8 Uncorrelated random fluctuations applied to each site molecule energy ϵ_0 and ϵ_1 . In this image, each molecule is affected by one fluctuator. 43

Figure 9	Implementation of one iteration of the system with decoherence algorithm. $ 1\rangle_{anc}$ is the ancilla qubit initialized at $ 1\rangle$. $ q_{system}\rangle$ is the system's qubit state <i>in the site basis</i> . The basis transformation operators T and T^\dagger are implemented with the gates $R_y(\theta)$ and $R_y(-\theta)$, respectively. Every set of fluctuators is identical so $g' = g'_m$. 45
Figure 10	C^n NOT decomposition where the work qubits are ancilla qubits. With n control qubits, $n - 1$ ancillas are required. This was the decomposition used in the simulations. Image taken from [43]. 47
Figure 11	Implementation of the one-level unitary matrix $O_4(1.767146)$. 55
Figure 12	Implementation of the one-level unitary matrix $O_3(2.3561945)$. 55
Figure 13	Implementation of the one-level unitary matrix $O_2(-2.8470683)$. 55
Figure 14	Implementation of the one-level unitary matrix $O_1(1.8653208)$. 56
Figure 15	Implementation of the two-level unitary matrix $R_{Z-X,6}(-2.159845, -1.2680365)$. 56
Figure 16	Implementation of the two-level unitary matrix $R_{Z-X,5}(-1.1780972, -0.103078015)$. 56
Figure 17	Implementation of the two-level unitary matrix $R_{Z-X,4}(-1.9634955, -0.37569928)$. 57
Figure 18	Implementation of the two-level unitary matrix $R_{Z-X,3}(-0.392699, -6.359089 \times 10^{-2})$. 57
Figure 19	Implementation of the two-level unitary matrix $R_{Z-X,2}(-0.7853982, -0.23925155)$. 57
Figure 20	Implementation of the two-level unitary matrix $R_{Z-X,1}(-1.5707964, -1.280839)$. 57
Figure 21	Time evolution of the occupation probabilities for a near-resonant system: simulated results (points) and theory (lines). 59
Figure 22	Time evolution of the occupation probabilities for a non-resonant system: simulated results (points) and theory (lines). 59
Figure 23	Time evolution simulation of the occupation probabilities for a four molecule system initialized at the state $ 00\rangle$. 60
Figure 24	Time evolution simulation of the occupation probabilities for a four molecule system initialized at the state $ 11\rangle$. 61
Figure 25	Time evolution simulation of the occupation probabilities for a near resonance system with decoherence for different values of fluctuation strengths. 62
Figure 26	Time evolution simulation of the occupation probabilities for a off resonance system with decoherence for different values of fluctuation strengths. 63
Figure 27	Time evolution simulation of the occupation probabilities for a near resonance system with decoherence for different values of switching rates. 64

Figure 28	Time evolution simulation of the occupation probabilities for a off resonance system with decoherence for different values of switching rates.	64
Figure 29	Evolution dynamics of the system with decoherence. The environment is modelled as two fluctuators in each set with different fluctuation strengths.	65
Figure 30	Comparison of the evolution dynamics obtained by employing the quantum and classical algorithms for the near-resonant system.	67
Figure 31	Comparison of the evolution dynamics obtained by employing the quantum and classical algorithms for the non-resonant system.	68
Figure 32	Implementation of the two-level unitary matrix decomposition example. The gate $CU(\delta, \gamma)$ is performed as $CR_Z(\delta)CR_X(\gamma)$.	81
Figure 33	Implementation of the one-level unitary matrix example. The Toffoli gates plus the CR_Z gate denote the decomposition of the C^2R_Z gate.	82
Figure 34	Quantum estimator used to measure the elements of the system density matrix. Image taken from [36].	87
Figure 35	Controlled-SWAP gate or Fredkin gate decomposition [49].	89
Figure 36	Optimized quantum circuit for the near-resonance system simulation.	93
Figure 37	Optimized quantum circuit for the off resonance system simulation.	93

INTRODUCTION

1.1 CONTEXT

Information physics is an emerging branch of physics, which tries to discover new physical ways to process and manipulate information. Diving into the field of research, several new technologies such as quantum computation begin to be applied to general problems, where older technologies, for instance transistors, are reaching an end state of improvement, evidenced by the saturation of Moore's law¹. Limitations imposed by quantum physics led the scientific community to turn their focus to other, newer technologies such as quantum computing. Thus, the notion of quantum computing was introduced by Richard Feynman [2] which could enable an extraordinary enhancement in the speed of processing information using the laws of quantum mechanics². Quantum digital simulation is being used to discover new phenomena in nature, in which classical computers are plausible soon to no longer catch up (by well-known limitations). In this context, quantum digital simulation also seems a very good candidate to be used, in an emerging field of quantum physics, the quantum biology.

Quantum biology is still in a preliminary stage, as only a few of biologic structures of nature have been found or believed to have relevant quantum effects which influence their behaviour. Some of them are: energy transport in photosynthesis, olfact and bird navigation (magnetoreception) [3]. While the former has been experimentally investigated, the later are yet to be. In this context, a reasonable approach to explore in detail such complex biologic mechanics resorts to quantum digital simulation, where complex interactions between the noisy environment and the system are responsible, at microscopic level, for the observed behaviour.

¹ Moore's law affirms that transistors would shrink its size to half, roughly doubling the computation performance, every year [1].

² As such, all the physical mechanisms, at microscopic level, of nature obey to quantum physics, therefore it seems logical that, to simulate nature, one use quantum computers, where the fundamental laws of the universe, given by quantum physics, govern everything. In the recent years, quantum computers are emerging as one of the most promising technologies of the future, thus the scientific community and companies have been improving them, whether on the hardware or software.

1.2 MOTIVATION

As one of the first applications of quantum computing in the field of quantum biology, the proposal of simulating an already experimentally observed quantum phenomenon in biology, in a quantum computer, can show that these machines can already be used in several fields of research. Not only a quantum system is being simulated by another quantum system, as the speed of simulation can exceed the standard ways of modelling quantum systems with classical computers.

Quantum biology works with noisy environments as those present in photosynthetic biologic structures. Therefore, simulating open quantum systems in a quantum computer is also a very recent application of these devices, while the current software still does not allow a generalized application of a quantum algorithm. In this way, creating or using already existent quantum algorithms to simulate open quantum systems is inevitably an advancement in quantum simulation.

The light harvesting in photosynthesis, a very small nature mechanism, has a great potential in changing our day-to-day lives. By understanding the physics of this extremely efficient phenomenon [3, 4], the transport, if implemented in a biomimetic technology, can be translated to artificial devices which collect and transport energy very efficiently, which would allow a transformation on energy-capture based technologies and on the information transport in society.

1.3 OBJECTIVES

This dissertation aims to develop an efficient and scalable quantum digital simulation of the time evolution of energy transport in photosynthesis. To achieve such a goal, our efforts seek to obtain

- A quantum simulation that provides answers about the mechanisms of the energy transport system, isolated and in contact with an environment.
- A quantum simulation verifiable with already developed classical algorithms.
- Clear physical and computational explanations about the algorithmic model.

1.4 OUTLINE

In chapter 2 the topics in quantum physics, quantum biology and quantum simulation are reviewed.

In chapter 3 the development and the decisions made are presented. The simulation model and implementation are introduced as well as the calculation of the required computational resources. A number of related quantum circuit optimizations are also explained.

In chapter 4 the setup of the quantum circuit is described, which contains the parameters used and their manipulation to conceive the simulation. The results and their discussion are then presented as well as a comparison between the classical algorithms and the quantum algorithm developed in this work.

Finally, chapter 5 summarizes the overall achievements of this work, and suggests possible paths to be taken in the future to pursue this line of research.

STATE OF THE ART

2.1 STRUCTURE OF A PHOTOSYNTHETIC SYSTEM

Photosynthesis is a process that converts electromagnetic energy into chemical energy. This process is found in some bacteria, algae and plants and consists mainly in light-harvesting followed by transformations of electronic excitation energy in membrane potentials [3]. It follows the production of the molecules required to create carbohydrates, which the living being needs.

Photosynthesis has two stages. The first one consists in light-dependent reactions, which is the focus of this work, and the second one is the Calvin cycle, i.e. a light-independent reactions stage [5]. The first stage begins with the absorption of photons by the light-harvesting molecules and ends with the production of ATP (Adenosine Triphosphate) and NADPH (Nicotinamide Adenine Dinucleotide Phosphate).

A photosystem is composed by a light-harvesting system and reaction centers, existent in a lipid bilayer structure called the thylakoyd membrane present in plants (inside chloroplasts), algae and bacteria. An illustration of the structure of chloroplasts and the thylakoid is presented in figure 1.

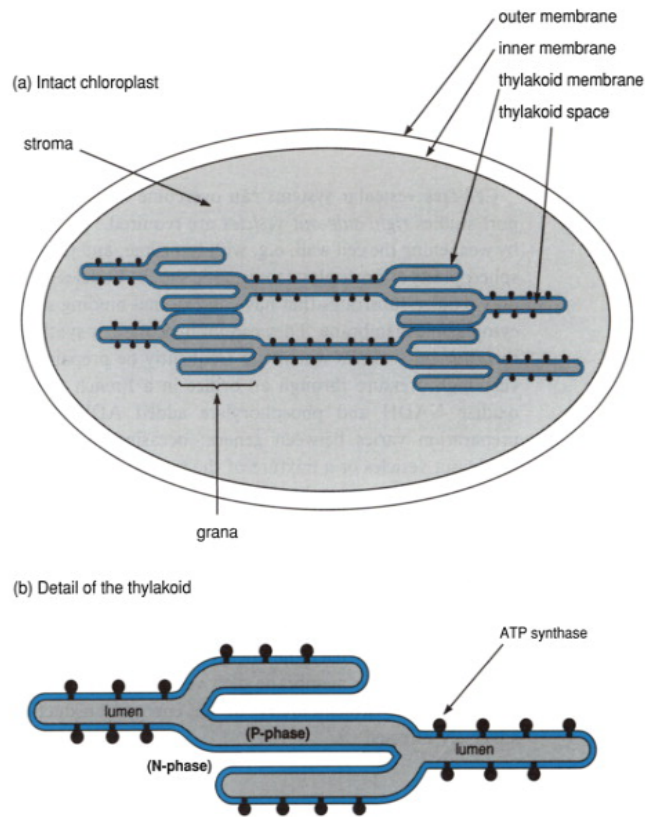


Figure 1: Structure of the chloroplast (a) and its thylakoid (b) in plants. In chloroplasts, first stage of photosynthesis occur at the thylakoyd membrane, while the second stage occurs outside the thylakoid [5]. Image taken from [6].

The structure of the purple bacteria is introduced in the next subsection. This widely studied living being has a simpler apparatus than plants, thus being a good start in this discussion. The structure of photosynthesis in plants is then introduced.

2.1.1.1 *Photosynthesis in bacteria*

In the purple bacteria, the light-harvesting system is composed by the LH-I (Light-Harvesting I) complex and the LH-II complex, whose main goal is to harvest light [5, 3]. The reaction center (RC) is also present where the primary energy conversions in photosynthesis take place. LH molecules, in bacteria called bacteriochlorophyll (BChl), are electronically coupled to each other. They can either absorb solar light or receive excitations from other BChl by Electronic Energy Transfer (EET) [3, 4].

The BChl molecules absorb light in the wavelength interval $[800, 900] \text{ nm}$ while, carotenoids, also located in the LH complexes, harvest light in the middle of the visible spectrum at around $\sim 500 \text{ nm}$. The excitation of these molecules is transferred very rapidly to the BChl,

in about 100 fs [3]. Carotenoids are not only an auxiliary light-harvesting molecule but also help the photosystem to get rid of any excess of energy under intense light, harmful to the bacteria, as heat dissipation [5].

Reaction centers also have BChl, although in a lower quantity, which can receive the excitation from LH-I molecules or absorb light by its own. When the excitation energy is delivered to RC, a charge separation process occurs. This charge (electron) is transferred along a chain of molecules, which generates a membrane potential [3]. In the green sulphur bacteria also exists the Fenna-Matthews-Olson complex (FMO), which connects LH complexes to the RC [3].

In the widely studied purple bacterium *Rhodobacter (Rba.)*, the photosynthetic apparatus is organized in chromatophore vesicles of almost spherical shape of about 60 nm diameter as shown in figure 2 [3, 7]. In this figure, it can be seen 4 BChl (blue) at each RC, 56 BChl (red), in LH-I, form a eight-line shape and at the LH-II complex there are 27 BChl (green) in a crown-like ring. This ring has 18 BChl while the crown has 9 BChl. There is a total of ~ 3000 BChl and ~ 1000 carotenoids in a single chromatophore.

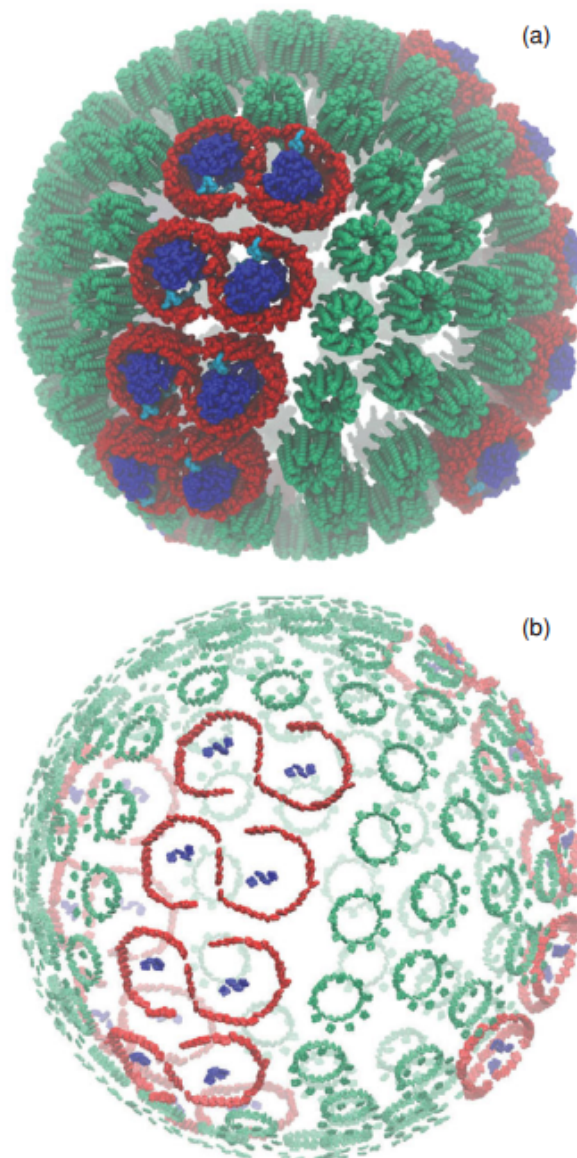


Figure 2: *Rhodospirillum rubrum* (Rba.) spheroides: chromatophore. (a) The structure of the chromatophore shown in 3 different colours: blue for RC, green for LH-II and red for LH-I. (b) Here only BChl are shown (without carotenoids). It is worth noticing that plant's photosystems do not exhibit such symmetric shapes as bacteria [3]. Image and legends adapted from [3].

Some remarks should be made concerning the efficiency of the energy transport along the light-harvesting system, which goes from 50% up to more than 95% efficiency of energy absorption and transport to the RC [4, 3] (under normal environment conditions, usually the efficiency is higher than 95%). The efficiency depends on the size of the complexes, the excited state lifetime of the light-harvesting molecules, the arrangement of the light-harvesting apparatus and the light conditions [4]. The observed lifetime of an excitation in

the light-harvesting system of a bacteria is around 50 *ps* [8, 9] while in the light-harvesting system of plants it is found to be 4 *ns* [4].

2.1.2 *Photosynthesis in plants*

In plants, chlorophyll *a* and chlorophyll *b* [5, 3] are the pigments that drive energy transport in the light-harvesting systems through EET. Chlorophyll *a* absorbs light within the [670, 680] *nm* wavelength interval, chlorophyll *b* at around 650 *nm* and the carotenoids at [400, 500] *nm* [3]. Chlorophyll *a* is the main component in excitation transfer and photon absorption, while other components are auxiliary, in lower number, but important because they broaden the wavelength interval of radiation absorption of the plant photosystem [5].

In plants, there are two photosystems, I and II (PS-I and PS-II respectively), which contain a light-harvesting system and a reaction center [3]. In short, photosystem II is responsible for the split of water into oxygen and it is the first photosystem to act. Photosystem I is responsible for the production of NADPH and it is the second photosystem to act [5]. Each photosystem has about 300-400 chlorophyll molecules [3]. The light-dependent stage in plants is slightly different from that in bacteria (mainly in the RC processes). In the next paragraph, the reaction center processes which occur in photosynthesis (only in plants) are explained [10]. A summary of this stage is illustrated in figure 3.

After the absorption of a photon and its energy transport to RC in PS-II, a *special pair* (in plants, constituted by two chlorophyll molecules) boosts an electron to a higher energy level. This electron is then passed to an acceptor molecule (pheophytin) and is replaced in the special pair by an electron delivered from water, H₂O. This process splits water into hydrogen and oxygen. This high energy electron goes through a transport chain, losing energy. The transport chain consists in the following: the electron is passed to a plastoquinone (Pq, which is a type of molecule), then to a cytochrome (Cyt) (a protein which helps the energy transport) and finally to a copper-containing protein called plastocyanin (Pc). This released (or lost) energy pumps H⁺ ions from the stroma (outside of the thylakoid membrane) into the thylakoid membrane, building a charge gradient. Later, as these ions flow from inside the thylakoid membrane to the stroma, driven by the proton-motive force originated by the gradient, they pass through ATP synthase (an enzyme) and ATP is synthesized.

The same process occurs in PS-I, but now the *special pair* in the corresponding RC is reduced by the electron which travelled across the transport chain in PS-II. After neutralization of the special pair, just like the process in PS-II, the high energy electron is transferred to an acceptor molecule (pheophytin), where it follows an electron transport through transport chain: it is passed to ferredoxin (Fd, a type of molecule) and then to an enzyme called NADP⁺ reductase. At the end of this transport chain, the electron is passed to the molecule NADP⁺, along with a second electron which has been boosted to a higher energy level and similarly transported

across the electron transport chain. This latter electron was originated from the photon absorption at the light-harvesting system in PS-I and transported to the corresponding RC, through EET. The transport chain finishes with the production of NADPH.

After NADPH and ATP have been produced, the light-independent stage occurs.

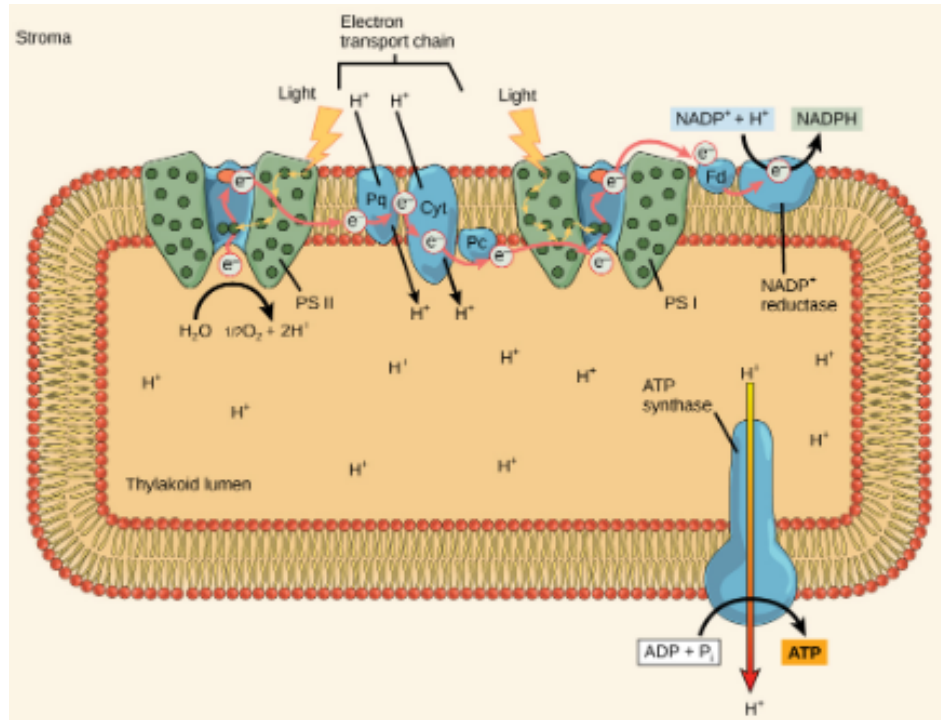


Figure 3: Summary of photosynthesis in plants. Image taken from [10].

2.2 OPEN QUANTUM SYSTEMS THEORY

The biological structures briefly described above, quite complex in themselves, such as e.g. the chlorophyll molecules interacting with the environment, are open systems. In this section, the most relevant mathematical approaches to open quantum systems will be presented.

The most used formalism to describe a system's state in open quantum systems is that of *density matrix*. This matrix can describe a system in a mixed state, which cannot be attributed a state vector. This is a matrix ρ which has diagonal terms (population terms) $\sum_{\alpha} P_{\alpha} |\Psi_{\alpha}\rangle \langle \Psi_{\alpha}|$, where each element represents the probability P_{α} of being in a certain pure state $|\Psi_{\alpha}\rangle$, and off-diagonal terms (coherence terms) $\sum_{\alpha \neq \beta} A_{\alpha, \beta} |\Psi_{\alpha}\rangle \langle \Psi_{\beta}|$, which describe correlations between

different states. The sum of the diagonal terms must be $\sum_{\alpha} P_{\alpha} = \text{Tr}[\rho] = 1$. The following example shows a general form of the density matrix for a two-level system:

$$\rho = \begin{pmatrix} P_0 & A_{0,1} \\ A_{1,0} & P_1 \end{pmatrix} \quad (1)$$

2.2.1 Kraus operators

One way of modeling open quantum systems is to consider the whole environment plus the open quantum system as a single *closed* system. Quantum systems can be composed and form new larger systems through the *Kronecker* product of the Hilbert spaces, corresponding to two sub-systems (in this case the open system S and the environment E):

$$\mathcal{H}_S \otimes \mathcal{H}_E \quad (2)$$

The state of such a closed system can be given, at the initial time $t = 0$, by

$$\rho(0) = \rho_S(0) \otimes \rho_E(0) \quad (3)$$

where ρ_S corresponds to the open system (denoted from now on as just *system*) and ρ_E to its environment. The environment plus the system maintain a unitary evolution $U_{SE}(t)$. The overall system evolution can be given as follows

$$\rho(t) = U_{SE}(t)[\rho_S(0) \otimes \rho_E(0)]U_{SE}^{\dagger}(t) \quad (4)$$

where U_{SE} is the unitary evolution operator of the pair *system plus environment*. Generally, one is only interested in the system and for such, the environment can be disregarded by *tracing* it out over an arbitrary environment basis $\{|k\rangle\}$ as

$$\rho_S(t) = \text{Tr}_E\{\rho(t)\} = \sum_k \langle k| U_{SE}(t)[\rho_S(0) \otimes \rho_E(0)]U_{SE}^{\dagger}(t) |k\rangle \quad (5)$$

where we define the initial environment density matrix to be

$$\rho_E(0) = \sum_m p_m |m\rangle \langle m| \quad (6)$$

Inserting this definition in equation (5),

$$\rho_S(t) = \text{Tr}_E\{\rho(t)\} = \sum_{k,m} p_m \langle k| U_{SE}(t) |m\rangle \rho_S(0) \langle m| U_{SE}^{\dagger}(t) |k\rangle \quad (7)$$

$$\rho_S(t) = \mathcal{M}[\rho_S(0)] = \sum_k E_k \rho_S(0) E_k^\dagger \quad (8)$$

\mathcal{M} is a superoperator that maps operators to operators. This superoperator preserves linearity, is trace-preserving (in time evolution mappings) and complete positive [11, 12]. E_k , in equation (8), is a Kraus operator defined as

$$E_k = \sum_m \sqrt{p_m} \langle k | U_{SE} | m \rangle \quad (9)$$

The set of Kraus operators, if trace-preserving, fulfill the following condition

$$\sum_k E_k E_k^\dagger = I \quad (10)$$

Next we will introduce the different types of decoherence.

2.2.2 Decoherence

It is possible that, throughout time, correlations are created between a system and its environment. Such correlations affect the pure states in the system, introducing *errors* in states, and ultimately destroy superposition and entangled states in an irreversible manner. This is the so-called process of *decoherence*, which has been the main obstacle to the practical implementation of quantum computation. Decoherence can be split in three categories: (i) amplitude damping, (ii) dephasing and (iii) depolarization, which are briefly characterized below.

Amplitude damping: Environment interactions with the system causing the loss of the amplitude of one or more system's states. The spontaneous emission of a photon from the system to the environment from a two-level atom is an example of this kind of process, where the atom has a probability decay of being in its excited state [11]. In a two level system, this type of decoherence contracts the Bloch sphere along the z axis [12].

Phase damping or dephasing: Such interactions conserve the energy of the system, contrary to the amplitude damping. A phase damping channel removes the superposition of the system's state, i.e. the off-diagonal terms of the system's density matrix decay over time down to zero. It is a process of removing the coherence of the system, causing a classical probability distribution of states and, therefore, imposing some classical behaviour in a quantum system. A simple way to look at this type of decoherence is also to think of the system interacting with the environment where the relative phases of the system's states become randomized by the environment. This randomness comes from a distribution of energy eigenvalues of the environment. Over time, the coherence between the system's states is lost by averaging this interaction.

Let us consider a qubit interacting with the environment via phase damping [11] and let $|\psi\rangle = a|0\rangle + b|1\rangle$ be the initial state of the qubit. Averaging the random effect of the environment on the qubit (given by z -rotations on the Bloch's sphere) over a Gaussian distribution of angles θ with zero mean value and variance 2λ yields

$$\rho = \frac{1}{\sqrt{4\pi\lambda}} \int_{-\infty}^{+\infty} d\theta R_z(\theta) |\psi\rangle \langle\psi| R_z^\dagger(\theta) e^{-\frac{\theta^2}{4\lambda}} \quad (11)$$

$$= \begin{pmatrix} |a|^2 & ab^*e^{-\lambda} \\ ba^*e^{-\lambda} & |b|^2 \end{pmatrix} \quad (12)$$

This is a characteristic result of dephasing. The off-diagonal elements decay exponentially to 0 as λ increases. The variance λ can be taken proportional to a time variable, which means that coherence decays over time [11]. In a two-level system with a dephasing interaction, the Bloch sphere contracts in the xy plane [12].

Depolarization: This type of decoherence changes the (pure) system's state to a mixed state with a probability P , while with probability $(1 - P)$ the system remains in its pure state. It is equivalent to saying that, for a single qubit, an initial pure state represented on the Bloch sphere has suffered a contraction over all dimensions of the sphere (with the contraction degree depending on the probability P) turning the initial pure state into a mixed state. It can be thought as a combination of the other two types of decoherence [12].

2.2.3 Redfield equations

Redfield equations are a set of time differential equations widely used in open quantum systems theory to describe the evolution of the system. A weak interaction between the bath (environment at thermal equilibrium) and the system (weak system-bath coupling) must exist [3, 12], so that the *second-order perturbative time-convolution* equation (TC2) or the *second-order perturbative time-convolutionless* equation (TCL2, or also called *time-dependent Redfield equation*) can then be formulated using a second order perturbation with respect to the system-bath interaction [3].

Consider the following Hamiltonian [3],

$$H = H_S + H_B + H_{SB} \quad (13)$$

where

$$H_S = \sum_m \hbar\Omega_m |m\rangle \langle m| \quad (14)$$

H_S is the system Hamiltonian in the energy eigenbasis composed by the energy eigenstates $|m\rangle$ with the respective energy eigenvalues $\hbar\Omega_m$.

$$H_B = \sum_{\xi} \hbar w_{\xi} (b_{\xi}^{\dagger} b_{\xi} + \frac{1}{2}) \quad (15)$$

This is the bath Hamiltonian. The bath is modelled as a set of harmonic oscillators. b_{ξ} and b_{ξ}^{\dagger} are the creation and annihilation operators for a phonon ξ and w_{ξ} is the normal mode of the phonon ξ .

$$H_{SB} = \sum_{l,\xi} \hbar w_{\xi} g_{l,\xi} (b_{\xi} + b_{\xi}^{\dagger}) S_l \quad (16)$$

This is the system-bath interaction Hamiltonian. $g_{l,\xi}$ is the coupling strength of a phonon ξ with the system via the operator S_l , which is an operator acting on the system's Hilbert space. Here, as can be observed, one assumes that the system-bath interaction is linear.

The equations TC2 or TCL2 can be derived with the previous Hamiltonians so that they take a simple form considering the following conditions [3]: the density matrix can be initialized as $\rho(0) = \rho_S(0) \otimes \rho_B(0)$ and $Tr_B[\mathcal{L}_{SB,I}(t)\rho_B(0)] = 0$, (static environment throughout time), where $\mathcal{L}_{SB,I}(t)\rho_B(0) = [H_I(t), \rho_B(0)]$ and $H_I(t) = e^{i(H_S+H_B)t} H_{SB} e^{-i(H_S+H_B)t}$ is the interaction Hamiltonian in the interaction picture. Then, the bath correlation function which defines the correlations between the system and the environment is [3]

$$C_{ll'}(t) = \int_0^{\infty} dw F_{ll'}(w) (\coth(\frac{\beta\hbar w}{2}) \cos(wt) - i \sin(wt)) \quad (17)$$

where $\beta = \frac{1}{k_B T}$, being k_B the Boltzmann constant and T the temperature of the bath. The function $F_{ll'}(w)$ is the spectral density of the bath respective to the system's operators S_l and $S_{l'}$ defined for a continuum of vibrations as

$$F_{ll'}(w) = \sum_{\xi} g_{\xi,l} g_{\xi,l'} \delta(w - w_{\xi}) w^2 \quad (18)$$

Defining the spectral density, one defines the type of bath present (more about spectral densities at the end of the section).

Then one can find a time non-local quantum master equation (TC2), in the interaction picture characterized as [3]

$$\frac{d\rho_{S,I}(t)}{dt} = - \sum_l \sum_{l'} \int_0^t d\tau \{ C_{ll'}(t-\tau) [S_l(t), S_{l'}(\tau) \rho_{S,I}(\tau)] - C_{l'l}(t-\tau) [S_l(t), \rho_{S,I}(\tau) S_{l'}(\tau)] \} \quad (19)$$

where $S_l(t) = e^{iHt} S_l e^{-iHt}$ is also defined in the interaction picture. This is the most used form for the TC2 equation whose derivation resorts to the previously defined Hamiltonians

[3]. The TCL2 equation can also be derived as a time local equation (with a time local additional approximation) [3], as follows

$$\frac{d\rho_{S,I}(t)}{dt} = \sum_{I'} \mathcal{R}_{I'}(t)\rho_{S,I}(t) \quad (20)$$

where $\mathcal{R}_{I'}(t)(\cdot)$ is a super-operator applied to some operator (\cdot) defined as

$$\mathcal{R}_{I'}(t)(\cdot) = - \int_0^t d\tau \{C_{I'}(t-\tau)[S_I(t), S_{I'}(\tau)(\cdot)] - C_{I'}(\tau-t)[S_I(t), (\cdot)S_{I'}(\tau)]\} \quad (21)$$

By employing a Markovian¹ bath (an additional approximation), one can reach the following simpler Bloch-Redfield equation from the TC2 or TCL2 equations in the Markovian limit [3]:

$$\frac{d\rho_{nm}(t)}{dt} = -i\hbar\Omega_{nm}\rho_{nm} + \sum_{n',m'} \Gamma_{nmm'n'}\rho_{n'm'} \quad (22)$$

where $\rho_{nm} = \langle n|\rho_S|m\rangle$ is a term of the system's density matrix in the energy eigenbasis. $\Omega_{nm} = \Omega_n - \Omega_m$ and the Redfield tensor $\Gamma_{nmm'n'}$ is:

$$\Gamma_{nmm'n'} = \Lambda_{m'mnn'} + \bar{\Lambda}_{nn'm'm} - \sum_k \Lambda_{nkkn'}\delta_{mm'} + \bar{\Lambda}_{kmm'k}\delta_{nn'} \quad (23)$$

with $\Lambda_{m'mnn'} = \frac{1}{2}S_{nm}S_{n'm'}\tilde{C}(\Omega_{m'} - \Omega_n)$, $\bar{\Lambda}_{m'mnn'} = \frac{1}{2}S_{nm}S_{n'm'}\tilde{C}^*(\Omega_{m'} - \Omega_n)$ where $\tilde{C}(w) = \int_0^\infty dt e^{iwt} C(t)$ and $C(t)$ is the system-bath correlation function for a single system operator l (for more operators, i.e. $l > 1$, the equation is described in [13]). Also, $S_{nm} = \langle n|S|m\rangle$ and $\delta_{mm'}$ is the Delta-Kronecker function.

Note that in a Markovian bath the correlation function must have a fast decay. Since the bath has no memory, one must ensure that the timescale of the correlation decay is much shorter than the decoherence timescale (the inverse of the system-bath interaction rate) [3].

By using a secular approximation (also called rotating wave approximation), one can find the dynamics in the Lindblad form (defined in the next subsection) from the Bloch-Redfield equation [13]. The approximation can only be applied if $|\Omega_m - \Omega_n|^{-1} \ll \tau_D$ for all unequal n 's and m 's [3, 13], where τ_D is the decoherence timescale of the system. Sometimes, the Bloch-Redfield equation does not yield a valid system's density matrix [3, 13]. In such cases, the conversion to the Lindblad form, using the secular approximation must be performed [3, 13].

¹ A Markovian approximation means that the dynamics of the system are local in time, i.e. $\rho_S(t+dt)$ is completely determined by $\rho_S(t)$. Because information can flow from the system to the environment, and vice-versa, the information that has flown to the environment can be, after a while, dissipated back to the system. A Markovian approximation consists in saying that the environment has a certain time to "forget" the information that flows to it and after this time, the information received from the system is forever lost in the environment. If the timescale of the overall system evolution one wants to observe is higher than the time scale of the environment to "forget" the information, one can apply the approximation.

2.2.4 Lindblad quantum master equation

The Lindblad master equation is also a time differential equation which follows from the rotating wave approximation applied to the Bloch-Redfield equation [3, 13]. It is defined as:

$$\frac{d\rho_S}{dt} = \mathcal{L}[\rho_S] = -i[H, \rho_S] + \sum_k (L_k \rho_S(t) L_k^\dagger - \frac{1}{2} \rho_S(t) L_k^\dagger L_k - \frac{1}{2} L_k^\dagger L_k \rho_S(t)) \quad (24)$$

where $\mathcal{L}[\cdot]$ is the *Lindblad superoperator*. This equation divides in the H , which is usually the system Hamiltonian term [13], where $-i[H, \rho_S]$ is the right-hand side term of the *quantum Liouville equation* corresponding to the system evolution alone. The remaining terms, correspond to the dissipative evolution, given by the Lindblad operators L_k . This time continuous system description can be converted to the Kraus operator representation and vice-versa [14].

2.2.5 Quantum beating

Quantum beating is an effect of superposed states within the system (coherence). By measuring this phenomenon, one can directly detect quantum effects, i.e. superposition [3]. This is a property which goes beyond open quantum systems, and of extreme importance to understand the energy transport in photosynthesis.

Consider the quantum Liouville equation that finds the evolution of a closed system ρ subjected to an Hamiltonian H ($\hbar = 1$),

$$\frac{d\rho}{dt} = -i[H, \rho] \quad (25)$$

If the density matrix is written in the energy eigenbasis where the Hamiltonian H is diagonal, then

$$\frac{d\rho_{ij}}{dt} = -i(\epsilon_i - \epsilon_j)\rho_{ij} \quad (26)$$

where ϵ_i is the energy eigenvalue of i th energy eigenstate. The populations (matrix elements ρ_{ii}) remain constant and the coherence terms (matrix elements ρ_{ij} , where $i \neq j$) evolve oscillating in time as

$$\rho_{ij}(t) = e^{-i(\epsilon_i - \epsilon_j)t} \rho_{ij}(0) \quad (27)$$

A wrong way to measure the oscillations would be to measure the energy observable as

$$\langle H \rangle = \text{Tr}(H\rho) = \sum_i \epsilon_i \rho_{ii} \quad (28)$$

As already seen, populations in the energy eigenbasis are constant under unitary evolution, so quantum coherence can not be measured by using the energy observable.

The best way to measure this oscillation is by using an observable operator that does not commute with the Hamiltonian. This procedure works because the observable operator written in the Hamiltonian eigenbasis is not diagonal. Therefore, oscillations present in the coherence terms of the system's density matrix, in the energy eigenbasis, will be observable at the population terms in the chosen operator eigenbasis.

In spectroscopy, the dipole moment operator is the chosen operator, \hat{A} , to detect quantum coherence [3]. One example is the detection of quantum coherence in the energy transport of photosynthesis [15, 16, 17]. These experiments show evidence of coherent energy transport, in the FMO complex and algae. The oscillations (quantum beating) last for hundreds of femtoseconds, thus providing evidence that coherence is not rapidly destroyed by the environment and that it can not be discarded in theoretical energy transport models.

2.2.6 Spectral density

Spectral densities are used to encapsulate the effect of the environment in the system's dynamics because it is impossible to know the evolution of all of the environment degrees of freedom. While the spectral function of the environment is the Fourier transform of the correlation function, which defines the noise spectrum and the strength of spatial correlations between sites, the spectral density defines, temperature-independently, the number of environmental fluctuators and their coupling strength to the system at a certain frequency [18, 19]. The spectral density for an environment of harmonic oscillators is defined as:

$$F(\omega) = \pi \sum_{i=1}^N \frac{c_i^2}{2m_i\omega_i} \delta(\omega - \omega_i) \quad (29)$$

where i is the subscript for a harmonic oscillator, c_i is the coupling strength between the harmonic oscillator i and the system and m_i is the mass of the harmonic oscillator [19, 20].

It can also be defined (for a continuum of harmonic vibrations [3]) as:

$$F(\omega) = \sum_{\zeta} g_{\zeta}^2 \delta(\omega - \omega_{\zeta}) \omega^2 \quad (30)$$

where g_{ζ} denotes the coupling strength of each phonon ζ to the system. In the limit of an high density bath, where $N \rightarrow \infty$, the sum can be converted to an integral over the frequencies ω .

Usually, the environment is modelled as:

$$F(\omega) = A\omega^s e^{-\omega/\omega_c} \quad (31)$$

This is a common type of spectral density referred to as an Ohmic form. A is a constant parameter, s is a number that defines the type of the Ohmic spectral density and w_c is the cut-off frequency. When $s < 1$, the spectral density is of the sub-Ohmic type, if $s = 1$ it is an Ohmic spectral density and if $s > 1$ the spectral density type is super-Ohmic. The cut-off frequency w_c is important because up to this frequency, the spectral density (for the Ohmic type) is approximated as $F(w) = haw$ when $w < w_c$, where a is a dimensionless strength system-bath coupling [19] and h is the Planck's constant. Note that the frequency w defines the rate of dynamics of the environment. These environment dynamics affect the system, which also depend on the system-environment coupling strength. The bath motions with frequencies higher than the cut-off frequency can be thought as if they are too fast to the system to follow, thus they average out over the system's dynamics [19], causing the system to not feel these fast dynamics of the environment. By defining a spectral density, one can have different environments represented [13, 21, 3].

2.3 DESCRIPTION OF THE ENERGY TRANSPORT DYNAMICS

This section will introduce the quantum mechanics of the energy transport in the light harvesting molecules, such as chlorophyll.

The photosynthesis starts by the absorption of photons by the molecules of a light-harvesting chain, which excite them by creating quasi-particles, generally called *excitons*. Such excitons can be transported, along the chain, from excited molecules (donors) to non-excited ones (acceptors), until they reach a reaction centre, where the energy is *trapped*, and the photosynthesis passes to the charge separation stage. Such transport phenomena between molecules are well-known and pervasive across physics, and can happen by several mechanisms as it will be discussed.

Two different theories try to explain this transport: Förster theory or incoherent EET (also called Förster resonance energy transfer, FRET) and coherent EET (coherent electronic energy transfer). Förster theory is a dissipative theory of electronic energy transfer in a weak donor-acceptor electronic coupling compared to the high system-environment coupling resulting in random incoherent hopping jumps of the excitation, from molecule to molecule. Coherent EET consists of the isolated system evolution (defined by a system Hamiltonian) which competes against dissipative evolution (defined by the system-environment interaction Hamiltonian), i.e. it is an unitary evolution of the system plus environment. This theory can exhibit coherent excitations among the molecules.

The widely studied Förster and Redfield theories are used as approaches based in the quantum-mechanical perturbation theory, which represent two opposite limits of the energy transport regime. Förster theory is the first theory to be discussed, then the Redfield theory, which is based on the master equations of subsection 2.2.3, will be connected to the coherent

model of energy transport. The main differences between coherent EET and Förster theory will be explained, followed by an insight about other EET mathematical treatments, different from these perturbative methods.

2.3.1 Förster Theory

A simple model consists of two molecules where the state $|m\rangle$ denotes the excited state of the molecule m and all other molecules (in this case, only one) are in the ground state.

Consider two baths, one for the acceptor molecule and one for the donor molecule, which are uncorrelated. The Hamiltonian, in Förster theory, takes the form [3]

$$H = H_0 + H_{DA} + H_{eb} \quad (32)$$

where

$$H_0 = E_D |D\rangle \langle D| + E_A |A\rangle \langle A| + H_b \quad (33)$$

This is the unperturbed Hamiltonian of the system and the baths. E_A and E_D are the energies of the acceptor and donor molecules in the excited state, respectively, and H_b is the unperturbed Hamiltonian of the two baths defined as

$$H_b = H_{b_D} + H_{b_A} \quad (34)$$

with the terms H_{b_D} and H_{b_A} denoting the bath Hamiltonians of the donor and acceptor molecules, respectively. The other Hamiltonian terms are

$$H_{DA} = J(|D\rangle \langle A| + |A\rangle \langle D|) \quad (35)$$

which define the interaction between the donor and acceptor molecules with a constant coupling strength J and

$$H_{eb} = B_D |D\rangle \langle D| + B_A |A\rangle \langle A| \quad (36)$$

is the exciton-bath Hamiltonian where B_D and B_A are the operators acting on the baths of the donor and acceptor molecules, respectively.

The density matrix of the system plus bath, at the initial time $t = 0$, is given as [3] by

$$\rho(0) = |D\rangle \langle D| \otimes \frac{e^{-\beta H_b}}{Z_b} \quad (37)$$

where $Z_b = \text{Tr}_b[e^{-\beta H_b}]$ is the bath partition function. The probability of finding the acceptor molecule in the excited state is

$$P_A(t) = \text{Tr}_b\{\langle A| e^{-iHt} \rho(0) e^{iHt} |A\rangle\} \quad (38)$$

where the evolution of the density matrix is given in the interaction picture. By differentiating this probability with respect to time, a energy transfer rate equation can be obtained. Therefore, using a first order approximation of the evolution operator with respect to H_{DA} , i.e. J must have a small value, and considering the approximation that the energy transfer only significantly occurs after the bath of the donor molecule reaches its thermal equilibrium state, the energy transfer rate can be calculated using the Fermi's Golden Rule and written as [22]

$$k_F = \frac{9000 \ln(10) \kappa^2}{128 \pi^5 N_A \tau_D n_r^4 R^6} \int_{-\infty}^{+\infty} dv \frac{f_D(v) \epsilon_A(v)}{v^4} \quad (39)$$

where $f_D(v)$ is the area-normalized emission spectrum of the donor, $\epsilon_A(v)$ is the molar extinction coefficient of the acceptor or, in other words, the attenuation coefficient per molar concentration (can be thought as the absorption spectrum), R is the distance between the donor and acceptor molecule, n_r is the refractive index of the medium, N_A is the Avogadro number, τ_D is the spontaneous decay lifetime of the donor molecule, κ is the orientational factor which is usually $\frac{2}{3}$ and v is equal to $\frac{1}{\lambda}$, being λ the wavelength. The energy transfer rate can also be defined as [3]

$$k_F = \frac{J^2}{2\pi\hbar^2} \int_{-\infty}^{+\infty} dw I_A(w) L_D(w) \quad (40)$$

where $I_A(w)$ is the lineshape function of the acceptor molecule, $L_D(w)$ is the lineshape function of the donor molecule and w is the angular frequency. The lineshape function is equivalent to the molecule energy spectrum, describing a probability distribution of the excited state having a certain energy. The energy of it is not completely determined due to the fluctuations of the environment which broaden the distribution, making the energy of the excited state to fluctuate.

As can be seen from equations (39) and (40), there must be a considerable overlap between the acceptor absorption spectrum and the donor emission spectrum to exist a significant energy transfer rate (this integral is also called spectral overlap). There are two principal regimes which control the energy transfer. The near-resonance regime, where the difference of the excited state energies (energy gap) is smaller than their coupling strength, i.e. $|E_D - E_A| \leq J$ and the non-resonant regime where $|E_D - E_A| > J$. In the first, the energy transfer rate is high, leading to the maximum transfer rate when $|E_D - E_A| = 0$ (resonance regime). In a non-resonant system, the energy transfer rate is small. Thus if the coupling strength is higher than the difference of the excited state energies of both molecules then the

near-resonance regime is present in the system and the energy transfer is fast. If the coupling strength is smaller than the difference of the excited state energies of both molecules then the non-resonant regime is present and the energy transfer is slow.

The coupling strength J can be expressed as [3]:

$$\frac{J^2}{\mu_D^2 \mu_A^2} = \frac{\kappa^2}{n_r^4 R^6} \quad (41)$$

where μ_D and μ_A are the transition dipole moments of the donor and acceptor molecule which define the transition from the ground state to the excited state of the molecule (creation of a dipole). This equation is a dipole-dipole approximation which is only valid for relatively large distances between molecules (10-20 *nm*).

Dexter considered [23] a generalization of the Förster coupling which includes multipole-multipole interaction. This coupling is relevant for closer distances between molecules or when there is a forbidden transition dipole moment in a molecule. In such cases, one needs to consider an higher order expansion of the Coulomb interaction. In particular, Dexter considered dipole-quadrupole interaction (forbidden transition in the acceptor) where a R^{-8} dependence in the transfer rate is present [23]. Finally, at very small distances, when there is an overlap of the wavefunctions, an electron exchange via tunneling can take place. This type of interaction decays exponentially with the inter-molecular distance.

The energy transfer equation (39) or (40) can be defined taking account some generalizations [3]:

- **Non-equilibrium generalization (N-FRET):** The energy transfer occurs before the equilibrium in the donor excited state becomes complete. If it does, the emission profile of the donor has a dependence on time. Then the energy transfer rate is changed to:

$$k_F = \frac{J^2}{2\pi\hbar^2} \int_{-\infty}^{+\infty} dw I_A(w) L_D(t, w) \quad (42)$$

If $t \rightarrow \infty$, $L_D(\infty, w) = L_D(w)$ and the original expression is recovered. This means the energy transfer in the original Förster Theory only occurs when the stationary equilibrium is reached in the donor excited state, i.e. the energy only jumps to the next molecule after the donor molecule reaches the equilibrium of its excited state (passed a long time).

- **Inelastic generalization (I-FRET):** The coupling strength J is not constant. The molecules can be in a soft environment or locked by a bridge molecule thus the coupling strength J can be modulated by the bath. Then, the energy transfer rate must be changed to:

$$k_F = \frac{1}{2\pi\hbar^2} \int_{-\infty}^{+\infty} dw \int_{-\infty}^{+\infty} dw' I_A(w') L_D(w) K_J(w - w') \quad (43)$$

The function $K_J(w - w')$ modulates the spectral overlap because it depends on the frequency of the dynamics of other physical objects (caused by orientational fluctuations of the dipoles). The original Förster theory is recovered when $K_J(w - w')$ approaches a delta-Dirac function.

- **Multichromophoric generalization (MC-FRET):** The original Förster theory only considered two molecules in the system. This is not the case in most photosystems, where light harvesting molecules can feel the electronic coupling of multiple molecules. Therefore it is added a sum over all the donors and a sum over all the acceptors in the Förster rate equation. This sum is only applied if the donors group is separated from the acceptors group so they have a clear distinction between them. The following equation represents the generalized Förster equation with diagonalized lineshapes:

$$k_F \approx \sum_j \sum_k \frac{J_{jk}^2}{2\pi\hbar^2} \int_{-\infty}^{+\infty} dw I_A^{kk}(w) L_D^{jj}(\infty, w) \quad (44)$$

If j and k represent the donor and acceptor molecule subscripts, this is a sum over the independent transfer rates of each pair where each exciton is completely localized at each molecule.

This equation can also be used for weak system-bath couplings in the exciton basis, where j and k represent delocalized excitons, i.e. superposition of excitations.

The Förster theory only allows an incoherent energy hopping between the molecules and at the multi-chromophoric generalization (MC-FRET), superposition of the excitation over several sites is allowed, but it is weak (due to the approximation of small J). If the inter-molecular coupling strength J has a medium or high value, then several molecules can feel the coupling and coherence can not be neglected, therefore one should adopt a different quantum theory formalism for coherent regimes.

2.3.2 Coherent EET

In this section, it will be explained how to formulate the Hamiltonians used in coherent EET. In this model, the resonance condition is still valid and a parameter called *reorganization energy* is introduced as the coupling of the environment with the system. In a more abstract

sense, the two couplings (molecule-molecule electronic coupling and system-environment coupling) compete with one another, and each one represents different dynamics. The system-environment coupling represents the *decoherence* process and the electronic coupling between molecules represents the isolated system dynamics. The review of coherent EET is adapted from [3].

To find the Hamiltonians which drive the coherent energy transport one considers a light-harvesting molecule m to have a restricted electronic spectrum composed by the ground state $|\Psi_{mg}\rangle$ and the first excited state $|\Psi_{me}\rangle$. At close proximity with another light-harvesting molecule, the excitation can be transferred to it. There is no orbital overlap, thus electrons can be completely assigned to one molecule or another. Then the Hamiltonian to describe EET in a system with N molecules is:

$$H_{EET} = \sum_{m=1}^N \sum_{a=g,e} H_{ma}(x) |\Psi_{ma}\rangle \langle \Psi_{ma}| + \sum_{m,n} \hbar J_{mn} |\Psi_{me}\rangle \langle \Psi_{mg}| \otimes |\Psi_{ng}\rangle \langle \Psi_{ne}| \quad (45)$$

where $H_{ma} = \epsilon_{ma}(x) + \text{nuclear kinetic energy}$, is the Hamiltonian describing the nuclear dynamics of an electronic state $|\Psi_{ma}\rangle$ where $\epsilon_{ma}(x)$ is the potential energy dependent of the nuclear coordinates x . The electronic coupling J_{nm} is also influenced by the nuclear dynamics, however it is considered to be very small [3]. Then, one can consider a state $[|m\rangle = |\Psi_{me}\rangle \prod_{k \neq m} |\Psi_{kg}\rangle]_{m=1, \dots, N}$ where each state $|m\rangle$ represents only one excited molecule in the entire system, as in the state representation used in Förster theory. Then the Hamiltonian is changed to:

$$H_{EET} = \sum_{m=1}^N \left[H_{me}(x) + \sum_{k \neq m} H_{kg}(x) \right] |m\rangle \langle m| + \sum_{m,n} J_{mn} |m\rangle \langle n| \quad (46)$$

Next, one defines the evolution of the environment and system-environment interaction. One considers the anharmonic motion is irrelevant to EET timescales [3] thus a normal mode treatment to the environment is employed. There are no large permanent dipoles in the molecule [3], thus the nuclear configurations are very similar in the ground and excited states. Then H_{mg} and H_{me} are modeled as a set of displaced harmonic oscillators:

$$H_{mg}(x) = \epsilon_{mg}(x_{mg}^0) + \sum_{\xi} \frac{\hbar \omega_{m\xi}}{2} (p_{m\xi}^2 + q_{m\xi}^2) \quad (47)$$

$$H_{me}(x) = H_{mg}(x) + \hbar \Omega_m - \sum_{\xi} \hbar \omega_{m\xi} d_{m\xi} q_{m\xi} \quad (48)$$

where x_{mg}^0 is the equilibrium configuration of the nuclear coordinates of the electronic ground state of the molecule m , $q_{m\xi}$ is the dimensionless normal mode coordinate with

frequency $w_{m\zeta}$ and momentum $p_{m\zeta}$ and $d_{m\zeta}$ is the dimensionless displacement between the minima of the ground and excited state's potential energy of the ζ phonon in the molecule m (sometimes called configurational coordinate). The last term in equation (48) describes the relaxation of the excited state caused by the accommodation of atomic nuclei's positions in the molecule, the Franck-Condon effect. One sets $\epsilon_{mg}(x_{mg}^0) = 0$ for convenience and the Franck-Condon transition energy is $\hbar\Omega_m = \epsilon_{me}(x_{mg}^0)$ which is also called site energy. After a vertical Franck-Condon transition, where the electronic transition is much faster than the nucleus motion, nucleus reorganization takes place from the ground state equilibrium coordinate x_{mg}^0 to the excited state equilibrium coordinate x_{me}^0 , thus the so called reorganization energy $\hbar\lambda = \epsilon_{me}(x_{mg}^0) - \epsilon_{me}(x_{me}^0)$ is dissipated. This energy can also be defined, site-dependently, as $\hbar\lambda_m = \sum_{\zeta} \hbar w_{m\zeta} d_{m\zeta}^2 / 2$ [24]. The reorganization process has a definite timescale defined by τ_B , which depends on the bath dynamics; see figure 4 for a simple illustrated example of the molecule-phonons dynamics previously described. The molecule passes to the vibrational excited state that contributes to the higher wavefunction overlap with the vibrational ground state the molecule is in before absorbing the photon.

The Hamiltonian defining EET can be then constructed as an electronic system (electronic degrees of freedom) coupled to a phonon bath (nuclear degrees of freedom) as:

$$H_{EET} = H_S + H_B + H_{SE} \quad (49)$$

where the first term is the electronic excitation Hamiltonian (system Hamiltonian) with respect to the equilibrium nuclear configuration of the ground state x_{mg}^0 :

$$H_S = \sum_m \hbar\Omega_m |m\rangle \langle m| + \sum_{m,n} J_{mn} |m\rangle \langle n| \quad (50)$$

The second term in equation (49) describes the environment. It is the normal mode Hamiltonian (or phonon Hamiltonian):

$$H_E = \sum_{\zeta} \frac{\hbar w_{\zeta}}{2} (p_{\zeta}^2 + q_{\zeta}^2) \quad (51)$$

The third Hamiltonian term describes the coupling between the nuclear motion and the electronic excitations (or between the system and the environment):

$$H_{SE} = \sum_m S_m V_m \quad (52)$$

where $S_m = |m\rangle \langle m|$ and $V_m = -\sum_{\zeta} \hbar w_{\zeta} d_{\zeta} q_{\zeta}$. Note that the definition of H_E and H_{SE} depend on the nuclear coordinates one chooses. One also supposes that the initial density matrix at $t = 0$, is in a factorized product $\rho(0) = \rho_S(0) \otimes \rho_E(0)$ and that the environment is in thermal equilibrium, thus it is initialized as $\rho_E(0) = e^{-\beta H_E} / \text{Tr}_E[e^{-\beta H_E}]$. This factorized

initial condition is in accordance with the definition of the electronic states in a vertical Franck-Condon transition, i.e. the transition is much faster than the nuclear motion, thus the transition is not correlated with the nucleus dynamics.

Note that in Redfield equations, one uses these Hamiltonians in the second quantization formalism, where $S_l = S_m$ and $g_{l,\xi} = d_{m,\xi}$ in equation (16). Therefore, in the weak system-bath coupling regime, the Redfield equations describe the dynamics of the coherent EET in a perturbative approximation.

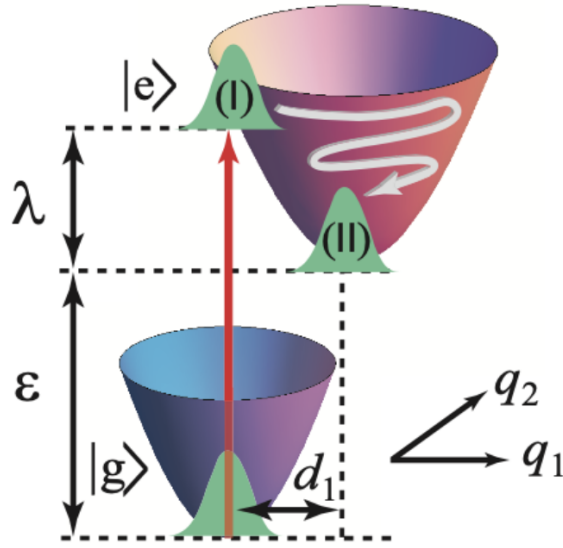


Figure 4: Molecular states' dynamics with two dissipative vibrational normal modes w_1 and w_2 (two dimensional coordinate system). (I) is the vertical Franck-Condon transition followed by the reorganization dynamics (II), which dissipate the reorganization energy λ ($\hbar = 1$). $\epsilon + \lambda$ is the site energy of the molecule. d_j is the equilibrium displacement for each normal mode j and q_j is the coordinate of each normal mode j . The model of the bath as a set of displaced harmonic oscillators induces a potential energy, in function of the displacement, in the form of a parabola. Image taken from [24].

The model described in this section is the one used to model the energy transport in photosynthesis. The Hamiltonians derived in this subsection as well as the defined environment can be used in quantum master equations beyond the weak system-bath coupling and Markovian baths, to calculate the evolution of the energy transport in photosynthesis.

2.3.3 Differences between Förster theory and coherent EET

In this section, some differences between the Förster theory and coherent EET will be presented. The electronic coupling between molecules and the reorganization energy essentially define the regime in which the energy transfer occur. Experimentally, the

inter-molecular coupling J is usually in the interval $[0.5, 500] \text{ cm}^{-1}$ and the reorganization energy is typically in the interval $[50, 100] \text{ cm}^{-1}$ [4]. Two different perturbative formalisms have derived two different theories (Förster theory and Redfield theory). If the electronic coupling between molecules J is small in comparison to the system-bath coupling, which is characterized by the reorganization energy λ , the Förster regime is present (incoherent transport). If the system-bath coupling is small it is possible to derive a quantum master equation by the Redfield theory which treats this coupling perturbatively. Just as the parameters J and λ are important, the timescale of the relaxation to the nucleus equilibrium position induced by the bath, τ_B , and the timescale of the inter-molecular energy transfer with no additional perturbations, J^{-1} , also are [3]. When² $\tau_B \ll J^{-1}$ coherence is not allowed over multiple molecules. The nuclear reorganization introduces fast dephasing in the system and the energy transfer only occurs after the nuclear reorganization. In this case, diffusive dynamics appear, where coherence (quantum beating) is not present thus one can use the energy transfer rate equation provided by the Förster theory, i.e. this is the Förster regime [3]. If $\tau_B \gg J^{-1}$, the energy is transferred over several molecules with no perturbation of the environment (nucleus relaxation). Thus coherent energy transfer is allowed and the evolution of the excitation transfer is given by wave packets traveling across the molecules keeping its phase coherence, i.e. very small dephasing rates are present because the energy transfer dynamics occur at timescales much smaller than the reorganization timescale [3]. In the coherent EET regime, the Förster energy transfer rate law fails, and one must use other quantum theories, as the previously overviewed Redfield theory, for small system-bath couplings.

Nowadays, coherent energy transport is mostly believed to drive the energy transfer faster than the (incoherent) Förster theory [4, 16, 25]. Quantum beating makes the populations oscillate, which can yield a momentarily higher probability to the acceptor molecule be excited than simple diffusive dynamics, which is the typical system's behaviour of incoherent energy transport. However a full coherent energy transport is not desired for reasons will be discussed in the section 2.3.5 and dephasing can help to enhance the energy transfer. Therefore, the two limits, Förster and Redfield theories, do not allow the fastest energy transport. When $\tau_B \sim J^{-1}$, i.e. the intermediate (fastest energy transport) regime at which energy transfer in photosynthesis usually occurs, perturbative and Markovian methods fail to give an appropriate answer, thus one needs to introduce other quantum theory formalisms.

² J is usually measured in spectroscopic units of frequency, cm^{-1} .

2.3.4 *Other approaches to the energy transport*

Other theories to explain the dynamics of energy transport exist [4, 3] such as the Hierarchical Equation of Motion (HEOM), which is based on exact numerical calculations, Polaron Transformation Redfield Theory (PTRT), etc. They are briefly discussed below [26, 3].

The PTRT approach can give answers beyond the weak system-bath coupling as a second order perturbation approach to the system-bath interaction, that accounts for non-Markovian effects [3]. This approach consists of applying a unitary transformation to the Hamiltonian, so that a quantum master equation in the moderate system-bath coupling is constructed. A second order approximation with respect to the system-bath couplings is used which can indeed be treated perturbatively and still ensuring good results in the limit of strong system-bath couplings of the original Hamiltonian [3]. Using super-ohmic spectral densities, the polaron transformation approach can be used in the intermediate regimes, in which neither Förster theory or the Redfield theory can give the correct results. For other types of environment one can use the variational polaron transformation which is derived in [26].

HEOM is derived in a non-Markovian context and applies to all the system-bath coupling regimes. It is a powerful technique because it is derived in a non-perturbative way and has an exact formalism with no approximations. It can give answers about site-dependent reorganization dynamics as well as an appropriate description of Gaussian fluctuations in the electronic energies to produce the lineshapes used in Förster theory. Thus, all regimes can be described by this theory. The downside of using it is that it suffers from heavy numerical calculations of the system density matrix because it needs to solve a high number of coupled differential equations [27].

Figure 5 shows the different existent theories currently used in order to derive a description of the energy transport.

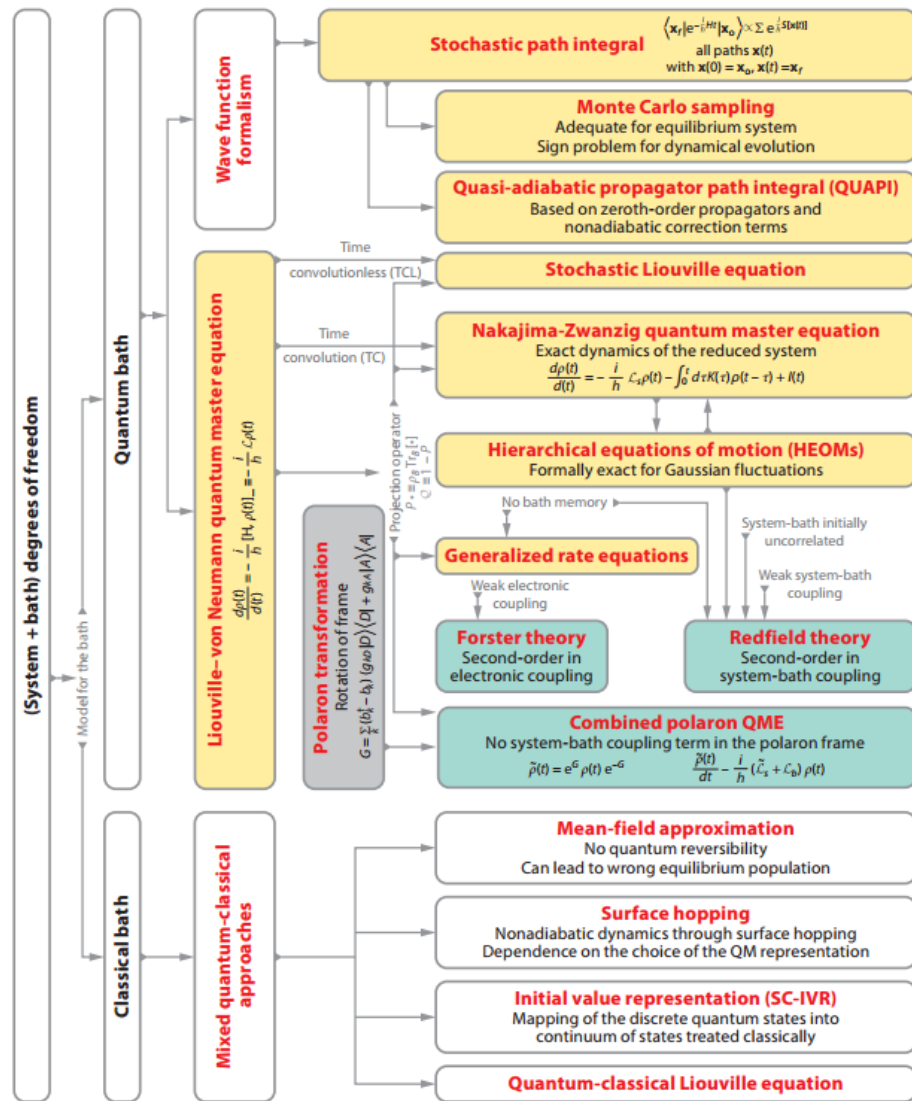


Figure 5: Summary of the approaches to the energy transport in photosynthesis. Image taken from [4].

2.3.5 The role of decoherence in coherent EET

For a chain of *light-harvesting* molecules in which the last one is the reaction centre where energy is trapped, it can be shown that the transport of energy throughout the chain is more efficient when it is coherent [4]. Therefore, coherence increases the probability of the excitation being found in the reaction centre [25]. However, the action of the *dephasing* processes, caused by the environment in realistic conditions, progressively eliminates the coherence (off-diagonal) elements in the system's density matrix, causing the oscillation amplitude to decay (*quantum beating suppression*). It eventually turns the diagonal matrix

elements (populations) into (non-correlated) classical probabilities, a process known as thermal relaxation, for which the existence of coherence in a system is time limited.

For the relevant mathematical formalism, let us consider the system Hamiltonian:

$$H_S = \sum_m \epsilon_m |m\rangle \langle m| + \sum_{m \neq n} J_{mn} |m\rangle \langle n| \quad (53)$$

where ϵ_m corresponds to each site energy m (site basis) and J_{mn} is the electronic coupling (e.g. Förster coupling) between the states. One can employ the Haken–Ströbl pure-dephasing model [28] where only dephasing is introduced in the system, making it to loose the phase coherence as time elapses [29].

Using Lindblad equation to model the system and its interaction with the environment [28],

$$\frac{d\rho}{dt} = \mathcal{L}[\rho] = -i[H_S, \rho] + \gamma \sum_m (L_m \rho(t) L_m^\dagger - \frac{1}{2} \rho(t) L_m^\dagger L_m - \frac{1}{2} L_m^\dagger L_m \rho(t)) \quad (54)$$

where $L_m = |m\rangle \langle m|$ and γ is the dephasing rate. This equation corresponds to the high temperature limit [13, 29]. One wants to find the energy transfer efficiency when the system is subjected to different dephasing rates. To account for exciton recombination and exciton trapping, the system Hamiltonian is changed to $H_S - iH_{trapp} - iH_{recomb}$ where $H_{trapp} = \sum_m \kappa_m |m\rangle \langle m|$ and $H_{recomb} = \Gamma \sum_m |m\rangle \langle m|$ [29]. κ_m is the trapping rate of the excitation and Γ is the exciton recombination rate assumed independent of m (i.e. it represents the lifetime of an excitation, which is usually very long in comparison with the energy transfer dynamics).

The probability of the exciton being captured at site m in the time interval $[t, t + dt]$ is $2\kappa_m \langle m | \rho(t) | m \rangle dt$ so the transport efficiency within an interval $[0, t]$, for a set of M energy trapping sites is [29]:

$$\eta(t) = 2 \sum_{m=1}^M \kappa_m \int_0^t ds \langle m | \rho(s) | m \rangle \quad (55)$$

For a two site system, the optimal dephasing rate for an optimal noise assisted transport is found to be, using equation (55) [3]:

$$\gamma_{opt} = \frac{|E|}{\hbar} - \kappa - 2\Gamma \quad (56)$$

The energy gap $E = \epsilon_0 - \epsilon_1$ is matched by the dephasing, trapping and exciton recombination rates [3]. Thus, a non-resonant system can achieve resonance with the help of dephasing.

At a more abstract physical point of view, it can be explained how dephasing can enhance the energy transfer in coherent EET, as well. Firstly, it yields random fluctuations in the

energy spectrum of each molecule, which can bridge the energy gap between the molecules, momentarily turning a non resonant system into a resonant one [3]. This process is illustrated in figure 6.

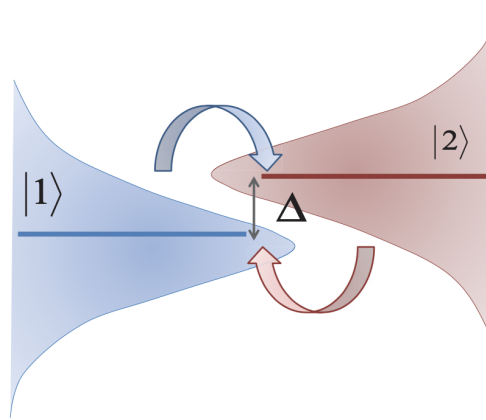


Figure 6: The molecule excited states $|1\rangle$ and $|2\rangle$ fluctuate, eventually having their energy gap $\Delta = 0$. The lineshape functions, in light-blue and light-red, establish the type of fluctuations present in each molecule. Image taken from [3].

Secondly, *dephasing* can also help avoiding the existence of *coherence traps*, a kind of *deadlocks* in energy transport. In system with a deviation from the linear chain of molecules, antisymmetric superposition excited states that can eventually form in the middle of the structure can block the energy transfer [3]. Dephasing can destroy the superposition, thus removing such a *coherent trap*.

However, very low or very high dephasing rates can bring undesired effects to the energy transfer process, the latter diminishing the transfer probability and leading, as the limiting case, to a *static, non-evolving* system (so called quantum Zeno regime) [29].

One can observe now, that a coherent energy transport can enhance the energy transport, although a complete coherent energy transfer is also undesired. Coherent traps can block the energy transfer and in non-resonant molecules, even coherent energy transport alone, can not enhance the energy transfer because the energy gap is too high. Thus, dephasing can destroy coherence and induce fluctuations in the site energies which help the molecules overcome the energy barrier. These effects are desired to enhance the energy transfer, but note that this enhancing requires only an appropriate (intermediate) degree of dephasing.

2.4 QUANTUM SIMULATION

Quantum systems can be simulated through quantum analog simulation or quantum digital simulation. The former consists of simulating a physical system with other physical system.

The later consists of simulating the physical system in a quantum computer as a digital simulation. Different methods to simulate a temporal evolution are next presented.

2.4.1 Isolated quantum systems simulation

One starts by defining the initial state of the isolated system and then implements the evolution operator for a time-independent Hamiltonian H as

$$U(t) = e^{-iHt} \quad (57)$$

This operator is unitary. Simulating several system dynamics, multiple Hamiltonians can be used, thus $H = \sum_j H_j$. If the Hamiltonians commute with each others then

$$U(t) = e^{-i\sum_j H_j t} = \prod_j e^{-iH_j t} \quad (58)$$

The unitary evolution, in a quantum circuit, is done by applying the evolution operators of each Hamiltonian in sequence. If the Hamiltonians do not commute, an approximation to the unitary evolution operator must be implemented. There are several different methods with minimum computational resources such as Trotter formula based algorithms, the truncated Taylor series algorithm and the qubitization algorithm. These methods, except the last one, are briefly explained below.

Trotter formula based methods

Trotter product formula [30] is:

$$e^{-iHt} \approx \left[\prod_j e^{-iH_j \frac{t}{N}} \right]^N \quad (59)$$

where N is the number of iterations. It is bounded by an error $\epsilon = \mathcal{O}(\Delta t^2/N)$. The number of iterations required to achieve results within a given error is $N = \mathcal{O}(\Delta t^2/\epsilon)$ [30]. The former equation gives the scaling of the number of times that the approximated unitary operator must be implemented to simulate a system with an error ϵ . This scaling is also called the *query complexity*.

To generate an approximated unitary evolution, the first order Lie-Trotter-Suzuki formula [30] can be used, defined for a sum of m Hamiltonians H_j , as

$$\tilde{U}_1(\Delta t) = \left(\prod_{j=1}^m e^{-iH_j \frac{\Delta t}{2}} \right) \left(\prod_{j=m}^1 e^{-iH_j \frac{\Delta t}{2}} \right) \quad (60)$$

Higher order versions of this formula are obtained by employing the Suzuki recursive method [30]. The approximated error for a k th order formula is at most proportional to $\mathcal{O}(\Delta t^{2k+1})$ [30]. Applying a repetition of k th order unitary operators \tilde{U}_k , where each one evolves for an arbitrary time Δt , the query complexity gets $\mathcal{O}(\Delta t^{1+\frac{1}{2k}}/\epsilon^{\frac{1}{2k}})$ [31]. Note that using very high orders is disadvantageous because the number of terms, i.e. the number of gates, increases exponentially [30].

Truncated Taylor series method

In short, this method consists of expanding the evolution operator (57) in a (truncated) Taylor series [32] for a sum of time-independent Hamiltonians $H = \sum_{j=0}^L \alpha_j H_j$ where H_j is unitary and does not commute with other Hamiltonians, such that

$$e^{-iHt/r} \approx \sum_{k=0}^K \sum_{j_1, \dots, j_k=1}^L \frac{(-it/r)^k}{k!} \alpha_{j_1} \dots \alpha_{j_k} H_{j_1} \dots H_{j_k} \quad (61)$$

where r is the number of iterations needed to simulate the system at a time t . Then consider

$$e^{-iHt/r} \approx \tilde{U} = \sum_{l=0}^{m-1} \beta_l V_l \quad (62)$$

where the unitary operator $V_l = (-i)^k H_{j_1} \dots H_{j_k}$ and $\beta_l = \beta_{k, j_1, \dots, j_k} = \frac{(t/r)^k}{k!} \alpha_{j_1} \dots \alpha_{j_k}$. The previous sum is not exactly unitary due to the truncated series, so it is bounded by an error. Consider now an operator B applied to an ancilla state $|0\rangle$ such that

$$B|0\rangle = \frac{1}{\sqrt{s}} \sum_{l=0}^{m-1} \sqrt{\beta_l} |l\rangle \quad (63)$$

where $s = \sum_{l=0}^{m-1} \beta_l$. Next, it is defined an operator which selects the V_l operator to be applied to the system state $|\Psi\rangle$ with the help of the ancilla state as

$$(\text{select } V) |l\rangle |\Psi\rangle = |l\rangle V_l |\Psi\rangle \quad (64)$$

Defining an operator $W = (B_{anc}^\dagger \otimes I_S)(\text{select } V)(B_{anc} \otimes I_S)$ and applying it at the initial ancilla plus system state

$$W|0\rangle |\Psi\rangle = \frac{1}{s} |0\rangle \tilde{U} |\Psi\rangle + \sqrt{1 - \frac{1}{s^2}} |\Phi\rangle \quad (65)$$

where $|\Phi\rangle$ is an ancillary state orthogonal to the initial state $|0\rangle$ of the ancilla subspace. Applying oblivious amplitude amplification, i.e. applying an operator $A = -WRW^\dagger RW$, where $R = (I - 2|0\rangle\langle 0|)_{anc} \otimes I_S$, results in

$$A|0\rangle|\Psi\rangle = |0\rangle\tilde{U}|\Psi\rangle \quad (66)$$

Time-dependent Hamiltonians can also be simulated using a similar approach [32]. For a time-independent Hamiltonian H , a simulation with an error ϵ can be obtained by applying a truncated K th order Taylor series (query complexity), where the order is given by

$$K = \mathcal{O}\left(\frac{\log(T/\epsilon)}{\log\log(T/\epsilon)}\right) \quad (67)$$

where $T = (\alpha_1 + \dots + \alpha_L)t$ and $T/r = \ln(2)$ or if T is not a multiple of $\ln(2)$ then set $r = \lceil T/\ln(2) \rceil$ [32]. In this algorithm, an additional $\mathcal{O}(\log(L) \frac{\log(T/\epsilon)}{\log\log(T/\epsilon)})$ ancilla qubits are required and the operator B can be constructed with $\mathcal{O}(\log(L) \frac{\log(T/\epsilon)}{\log\log(T/\epsilon)})$ single qubit and CNOT gates. A detailed description of this algorithm can be found in [32].

Qubitization

Another simulation method with some similarities with the former, is the recently developed qubitization algorithm using quantum signal processing [33], which achieves a query complexity of $\mathcal{O}(\alpha t + \frac{\log(1/\epsilon)}{\log\log(1/\epsilon)})$, with $\alpha = \sum_{j=0}^L \alpha_j$. This method will not be discussed here but a description can be found in [33, 34].

2.4.2 *Open quantum systems simulation*

The energy transport in photosynthesis may include an environment interacting with the system. Hence, the open quantum system formalism may be used. Quantum algorithms which simulate such systems are still underdeveloped and there are only a few of them generally applied to any system. The process of irreversibility and non-unitarity of open systems when temporal evolution is simulated presents an obstacle because quantum gates must be reversible and unitary. Also if quantum open systems need to be simulated, the open system evolution can not be the only system one is interested in, as in isolated systems, because there is an environment which must also be simulated. In this context, a few open quantum system simulation algorithms have been already developed. Among them, we mention Kraus operators based algorithms [11, 35] and an algorithm which defines a qubit model of an environment, i.e. the Hilbert space of the overall system is dilated to include the environment Hilbert space, and its interactions with the system [36]. The latter algorithm was initially implemented, although discarded at an advanced state of the work.

Its model and implementation, as well as some comments, are explained in Appendix B. A different algorithm can be used to simulate pure-dephasing system-environment interaction dynamics, which was the one implemented in this work. It consists in applying random energy fluctuations in the system, thus creating a dephasing effect. This simulation method will not be explained in this section, but in the next.

Kraus operators based simulation

Kraus operators are density matrix maps that transform the system's density matrix at an initial time into another at a chosen final time t . The first step to simulate a open quantum system, through this method, is to calculate the Kraus operators (9) (for instance, using the evolution operator). Therefore the Hamiltonians of the system, the environment and the system-environment interaction must be known.

In simple systems and environments calculating the Kraus operators can be a rather easy task, they can be expressed through simple phase damping or amplitude damping operators applied to the system [11]. An exponential decay of a population term or a decay of the coherence terms is observed, a characteristic result of Markovian environments [13]. If these (Markovian) operators describe the dynamics of the system then the set of Kraus operators can be easily translated into a simple quantum circuit such as the ones described in [11]. Usually, open quantum systems are not so simple and the explicit evolution operator of the system, environment and their interaction is required. In such cases, these operators can have complex forms and their translation to quantum circuits can be done by the recently developed algorithm [35].

In this algorithm, the application of the Kraus operators is done by augmenting the Hilbert space of the system, adding an ancilla Hilbert space. Each Kraus operator E_k is then converted to a unitary operator U_k which is applied to the ancilla and system Hilbert space using a minimal Hilbert space dilation, i.e. using the minimum number of ancilla qubits. This is possible by making use of the *Sz.-Nagy theorem* [35]. Then the evolution of the system's density matrix modeled as

$$\rho_S(t) = \sum_k^m E_k \rho_S(0) E_k \quad (68)$$

is converted to

$$\rho_S(t) = \sum_k^m U_k (\rho_S(0) \otimes \rho_{anc}) U_k \quad (69)$$

where each U_k is computed separately, i.e. the evolution of the system's density matrix is given by m different quantum circuits, each with a different U_k . The population terms can be found by projection measurements, where the system's density matrix is assembled after all the measurements are over, i.e. $\rho_S(t) = \sum_{i,k} p_{i,k}(t) |\Phi_{i,k}\rangle \langle \Phi_{i,k}|$, where $\rho_S(0) =$

$\sum_i p_i(0) |\Psi_i\rangle \langle \Psi_i|$ is defined to be the initial state of the system. The coherence terms of the density matrix can be found by quantum state tomography [35, 11].

2.5 SUMMARY

The structure of photosynthetic systems, as well as their energy transport dynamics have been discussed in this chapter. Some of the open quantum systems theory approaches have been reviewed as well as their application to the most currently used models to explain the different regimes of energy transport. On the other hand, decoherence, injected by the environment into the system, was shown to produce undesired effects on the energy transfer as well as enhancing effects if taken at an appropriate rate. Finally, an introduction has been given to current quantum algorithms used to simulate the temporal evolution of a system. Among these, the open quantum systems simulation methods are particularly important in to work.

DEVELOPMENT

The focus in this chapter will be the model and the algorithmic theory used in the photosynthetic energy transport simulation.

This chapter is divided in the decisions taken to develop an algorithm followed by the explanation of its implementation. Then the computational resources of the proposed algorithm will be evaluated. Finally, possible optimizations of the quantum circuit will be discussed.

3.1 DECISIONS

The approach consisted firstly in the simulation of the energy transport in photosynthesis, considering a light-harvesting system as isolated, i.e. without decoherence. In this approach, it was used a simple Hamiltonian, the one described by equation (50), accounting only for the unitary system evolution. The second stage of this work consisted in injecting artificial decoherence in the previous isolated system, making it an open quantum system.

This section begins with a brief explanation of the methods used to synthesize a quantum circuit to implement the no decoherence model simulation. Then, the artificial decoherence simulation methods considered to simulate a real open quantum system will be presented. The section ends with the explanation of the qubit model used in the simulation.

3.1.1 *Quantum circuit synthesis*

To implement the evolution operator of the system Hamiltonian, diagonalization of it was required, so the software Mathematica was used. From a simple program, the eigenvalues and the unitary basis transformation matrices were found. Finding the quantum circuit that is equivalent to the diagonalized evolution operator of the system Hamiltonian is trivial. But modelling the basis transformation matrices, required for the simulation, into a quantum circuit is not so simple. A rotation decomposition algorithm based in [11, 37] was used. A first approach was to implement this algorithm using Matlab, with the code given by [37].

This algorithm did not result in the decomposition of two-level unitary matrices that were required to implement the basis transformation operators. The last two-level matrix to be calculated was not unitary, therefore it can not be applied in a quantum circuit. Due to this problem, this code, in [37], was not used for the basis transformation operator synthesis.

Another possible way to decompose an unitary matrix is to use the exact circuit synthesis [38]. However, this algorithm could not be used because the elements of the basis transformation matrices do not belong to the ring $\mathbb{Z}[\frac{1}{\sqrt{2}}, i]$ which means that the elements were not in the form $\frac{1}{2^n}(a + bi + c\sqrt{2} + id\sqrt{2})$ where $n \in \mathbb{N}$ and $a, b, c, d \in \mathbb{Z}$.

The approach adopted consisted of using the language Haskell with the Quipper library to transform an unitary basis transformation matrix in the multiplication of one-level and two-level unitary matrices. After this process, Gray code [11] was used to find the gates needed to implement the sequence of one-level and two-level unitary matrices in a quantum circuit. This was the option chosen to decompose the basis transformation matrices in quantum gates and discussed in detail in the Appendix A.

3.1.2 Artificial decoherence simulation methods

Three algorithms were initially proposed to model the artificial decoherence injection in the system which can be found, in detail, in [35, 36]. At the end of the decision process, it remained one algorithm that was implemented, i.e. two algorithms were discarded. The main differences between the three algorithms are presented below, in order to explain the decisions taken.

Dilation of the system Hilbert space

The first algorithm as proposed in [36] was not implemented in this work. It consists of maintaining the system Hamiltonian (50) and adding a bath (a dilated Hilbert space of the system) which evolves with its bath Hamiltonian (15) and interacts with the system via the interaction Hamiltonian (16). In this algorithm, there are environment qubits in thermal equilibrium and the system's qubits. The algorithm was discarded in the course of work, therefore its model and quantum circuit implementation are described in the Appendix B as well as some comments about what went wrong with it. Essentially, the bath model defined in [36] is not a convenient description for the simulation of any open quantum system dynamics such as the one of light-harvesting systems in photosynthesis and it unfolded some wrong physical assumptions described in Appendix B. Therefore, it was concluded that simulating photosynthesis with this algorithm was not the best path to follow.

Kraus operators

The second algorithm that was also discarded consisted of using the evolution operator to formulate the Kraus operators. Therefore, the system Hamiltonian (50) was kept, the environment Hamiltonian H_E was the one formulated in equation (15) and the interaction Hamiltonian H_{SE} was described by equation (16). To formulate Kraus operators, one needs to employ equation (9) where $\sqrt{p_m} |m\rangle$ is the initial environment state and $|k\rangle$ is the chosen final environment state. Thus, considering the final environment state to be a normal mode $|k\rangle = |w_k\rangle$ and the initial environment state to be a normal mode in thermal equilibrium, i.e. using $\hbar = 1$, one gets $\sqrt{p_m} |m\rangle = \sqrt{\frac{e^{-\beta E_k}}{Z}} |w_k\rangle$ where w_k is a normal mode of the environment, $\beta = \frac{1}{k_B T}$, $E_k = [n_k + \frac{1}{2}]w_k$ denotes the energy eigenvalue of the environment energy eigenstate (n_k is the number of excitations of the normal mode w_k , which at thermal equilibrium can be given by the Bose-Einstein statistics) and Z is the partition function of the bath. U is the unitary evolution operator applied to the environment and the system defined as

$$U(t) = e^{-i(H_S + H_E + H_{SE})t} \quad (70)$$

An effort has been made to calculate the Kraus operators with a similar approach to Ramsey-like dynamics in photosynthesis, as the one employed in the supplementary information section of [39] but these operators have not been found. As an alternative, it was thought to use a generalized amplitude damping Kraus operator [11], i.e. a thermal relaxation operator, and a phase damping Kraus operator as the ones derived in [11]. However, using these kind of operators can underestimate the role of decoherence in the system, where the only controllable environment parameters are the dephasing rate and the final state of the system, i.e. the thermal equilibrium state (controlled by the thermal relaxation operator). Employing a set of Kraus operators with thermal relaxation can also have a complex form, therefore it can be difficult to employ such operators in a quantum circuit.

Another issue arises if the Hamiltonians in the evolution operator do not commute. If this is the case, the Trotter product formula (59) can be used to separate the Hamiltonians in different exponentials, which requires a time segmentation. However, in the Kraus operator formulation one needs always to start from a defined initial environment state $|m\rangle$ and end in a definite environment end state $|k\rangle$. Therefore to apply the Kraus operators to a system density matrix at any time, one has to make sure that the environment state is always the same, $|m\rangle$, before the operator application. Using the Trotter product formula, the use of several iterations of the evolution operator is required. Hence, to employ these Kraus operators, it is required a Markovian approximation, where the environment state must be reset to its initial state at each iteration (forgetting the system-environment correlations created in the previous iterations). If a Markovian approximation can indeed be made, then using the algorithm in [35] explained in the subsection 2.4.2, each Kraus operator must be

computed in a different quantum circuit. This is computationally quite costly, because each quantum circuit defining a Kraus operator must be applied at each iteration. If K Kraus operators and N iterations are considered, then to simulate a system at a time $t = N\Delta t$, it would require K^N quantum circuits to perform the simulation!

This algorithm was discarded because if the Hamiltonians do not commute, which is the case for the photosynthesis dynamics (the Hamiltonians (16) and (50) do not commute), then the simulation becomes practically unfeasible. Another reason is that Kraus operators have also not been found. The option of using simpler Kraus operators which commute with the system Hamiltonian (50), such as thermal relaxation and dephasing operators, can underestimate the role of decoherence in the system's dynamics. For instance, not having an explicit system-environment coupling can cause a poor definition of the decoherence effects in the transport regimes, such as in the coherent EET and Förster regimes.

Implementing decoherence as a closed system

Following a proposal in [36], the third algorithm considered was implemented as a pure-dephasing model (which should be physically relevant at high temperatures). It consists of keeping the system Hamiltonian and adding a perturbation, which is defined by random fluctuations in the site energies of the molecules. This interaction does not need to originate from an external Hilbert space (as a bath) and can be implemented as a closed system. This algorithm is simple enough to give appropriate dynamics of the energy transport, even only containing pure dephasing. It is not heavy in computational resources and it is an algorithm which is "flexible" in the implementation whether the perturbation commutes or not with the system Hamiltonian. An important aspect of this algorithm is that it can model some types of Markovian environments, i.e. different types of spectral densities, and it can simulate coherent EET (it fails in the Förster regime).

This is also the algorithm which requires less quantum computational resources, specially in the number of qubits, which is a consequence of the non-dilation of the system's Hilbert space. The implementation of this algorithm is described, in detail, in the next section.

3.1.3 *The system's qubit model*

The model implemented in all the simulations consisted in considering each state of the qubits $|m\rangle = |q_1\rangle \otimes \dots \otimes |q_k\rangle$ to be the representation of an excited state of a molecule (and all other molecules in the ground state) in the computational basis, where 2^k denotes the dimension of the system's Hilbert space. The initial state prepared for most of the simulations was chosen as $|m\rangle = |0_1\rangle \otimes \dots \otimes |0_k\rangle$, i.e. the first molecule is excited. Each state denotes an excited state of a different molecule, thus a superposition of the qubit states is a superposition of excited molecules. This is the model for a system with no interaction with

the environment, introduced in the subsection 2.3.2. In this work, it was considered that the set of molecules represents a *chain* of molecules. Therefore, no other quantum effects derived from other geometries, such as *coherent traps*, will be present.

The molecule representation was chosen in order to perform a scalable quantum simulation. If each qubit would represent a molecule with states $|0\rangle$ and $|1\rangle$ for the ground state and the excited state respectively, a quantum simulation of a real system would require 200 – 300 qubits, so that the 200 – 300 molecules of a real photosystem can be represented. In the chosen representation where each system state is an excited molecule state, one would require 8 – 9 qubits for a real quantum simulation of a photosystem ($2^8 - 2^9$ light-harvesting molecules). A real quantum simulation of energy transport in photosynthesis in this chosen model can already be achieved with current available quantum computers *at least in terms of qubit resources*.

3.2 IMPLEMENTATION

3.2.1 Isolated system (no decoherence)

The first stage is to implement the isolated system's evolution as previously explained. The considered system Hamiltonian is described by equation (53). This Hamiltonian is in accordance with the modelled system Hamiltonian in several simulations as [24, 39, 3] and it is described in detail, in subsection 2.3.2. It has been considered that the spontaneous decay of the excited state occurs at very long times relatively to the energy transport timescale [3].

The Hamiltonian, in matrix form, for four molecules reads

$$H_S = \begin{pmatrix} \epsilon_1 & J_{12} & J_{13} & J_{14} \\ J_{21} & \epsilon_2 & J_{23} & J_{24} \\ J_{31} & J_{32} & \epsilon_3 & J_{34} \\ J_{41} & J_{42} & J_{43} & \epsilon_4 \end{pmatrix} \quad (71)$$

The temporal evolution is the process one wants to simulate, thus the unitary evolution operator needs to be applied ($\hbar = 1$)

$$U(t) = e^{-iH_S t} \quad (72)$$

After applying the unitary operator, for each time t , the system's qubit states at the site basis are measured.

Isolated system quantum circuit implementation

To find the evolution operator in matrix form (assume from now on, a four molecule system), diagonalization of the Hamiltonian is used, so that

$$H_S = T^\dagger H_{S-diag} T \quad (73)$$

where T is the basis transformation matrix with dimensions 4×4 which changes the site basis to the energy eigenbasis. H_{S-diag} is the diagonal Hamiltonian. This way,

$$e^{-iH_S t} = T^\dagger e^{-iH_{S-diag} t} T \quad (74)$$

After finding the basis transformation matrices, a rotation decomposition algorithm is employed [11]. The process of decomposing the basis transformation matrices in quantum gates is described in the Appendix A.

Knowing how to apply the basis transformation matrix T and its conjugate T^\dagger in a quantum circuit, one can apply the operator $e^{-iH_{S-diag} t}$ in the energy eigenbasis as

$$\begin{pmatrix} e^{-iE_1 t} & 0 & 0 & 0 \\ 0 & e^{-iE_2 t} & 0 & 0 \\ 0 & 0 & e^{-iE_3 t} & 0 \\ 0 & 0 & 0 & e^{-iE_4 t} \end{pmatrix} \quad (75)$$

The Hamiltonians are usually given in units cm^{-1} , so a conversion is performed to $rad.THz$, which can be straightforwardly done by the application of the following formula: $E'_j = 2\pi c E_j$, where $c \approx 0.029972 \text{ cm.ps}^{-1}$ is the speed of light in vacuum.

To implement the operator (75) in a quantum circuit, a gate $C^2R_Z(\theta)$ is applied with controls at the system's qubits and target at an ancilla qubit initialized at $|1\rangle$. The gate $C^2R_Z(\theta)$ can only be applied if the energy system eigenstate $|E'_j\rangle$ can be specifically selected, where $\theta = -2E'_j t$ (The coefficient 2 comes from the Qiskit implementation of the gate $R_Z(\phi)$ which is $e^{-i\frac{\theta}{2}\hat{Z}}$). To select the eigenstates, X -Pauli gates are used. This process can be applied in sequence to all the energy eigenstates as demonstrated in the following equation (76) and illustrated in the figure 7.

The unitary evolution is then modelled as

$$U(t) = e^{-iH_S t} = T^\dagger \left[\prod_{j=1}^4 e^{-iE'_j t} \right] T \quad (76)$$

where j is the subscript denoting each energy eigenstate.

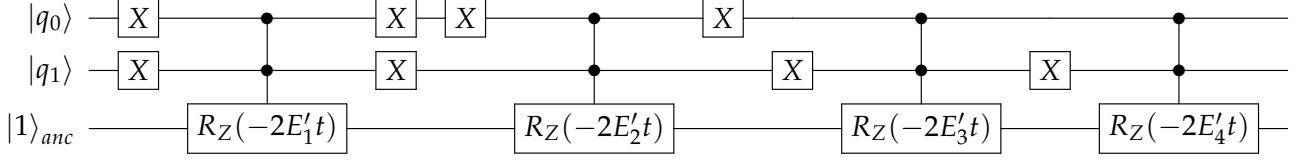


Figure 7: Implementation of the diagonal Hamiltonian evolution operator. $|1\rangle_{anc}$ is the ancilla qubit initialized at $|1\rangle$. $|q_i\rangle$ is the system's qubit state *in the energy eigenbasis*.

At the end of the quantum circuit (after applying T^\dagger), a measurement in each of the two system's qubits is performed. This way, the population terms of the system's density matrix can be known.

For a two molecule system (one qubit representing the system), the algorithm of the basis transformation decomposition given in the Appendix A does not need to be employed, because usually the basis transformation matrices are simple $T = R_Y(\theta)$ and $T^\dagger = R_Y(-\theta)$.

3.2.2 Artificial decoherence injection

System with decoherence model

It has been followed an approach to implement artificial decoherence as pure-dephasing, by taking into account Markovian fluctuations, which constitutes a good approximation in a *high-temperature* regime [40, 29, 13]. The actual algorithm that has been used is the one of [36], a quantum algorithm that simulates open quantum systems, with pure-dephasing, modeling the action of the decoherence as classical (Gaussian) random fluctuations (a telegraph-type classical noise affecting the system). The actual Hamiltonian of this system, reads as

$$H = H_S + H_F \quad (77)$$

and it consists of the system Hamiltonian H_S explained above, under the perturbation of a *bi-stable fluctuator environment*, H_F , i.e. sets of *fluctuators* representing the environment (at thermal equilibrium) which inject random energy fluctuations in a molecule. These objects switch between two values, $\pm g/2$, at a given fixed rate γ , where g is the fluctuation strength (or coupling strength to a molecule). Physically, the action of the fluctuations is typically stronger in the excited state energies than in the couplings between the molecules [40, 41], thus we resorted to the approximation that the fluctuations are only applied to the molecule excited states. In addition, we approximate the environment to be modeled by independent and identical sets of fluctuators with no interaction of any sort between them, as supported by [42], so that each set of fluctuators only affects the energy of a single molecule excited state (a diagonal term of the system's density matrix in the site basis).

The random fluctuations applied to a two molecule system are illustrated in figure 8. The fluctuator interaction Hamiltonian \hat{H}_F , can be defined following [36], as

$$H_F(t) = \sum_m \chi_m(t) A_m \quad (78)$$

where A_m is the *projection operator* $|m\rangle \langle m|$, and $\chi_m(t)$ is the *action* of a set of fluctuators on the molecule m . The action, for one fluctuator per set, is defined as follows

$$\chi_m(t) = g_m \xi_m(t) \quad (79)$$

where g_m is the fluctuation strength (or coupling strength of the fluctuator with the molecule m) and the function $\xi_m(t)$ is the generator of the random fluctuations, which switches between values $-1/2$ and $1/2$ at a rate γ_m . This type of action can, obviously, be generalized to a higher number of uncorrelated fluctuators per set

$$\chi_m(t) = \sum_j g_{jm} \xi_{jm}(t) \quad (80)$$

where g_{jm} is the coupling strength between the fluctuator j and the molecule m .

The random fluctuations have been generated with a classical algorithm. To generate the functions $\xi_m(t)$, it can be used a classical pseudo-random generator with a probability of 50% of outputting either value $-1/2$ or $1/2$. This pseudo-random generator is implemented before the execution of each quantum simulation and these values are stored in lists. Each time a switch of a fluctuator takes place in the simulation, a random value is picked from a list.

Another idea for generating the fluctuations is to model the functions $\xi_m(t)$ as a simple quantum circuit composed by an Hadamard gate applied to a qubit initialized at $|0\rangle$. The Hadamard gate sets the qubit state to $(|0\rangle + |1\rangle)/\sqrt{2}$ and then this qubit is measured. This way, the output will be a random value 0 or 1 with 50% probability each. Depending on the time t in which the system is simulated, several runs of the algorithm can be performed as well as several qubits can be used. Although one can achieve a true random generator with this quantum circuit, this is a costly process in quantum computational resources, so it was not implemented.

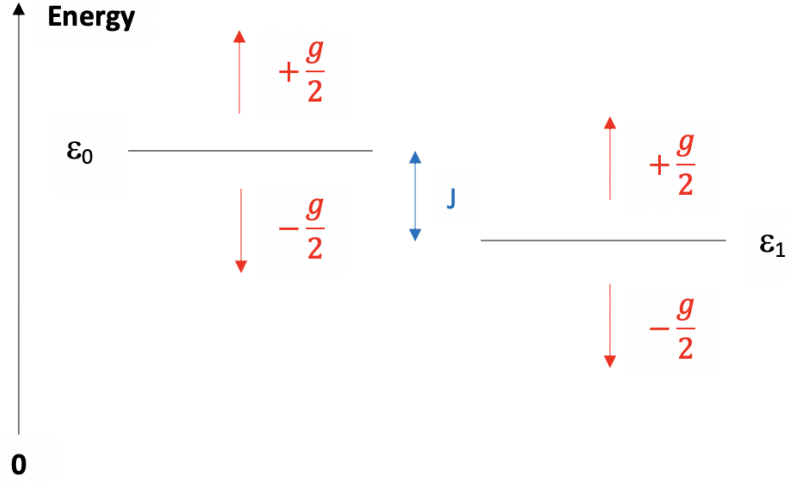


Figure 8: Uncorrelated random fluctuations applied to each site molecule energy ϵ_0 and ϵ_1 . In this image, each molecule is affected by one fluctuator.

Environment definition with fluctuators

The contribution of a fluctuator to the bath spectral density takes the Lorentzian form [36]

$$f_i(\omega) = \frac{g_i^2 \gamma_i}{4\pi(\omega^2 + \gamma_i^2)} \quad (81)$$

where g_i is the fluctuation strength of the fluctuator i and γ_i is the switching rate of the fluctuator i .

The spectral density of a set of fluctuators is given as a sum of the contributions of all fluctuators present in the set [36] as

$$F(\omega) = \sum_i \frac{g_i^2 \gamma_i}{\omega^2 + \gamma_i^2} \quad (82)$$

One can reproduce several types of environments by choosing the parameters accordingly. Note, however, that only low-frequency environments can be represented by a fluctuator environment.

Quantum circuit implementation: Two molecule system and one fluctuator per set

The usual approach to implement the system's evolution is to employ the evolution operator (57). The general Hamiltonian is given by a sum of Hamiltonians, i.e. $H = H_S + H_F(t)$, where $H_F(t)$ is time-dependent. Nevertheless, time-dependency is given by sudden switching acts which commute at different times. Therefore its evolution operator can be constructed as a product of evolution operators as long as the Hamiltonian stays constant as it freely evolves

in some constant time interval, i.e. there is no fluctuation switch between some time t' and $t' + \Delta t_f$. The unitary evolution, which defines the system-bath interaction, for a time $t = N_f \Delta t_f$, where N_f is the number of fluctuation switches and Δt_f is the fluctuator waiting time (interval of time between switches), is given by

$$U_f(N_f \Delta t_f) = \prod_{n_f=1}^{N_f} e^{-iH_F(n_f \Delta t_f) \Delta t_f} \quad (83)$$

where $H_F(n_f \Delta t_f)$ must have a constant *action* throughout the interval of time $[(n_f - 1)\Delta t_f, n_f \Delta t_f]$.

Both Hamiltonians H_S and H_F do not commute in the general case, therefore the Trotter product formula (59) must be applied, where each iteration time-step Δt must be considered smaller or equal to the previous fluctuator waiting time Δt_f . Therefore the switching act is performed at every $\frac{1}{\gamma \Delta t}$ iterations, where $a \Delta t = \Delta t_f = \frac{1}{\gamma}$, $a \in \mathbb{N}$. Note that the iteration time-step is dependent on the fluctuator switching rate, a requirement caused by the implemented evolution as iterations. The unitary evolution, for a time $t = N \Delta t$ where Δt is the iteration time-step and N is the number of iterations, becomes:

$$U(N \Delta t) = \prod_{n=1}^N \left(e^{-iH_F(n \Delta t) \Delta t} T^\dagger e^{-iH_S \Delta t} T \right) = \prod_{n=1}^N \left(\left[\prod_{m=0}^1 e^{\pm i \frac{g_m}{2} \Delta t} \right] T^\dagger \left[\prod_{m=0}^1 e^{-iE_m \Delta t} \right] T \right) \quad (84)$$

Note that the operator $|m\rangle \langle m|$ is not present in the fluctuator interaction evolution operator because it is employed in its eigenbasis, i.e. site basis, and therefore it is substituted by its eigenvalues. To implement one fluctuator interaction evolution operator $e^{\pm i \frac{g_m}{2} \Delta t}$ to the molecule m , one needs to apply X -Pauli gates to identify which molecule m , i.e. system's state $|m\rangle$, the fluctuation is applied, similarly to the implementation of $e^{-iH_S \Delta t}$. Then a controlled gate $CR_Z(\phi_m)$ where $\phi_m = \pm g_m \Delta t$ and the sign \pm is determined by the random output of the switch at every $\frac{1}{\gamma \Delta t}$ iterations, and applied with control at the system's qubit and target at the ancilla qubit (it can be the same ancilla used in the implementation of $e^{-iH_S \Delta t}$). The fluctuation strength is given in units cm^{-1} , thus the same unit conversion to $rad.THz$ as the performed on the computation of the system Hamiltonian is employed, i.e. $g' = 2\pi c g$. The circuit implementation for a complete iteration is shown in figure 9.

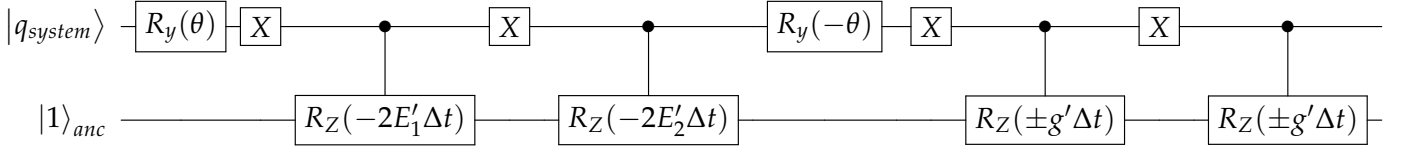


Figure 9: Implementation of one iteration of the system with decoherence algorithm. $|1\rangle_{anc}$ is the ancilla qubit initialized at $|1\rangle$. $|q_{system}\rangle$ is the system's qubit state *in the site basis*. The basis transformation operators T and T^\dagger are implemented with the gates $R_y(\theta)$ and $R_y(-\theta)$, respectively. Every set of fluctuators is identical so $g' = g'_m$.

Generalized quantum circuit implementation

If more than one fluctuator is present in each set, the procedure is very similar, although one must account for the different switching rates. The time-step of the iteration must be equal or smaller than the waiting time of the fluctuator with the highest switching rate γ_h in the set, i.e. $l\Delta t = \frac{1}{\gamma_h}$, $l \in \mathbb{N}$. Using this method, the switching rates of the other fluctuators (denoted by the subscript j) must fulfill the following condition: $p_j\gamma_j = \gamma_h$, $p_j \in \mathbb{N}$. These conditions are a requirement because the system's evolution is made by time iterations. For a number of F fluctuators in a set and M molecules,

$$U(N\Delta t) = \prod_{n=1}^N \left(\left[\prod_{m=0}^M \prod_{j=0}^F e^{\pm_j i \frac{g_{jm}}{2} \Delta t} \right] T^\dagger \left[\prod_{m=0}^M e^{-iE_m \Delta t} \right] T \right) \quad (85)$$

where \pm_j denotes the act of switching of the fluctuator j to be applied when $(n\Delta t) \bmod \frac{1}{\gamma_j} = 0$.

The generalized implementation of the fluctuator interaction evolution operator is the following:

- **Step 1:** Select a system's state $|m\rangle$ by applying X-gates. Then apply a $C^n NOT$, where n is the number of qubits that represent the system, with controls at the system's qubits and target at the ancilla qubit. Then proceed to step 2.
- **Step 2:** If all the fluctuators have already interacted with the molecule, then proceed to step 3. Otherwise, choose a fluctuator j with the corresponding coupling g_j . Then apply a $CR_Z(\phi)$ with control at the ancilla qubit and target at the same ancilla used in the system's Hamiltonian evolution operator. The sign of the angle $\phi = \pm \Delta t g_j$ depends on the switching rate of the fluctuator j . If the current iteration is the one where the switching act must be performed then a new random value must be picked from a list, generated with random values before the execution of the quantum circuit. If the current iteration is not the one where the fluctuator j switches its fluctuation sign,

then pick the random value in the list used in the previous iteration for the fluctuator j . Then repeat this whole step, by choosing another fluctuator $j + 1$.

- **Step 3:** Reverse the circuit in step 1. **If all the system's states $|m\rangle$ have been chosen**, the implementation of the fluctuator interaction evolution operator is over for this iteration. **If all the system's states have not been chosen**, then proceed to step 1 and choose another system's state $|m\rangle$ different from the ones already chosen.

Usually in an open quantum system with a dilated system's Hilbert space, one needs to perform different measurement techniques [11, 36] than the one used in the no decoherence algorithm, however the system here implemented is modelled in closed form so the measurement procedure is done directly at the system's qubits in the site basis.

The full algorithm (random values generator plus the actual simulation) must be performed several times, so that the results of all runs are averaged. The requirement of a high number of runs motivated the multiprocessing parallelization of the code for faster executions of the full algorithm in the quantum simulator. It was used the *Python multiprocessing* library to parallelize the code in different processes with concurrency control. The overall algorithm is sent to a number P of processes. Each process executes N different programs, each one with different random functions ζ . Each n program, $n \in \{1, 2, \dots, N\}$, in each p process, $p \in \{1, 2, \dots, P\}$, produces a list of random values 0 and 1 and then this list is used for the execution of the quantum circuit. Each process p and each program n perform a number of S shots. A shot s , $s \in \{1, 2, \dots, S\}$, is a run of the quantum circuit. At the end, one has $E = P \times N \times S$ executions of the algorithm with $P \times N$ different random-valued functions ζ for each fluctuator. The population terms, for a M molecule system, are found by calculating

$$\rho_S(t) = \sum_{i=1}^M \frac{E_i(t)}{E} |i\rangle \langle i| \quad (86)$$

where $E_i(t)$ is the sum of all the measurements of the system's qubits which resulted in the state $|i\rangle$ at time t and $E = P \times N \times S$. The value $E_i(t)/E$ is the probability of getting the state $|i\rangle$ by measuring the final system state $|\Psi(t)\rangle$.

The concurrency control was implemented with a *lock* when the number of measurements of a determined state in each process is added to the number of measurements of another process and when the parameters required for the implementation are read at the start of the simulation.

3.3 COMPUTATIONAL RESOURCES

In this section, the quantum computational resources required by both previous implemented algorithms are calculated, as well as the query complexity of the system with decoherence algorithm. Finally the number of required random numbers is calculated.

Qubit resources

The system and ancilla qubits are the only qubits required, therefore $n = \log_2(N_{mol})$ qubits represent the system's qubits, being N_{mol} the number of the system's molecules. Considering the ancilla qubits, then the simulation requires $\log_2(N_{mol}) + d$ qubits where d is the number of ancillas. A $C^n NOT$ decomposition requires $\log_2(N_{mol}) - 1$ qubits (see figure 10) and one more ancilla qubit is required to implement the diagonal evolution operator of the system Hamiltonian and the basis transformation matrix decomposition (the target qubit of the gates CR_Z , when decomposing the one-level matrices), thus the final number of needed ancilla qubits is $d = \log_2(N_{mol})$. The system's qubits plus the ancilla qubits gives a total of $2\log_2(N_{mol})$ required qubits for both previous algorithms.

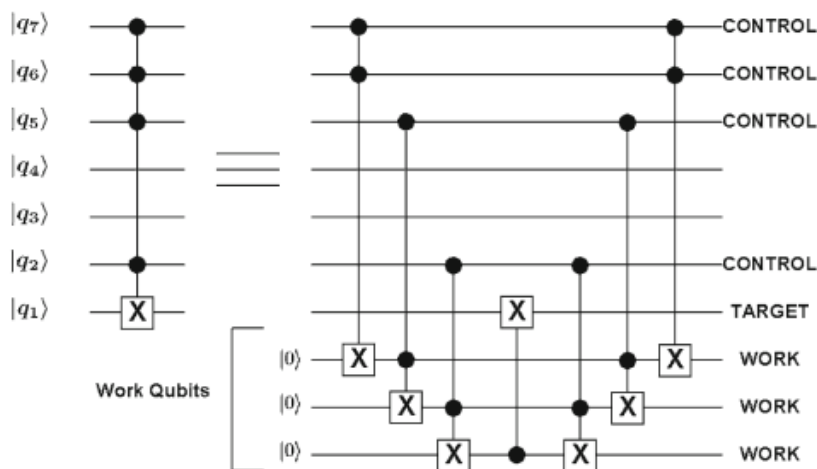


Figure 10: $C^n NOT$ decomposition where the work qubits are ancilla qubits. With n control qubits, $n - 1$ ancillas are required. This was the decomposition used in the simulations. Image taken from [43].

Quantum gate resources

Any $C^n NOT$ gate can be decomposed using $\mathcal{O}(n)$ CNOT gates [11].

The matrix T decomposition has a complexity of $\mathcal{O}(N_{mol}^2)$ two-level matrices (the one-level matrices are left out, for reasons that will be explained in the next section). Each two-level unitary matrix needs $\mathcal{O}(\log_2[N_{mol}])$ single qubit and $C^n NOT$ gates to reach the state $|k\rangle$

from the state $|j\rangle$ [11] (see Appendix A) and each $C^n NOT$ needs $\mathcal{O}(\log_2[N_{mol}])$ CNOT gates to be decomposed. Therefore, the final complexity of the basis transformation operator is $\mathcal{O}(N_{mol}^2 \log_2^2[N_{mol}])$ [11]. If the number of iterations, given by I , is taken into account $\mathcal{O}(I \times N_{mol}^2 \log_2^2[N_{mol}])$ single qubit and CNOT gates will be required.

The diagonal evolution operator of the system Hamiltonian can be applied using $\mathcal{O}(N_{mol} \log_2[N_{mol}])$ single qubit and CNOT gates. For each term in the diagonal evolution operator, $\mathcal{O}(\log_2[N_{mol}])$ gates are required to decompose the $C^n R_Z(\theta)$. The diagonal Hamiltonian has N_{mol} diagonal elements, so the gate complexity of the diagonal evolution operator is calculated as $\mathcal{O}(N_{mol} \log_2[N_{mol}])$. Considering the number of iterations I , the final complexity of the diagonal evolution operator of the system's Hamiltonian is $\mathcal{O}(I[N_{mol} \log_2(N_{mol})])$.

The no-decoherence algorithm has a final quantum gate complexity of

$$\mathcal{O}(N_{mol}^2 \log_2^2[N_{mol}]) \quad (87)$$

where the quantum gate computational cost is dominated by the decomposition of the basis transformation matrix in a sequence of single qubit and CNOT gates.

The complexity of the fluctuator interaction evolution operator is, for one iteration, $\mathcal{O}(N_{mol}[\log_2(N_{mol}) + F])$, where F is the number of fluctuators in a set. Each molecule interacts with its set of fluctuators, thus N_{mol} $C^n NOT$ gates are required to define the interaction of all the fluctuator sets which gives a complexity of $\mathcal{O}(N_{mol} \log_2[N_{mol}])$. It is also required to implement $F CR_Z$ gates for each molecule present in the system, i.e. the interactions between a molecule and the F fluctuators in a set, which gets a total of $\mathcal{O}(IN_{mol}[\log_2(N_{mol}) + F])$ single qubit and CNOT gates, for I iterations.

The quantum gate complexity for one run of the system with decoherence algorithm, for a time $t = I\Delta t$, is

$$\mathcal{O}\left(\frac{t}{\Delta t}\{N_{mol}^2 \log_2^2[N_{mol}] + N_{mol}F\}\right) \quad (88)$$

Note that the algorithm must be run several times to average the results. One can parallelize the algorithm in a quantum computer so that it requires less time to fully execute it, but comes with the cost of an higher number of qubits.

Query complexity

The system with decoherence algorithm used the Trotter product formula (59), therefore the query complexity for a single run is $\mathcal{O}(\Delta t^2/\epsilon)$, where ϵ is the desired error one wishes to obtain in the simulation by using an iteration time-step Δt .

Next, the calculation of the number of runs of the simulation required to obtain an error $\epsilon > 0$ by averaging the results is performed.

Each fluctuation can assume two random values (with signs + and -) and each set of the environment interacting with a molecule has F different fluctuators. Therefore after one iteration, a molecule has $2F$ different possibilities of having an excited state energy different from the initial site energy ϵ_m , in the worst case. At every iteration, the possible configurations of a molecule excited state increase by $2F$, because at each iteration each molecule interacts again with F fluctuators. This is, for a number of I iterations, $2FI$ configurations of the excited state of a molecule are possible. Converting the number of iterations to $I = \frac{t}{\Delta t}$, then the number of possible configurations, in function of time, is $2F \frac{t}{\Delta t}$. Each possible energy configuration of the system for a time t , has a well defined probability. Note that the random fluctuations applied to the system cause a discrete Gaussian probability distribution of measuring some possible energy state outcome in each molecule. For a chain of N_{mol} molecules, the fluctuations are *independently applied* to each molecule, which means that the probability of having a configuration of an excited state of a molecule as an outcome can be equal to the probability of outcome of a configuration of the excited state of another molecule. This means that for a chain of N_{mol} molecules, the probability of having a determined chain energy state outcome can be equal to another chain energy state outcome (this is called degeneration). Running R times the simulation and averaging the results, an error relatively to the average value of $\epsilon = \frac{\sigma}{\sqrt{R}}$ is obtained, where σ is the standard deviation which scales with $\mathcal{O}(F \frac{t}{\Delta t})$, i.e. it scales with the number of possible chain energy configurations with *different probabilities* of outcome, for a time t , because the probability distribution must be normalized to 1 for the discrete domain of energies. Therefore, to obtain an error ϵ by averaging the results, the number of times the simulation must be run is

$$\mathcal{O} \left(\frac{[F \frac{t}{\Delta t}]^2}{\epsilon^2} \right) \quad (89)$$

Number of required random numbers

The random numbers are calculated by taking into account how many switches are needed for the whole algorithm. Each fluctuator j needs a random value to be implemented at a rate γ_j , thus a set of fluctuators with F elements and a desired simulation for a time t , needs $\sum_{j=0}^F t\gamma_j$ random values. If N_{mol} molecules are present in the system, the number of required random numbers increases to $N_{mol} \times \sum_{j=0}^F t\gamma_j$. Using multiprocess parallelization with P processes where each executes N_{prog} programs with different random-valued functions, gives a total of $R = PN_{prog}$ runs of the simulation. The total of random values needed for the full implementation, for a time t , is:

$$\mathcal{O}(R \times N_{mol} \times \sum_{j=0}^F t\gamma_j) \quad (90)$$

3.4 QUANTUM CIRCUIT OPTIMIZATIONS

This section discusses some possible optimizations for the simulation.

3.4.1 *Simple optimizations*

One simple optimization that can be done is to not implement some types of quantum gates at the same qubits, consecutively. For instance, two X-Pauli or two CNOT gates consecutively applied to the same qubits can be removed because the final state is the same as if the two consecutive gates were not applied. This is a very small optimization which does not reduce the quantum gate complexity, however it still slightly reduces the number of quantum gates in the circuit.

Another simple optimization is to put the state of each ancilla qubit at $|0\rangle$ whenever it is possible. The T_1 (or longitudinal) relaxation time of the qubit is an important parameter of the quantum hardware, which can produce significant errors in the simulation. Therefore, not letting the qubit unexpectedly decay to the state $|0\rangle$ (its decay probability obeys to an exponential decay tendency in function of time) by changing it to that state on purpose, can reduce the error rate. In the performed simulations, an ancilla initialized at $|1\rangle$ has been used as a target qubit for the gates $C^n R_Z$. Whenever the basis transformation operator is performed, in a simulation with a high number of molecules or fluctuators, a X-Pauli gate can be implemented at the ancilla, before and after the basis transformation operator application. This operator requires a high number of gates to be implemented, i.e. a high interval of time to be fully applied, thus the ancilla qubit is not used along this time (considering that the one-level matrices are not applied, as it will be discussed next). Then the ancilla qubit should be set to the state $|1\rangle$ only when the diagonal system evolution operator or the fluctuator interaction evolution operator are to be implemented, because it is needed at the application of these operators. Obviously, adding the extra X-Pauli gates increases the number of gates, but by only implementing them when is strictly necessary, a balance between the minimum number of gates and the minimum error rate produced by the longitudinal relaxation decay can be achieved.

3.4.2 *Basis transformation matrix decomposition*

The most expensive method to implement the simulation is the basis transformation matrix decomposition. Considering an Hamiltonian with no imaginary terms, as the ones considered in this work, the energy eigenstates of the system are composed by a superposition of site eigenstates with 0 relative phase between them, i.e. the basis transformation matrix is given by real numbers only. Therefore, the unitary one-level matrices outputted by the

Quipper algorithm described in Appendix A can be neglected because they only apply a phase, which is not required. This optimization does not decrease the quantum gate complexity of implementing the basis transformation operator, because in the previous section, the complexity is formulated accounting only for the two-level unitary matrices, but it still reduces the overall number of gates of the quantum circuit by removing unnecessary quantum gates.

3.4.3 Query complexity optimization

If seeking for a simulation, using the system with decoherence algorithm, with an error $\epsilon > 0$, then the use of the Trotter product formula (59) to approximate the evolution operator gives an error scaling of $\epsilon = \mathcal{O}(\Delta t^2/N)$ [30]. Another approximation it can be used is the Lie-Trotter-Suzuki formula up to some k th order where the error scales with $\epsilon = \mathcal{O}(\Delta t^{2k+1}/N^{2k})$ [31], being N the number of iterations with iteration time-step Δt . It can be observed that using a different technique, the error derived from the approximation is smaller to the same N and (small) Δt than using Trotter approximation.

The other evolution operator decomposition techniques addressed in subsection 2.4.1 are also an optimization, concerning only the query complexity.

3.5 SUMMARY

The decisions made in order to develop a quantum algorithm which describes faithfully the energy transport in photosynthesis have been presented and justified. The model and the quantum circuit implementation have been theoretically formulated and demonstrated, for an isolated and open system quantum simulation. The algorithm has been evaluated in terms of its computational resources: the required qubits, quantum gate complexity, query complexity and the number of required random numbers. Finally, some optimizations which can be straightforwardly applied to the quantum circuit were presented.

 APPLICATION

4.1 COMPUTATIONAL SETUP

In this section, the calculations required to perform the quantum simulation in the no decoherence regime, for a two and four molecule system will be presented. Typical energy parameters for the site energies and inter-molecular coupling strengths have been used [39, 41].

The code used to diagonalize the Hamiltonians can be found in the following URL: https://github.com/jakumin/Photosynthesis_quantum-simulation_code.

4.1.1 One qubit system

The first case study consists of a two molecule non-resonant system, considered as isolated from the universe. The numerical Hamiltonian to implement this system is given by

$$H_S = \begin{pmatrix} 12900 & 132 \\ 132 & 12300 \end{pmatrix} cm^{-1} \quad (91)$$

This matrix is diagonalized and it yields

$$H_{S-diag} = \begin{pmatrix} 12927.8 & 0 \\ 0 & 12272.2 \end{pmatrix} cm^{-1} \quad (92)$$

where the energy eigenvalues are later converted to *rad.THz*. The unitary basis transformation matrices are

$$T = \begin{pmatrix} -0.9786 & 0.205773 \\ -0.205773 & -0.9786 \end{pmatrix} \quad (93)$$

and its conjugate T^\dagger . It can be seen that the energy eigenstate $|E_0\rangle$ can be decomposed in a superposition of the site eigenstates as $|E_0\rangle = -0.9786 |0\rangle + 0.205773 |1\rangle$ and $|E_1\rangle$ can also be decomposed in a similar superposed form. For a two molecule system, the basis

transformations matrix T is given as an unitary $R_Y(\theta)$ gate applied to the system qubit where $\theta/2 \approx -2.934$. The basis transformation T^\dagger is applied as $R_Y(-\theta)$.

A second case study of the no decoherence algorithm is performed with a system of two molecules in near resonance. In this case the Hamiltonian is

$$H_S = \begin{pmatrix} 13000 & 126 \\ 126 & 12900 \end{pmatrix} cm^{-1} \quad (94)$$

Diagonalizing it, one gets

$$H_{S-diag} = \begin{pmatrix} 13086 & 0 \\ 0 & 12814 \end{pmatrix} cm^{-1} \quad (95)$$

The corresponding unitary basis transformation matrix is

$$T = \begin{pmatrix} -0.8273 & 0.5618 \\ -0.5618 & -0.8273 \end{pmatrix} \quad (96)$$

The T matrix can be implemented with a gate $R_Y(\theta)$ where $\theta/2 \approx -2.545$.

4.1.2 Two qubit system

We shall consider now a system consisting of two pairs of molecules (four in total); its simulation requires two qubits. The model of the four molecule system simulation was explained in subsection 3.2.1.

The first pair (first and second molecules) is near-resonant as well as the second pair (third and fourth molecules), while the two pairs are in off resonance between them. The Hamiltonian of the system is

$$H_S = \begin{pmatrix} 13000 & 126 & 16 & 5 \\ 126 & 12900 & 132 & 16 \\ 16 & 132 & 12300 & 126 \\ 5 & 16 & 126 & 12200 \end{pmatrix} cm^{-1} \quad (97)$$

After diagonalization it reads

$$H_{S-diag} = \begin{pmatrix} 13096 & 0 & 0 & 0 \\ 0 & 12834 & 0 & 0 \\ 0 & 0 & 12360 & 0 \\ 0 & 0 & 0 & 12109 \end{pmatrix} cm^{-1} \quad (98)$$

and the basis transformation matrix is given as

$$T = \begin{pmatrix} -0.7957 & 0.6054 & -0.0176 & -0.0057 \\ -0.5923 & -0.772421 & 0.2119 & 0.0829 \\ -0.1193 & -0.1850 & -0.7779 & -0.5886 \\ -0.0318 & -0.0515 & -0.5913 & 0.8042 \end{pmatrix} \quad (99)$$

The procedure is to input this matrix to the Quipper program to know how to implement it in a quantum circuit. The procedure of the basis transformation decomposition is detailed in Appendix A. The code used to decompose matrix (99) is available at the URL: https://github.com/jakumin/Photosynthesis_quantum-simulation_code.

First, recall the matrices that the Quipper program outputs:

$$R_{Z-X}(\delta, \gamma) = \begin{pmatrix} I & \vdots & \mathbf{o} & \vdots & \mathbf{o} \\ \dots & e^{-i\delta/2}\cos(\gamma/2) & \dots & -ie^{-i\delta/2}\sin(\gamma/2) & \dots \\ \mathbf{o} & \vdots & I & \vdots & \mathbf{o} \\ \dots & -ie^{i\delta/2}\sin(\gamma/2) & \dots & e^{i\delta/2}\cos(\gamma/2) & \dots \\ \mathbf{o} & \vdots & \mathbf{o} & \vdots & I \end{pmatrix} \quad (100)$$

Where the bold \mathbf{o} are square 0-matrices, the dots denote 0 columns or rows and I is the identity matrix. The unitary square one-level matrix $e^{i\theta}$ is:

$$O(\theta) = \begin{pmatrix} I & \vdots & \mathbf{o} \\ \dots & e^{i\theta} & \dots \\ \mathbf{o} & \vdots & I \end{pmatrix} \quad (101)$$

The output of the program is given in the order of mathematical application (left-to-right) but note that in the quantum circuit the application is from right to left.

The T basis transformation matrix outputted by the Quipper program is:

$$\begin{aligned} T = & R_{Z-X,1}(-1.5707964, -1.280839)R_{Z-X,2}(-0.7853982, -0.23925155) \\ & R_{Z-X,3}(-0.392699, -6.359089 \times 10^{-2})R_{Z-X,4}(-1.9634955, -0.37569928) \\ & R_{Z-X,5}(-1.1780972, -0.103078015)R_{Z-X,6}(-2.159845, -1.2680365) \\ & O_1(1.8653208)O_2(-2.8470683)O_3(2.3561945)O_4(1.767146) \end{aligned}$$

The Gray Code is then applied where each matrix contains the numbers j and k (or only j) outputted by the Quipper program. The quantum circuit optimizations discussed in the

previous chapter are neglected in the following application of the Gray Code. Each matrix is implemented in a circuit sequence as provided below,

$$O_4(1.767146) \tag{102}$$

where $j = 0$. Using the system qubit notation $|q_0\rangle \otimes |q_1\rangle$, the $e^{i\theta}$ term is applied to state $|00\rangle$ in the matrix (101). Therefore the quantum circuit for this gate is depicted in figure 11.

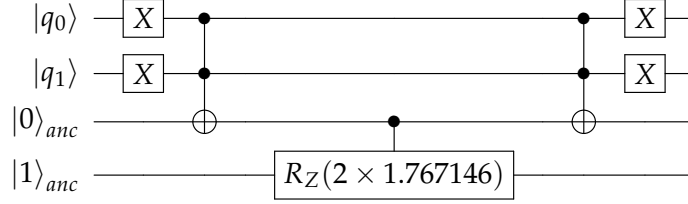


Figure 11: Implementation of the one-level unitary matrix $O_4(1.767146)$.

$$O_3(2.3561945) \tag{103}$$

This matrix has $j = 1$, so it corresponds to the state $|01\rangle$. The matrix is then implemented as depicted in figure 12.

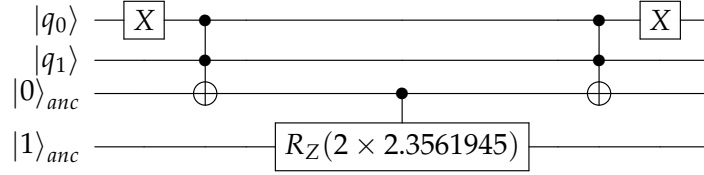


Figure 12: Implementation of the one-level unitary matrix $O_3(2.3561945)$.

$$O_2(-2.8470683) \tag{104}$$

where $j = 2$ corresponds to the state $|10\rangle$. The quantum circuit representing this gate is illustrated in figure 13.

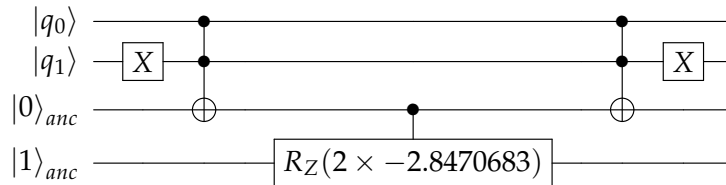


Figure 13: Implementation of the one-level unitary matrix $O_2(-2.8470683)$.

$$O_1(1.8653208) \tag{105}$$

where $j = 3$ corresponds to the state $|11\rangle$. This gate is implemented as in figure 14.

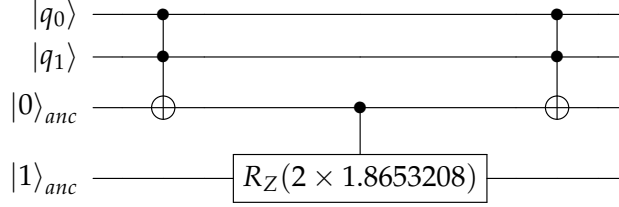


Figure 14: Implementation of the one-level unitary matrix $O_1(1.8653208)$.

$$R_{Z-X,6}(-2.159845, -1.2680365) \tag{106}$$

where $j = 2$ and $k = 3$, thus $|j\rangle = |10\rangle$ and $|k\rangle = |11\rangle$. Using notation $U_3(\gamma) = U_3(\gamma, -\pi/2, \pi/2)$, the quantum circuit representing this matrix is presented in figure 15.

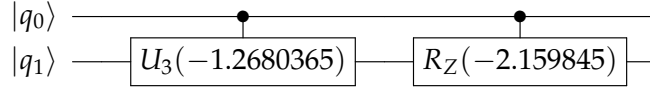


Figure 15: Implementation of the two-level unitary matrix $R_{Z-X,6}(-2.159845, -1.2680365)$.

$$R_{Z-X,5}(-1.1780972, -0.103078015) \tag{107}$$

where $j = 1$ and $k = 3$. Thus the respective states are $|01\rangle$ and $|11\rangle$. The matrix is implemented as in figure 16.

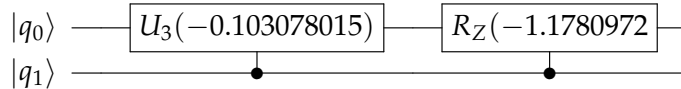


Figure 16: Implementation of the two-level unitary matrix $R_{Z-X,5}(-1.1780972, -0.103078015)$.

$$R_{Z-X,4}(-1.9634955, -0.37569928) \tag{108}$$

where $j = 1$ and $k = 2$. The respective states are $|01\rangle$ and $|10\rangle$. The quantum circuit which represents this gate is illustrated in figure 17.

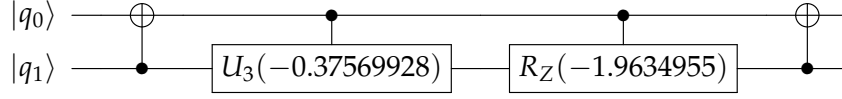


Figure 17: Implementation of the two-level unitary matrix $R_{Z-X,4}(-1.9634955, -0.37569928)$.

$$R_{Z-X,3}(-0.392699, -6.359089 \times 10^{-2}) \quad (109)$$

where $j = 0$ and $k = 3$. Here, $|j\rangle = |00\rangle$ and $|k\rangle = |11\rangle$. The quantum circuit is implemented as in figure 18.

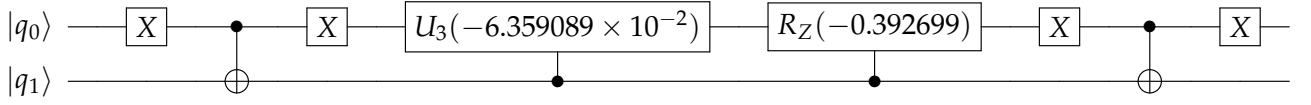


Figure 18: Implementation of the two-level unitary matrix $R_{Z-X,3}(-0.392699, -6.359089 \times 10^{-2})$.

$$R_{Z-X,2}(-0.7853982, -0.23925155) \quad (110)$$

where $j = 0$ and $k = 2$, i.e. $|00\rangle$ and $|10\rangle$, respectively. This matrix is modeled as presented in figure 19.

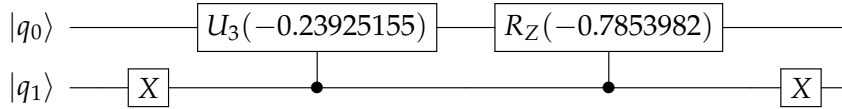


Figure 19: Implementation of the two-level unitary matrix $R_{Z-X,2}(-0.7853982, -0.23925155)$.

$$R_{Z-X,1}(-1.5707964, -1.280839) \quad (111)$$

where $j = 0$ and $k = 1$. The corresponding states are $|00\rangle$ and $|01\rangle$. This final matrix is applied with the circuit depicted in figure 20.

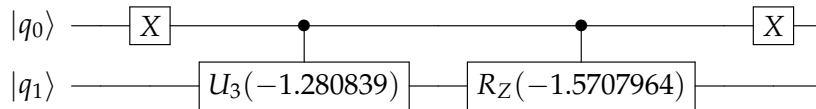


Figure 20: Implementation of the two-level unitary matrix $R_{Z-X,1}(-1.5707964, -1.280839)$.

The basis transformation matrix implementation is now completed. To apply T^\dagger , the reversed matrix sequence is implemented and the two-level matrices are applied with the

gate $CU_3(\gamma, \pi/2, -\pi/2)CR_Z(-\delta)$. The one-level matrices are applied with negative angles as $C^2R_Z(-2\theta)$.

The implemented operator T is correct if it represents the basis transformation matrix, i.e. if both matrices are equal. To check this, the system's qubits are prepared in a non superposed state, the T operator is applied to them and measurements are performed in the corresponding qubits. Then, Qiskit outputs the amount of times the qubit states were measured, which we denote by M_i for each measured state $|i\rangle$. Therefore, the amplitude α_i of some measured state i is $\alpha_i = \sqrt{\frac{M_i}{S}}$, where S is the number of shots performed. By initializing the qubits at a state $|m\rangle$, applying the operator T and measuring the resulting state a number of S times (shots), the amplitudes α_i of the resulting states $|i\rangle$ can be known. Therefore, each α_i must be equal to the element in row $|i\rangle$ of the column $|m\rangle$ (prepared initial state) of the basis transformation matrix. This process can be generally applied to check if all the elements of the basis transformation matrix are equal to all the elements of the implemented operator T .

4.2 RESULTS AND DISCUSSION

Experiments of simulation of the energy transport in photosynthesis, were conducted, for both the *isolated system* and *pure dephasing* regimes, in near-resonant and non-resonant scenarios, according to the algorithms described throughout the previous chapter and the computational setups of the previous section. For the purpose of validation, for the *isolated one system qubit*, the simulation results were compared with the theoretical prediction, whose derivation is available in Appendix C. Since the circuit for the *isolated one qubit system* simulation is small, it was directly implemented in the online Qiskit editor [44], while for the *isolated two qubit system* and *one system qubit decoherent* case, the QASM editor was used.

The code used for all the experiments can be found in the URL: https://github.com/jakumin/Photosynthesis_quantum-simulation_code.

4.2.1 Isolated system results

One qubit system

The results for both the *near resonance* and *non resonant* regimes are shown in figures 21 and 22, respectively. They were obtained in an actual quantum device (the IBMQ london with 5 qubits). Due to the stochastic nature of quantum computers, the experiments were conducted with 2048 shots for each time value. The specific optimized quantum circuits used in this experiment, are presented in Appendix D.

In the following results, the probabilities of the donor and acceptor molecules being excited are denoted by $P(0) = \langle 0 | \rho_S(t) | 0 \rangle$ and $P(1) = \langle 1 | \rho_S(t) | 1 \rangle$, respectively.

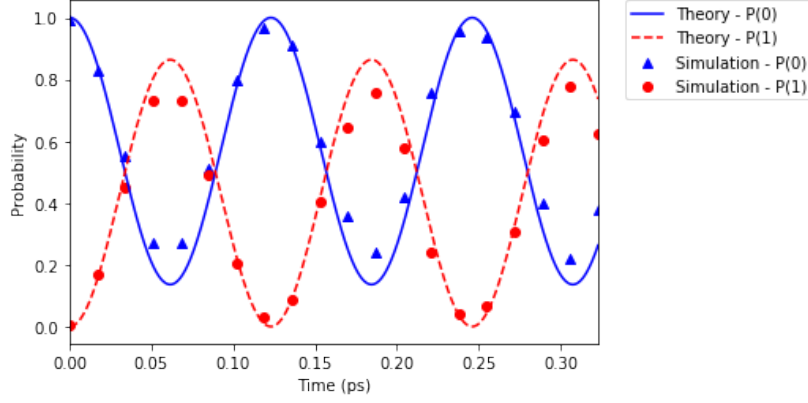


Figure 21: Time evolution of the occupation probabilities for a near-resonant system: simulated results (points) and theory (lines).

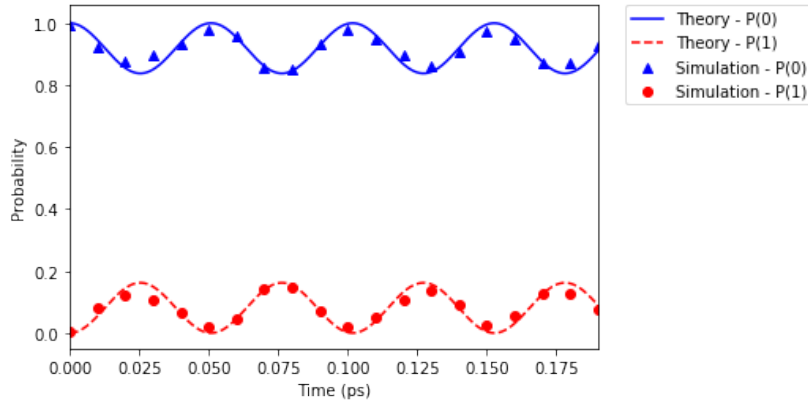


Figure 22: Time evolution of the occupation probabilities for a non-resonant system: simulated results (points) and theory (lines).

Taking the fluctuator's switching rate to be $\gamma = 0$ or the fluctuation strength to be $g = 0$, one has the no-decoherence regime. These simulations show the Redfield regime where there is a very weak system-environment coupling g , relatively to the inter-molecular coupling J , in the limit of null g , i.e. the *full coherent regime*. The quantum beating, observed in the simulation results, can be thought as a *reversible* transfer of energy between the molecules, where the excitation goes back and forward across the molecules [25], an equivalent of the Rabi oscillations.

In the performed simulations, the near-resonant and the non-resonant regime have a maximum probability of $\sim 90\%$ and $\sim 20\%$, respectively, of the energy being transferred to the acceptor molecule. Using the quantum Liouville equation [3] (the derivation is provided in Appendix E), the period of the quantum beating is $T_{near-res} \approx 123$ fs for the near-resonant

regime and $T_{non-res} \approx 51$ fs for the non-resonant regime. These periods are in the fs timescale according to the experimentally observable quantum beatings [15, 17, 16]. The simulation results show a similar behaviour as the ones predicted by the *Schrödinger* and *quantum Liouville* equation, where the off curve points are predominantly originated by errors in the quantum hardware.

Two qubit system

The results were obtained with 5000 shots for each time value t .

The elements of the system's density matrix shown in the following results are

$$\rho_S = \begin{pmatrix} P(0) & \rho_{0,1} & \rho_{0,2} & \rho_{0,3} \\ \rho_{1,0} & P(1) & \rho_{1,2} & \rho_{1,3} \\ \rho_{2,0} & \rho_{2,1} & P(2) & \rho_{2,3} \\ \rho_{3,0} & \rho_{3,1} & \rho_{3,2} & P(3) \end{pmatrix} \quad (112)$$

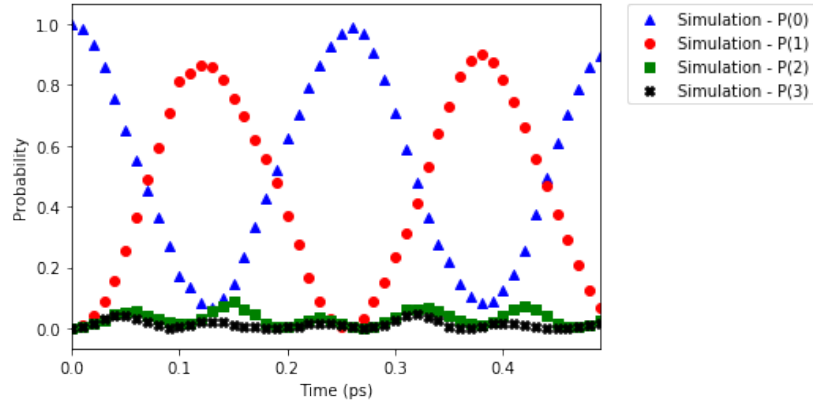


Figure 23: Time evolution simulation of the occupation probabilities for a four molecule system initialized at the state $|00\rangle$.

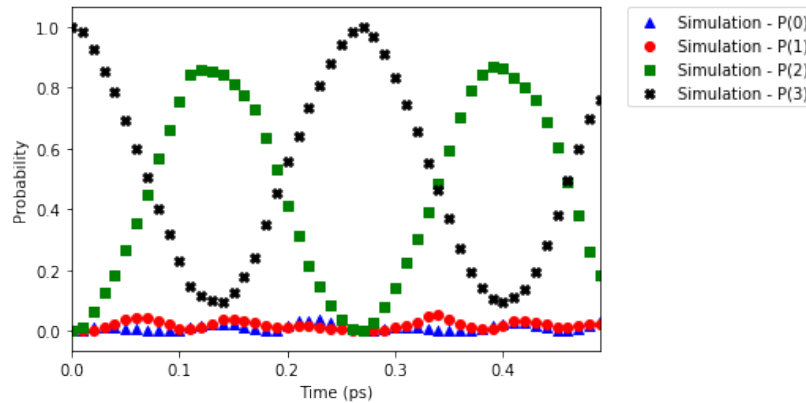


Figure 24: Time evolution simulation of the occupation probabilities for a four molecule system initialized at the state $|11\rangle$.

In figure 23, the first two molecules 0 and 1 exhibit approximately the same behaviour as in the previously discussed qubit system simulation, fig. 21. It can also be observed that the molecules 2 and 3 oscillate with very low amplitudes. The reason is the non resonance regime of the first pair of molecules with respect to the second pair, which strongly blocks the energy transfer between them. The initial state of the system is the excited molecule 0. Energy is only significantly transferred among near-resonant molecules, therefore the energy trapping in the first two molecules occurs. Still, quantum beating permits the second pair to have a small probability of becoming excited.

In contrast, figure 24 shows that energy is trapped in the second pair of molecules. The excitation is initially present in molecule 3, therefore the energy can only be significantly transferred to the near-resonant molecule 2.

4.2.2 Results for the system with decoherence

The simulations were performed with two molecules and only one fluctuator per set of the environment.

A large number of samples had to be measured in order to produce reliable results. The algorithm was implemented with 250 runs, where 5000 shots were performed for each time t .

Fluctuation strengths

In figures 25 and 26 the simulation results for different values of fluctuation strengths are presented, in the near resonant and non resonant systems, respectively. The switching rate was chosen to be 125 THz.

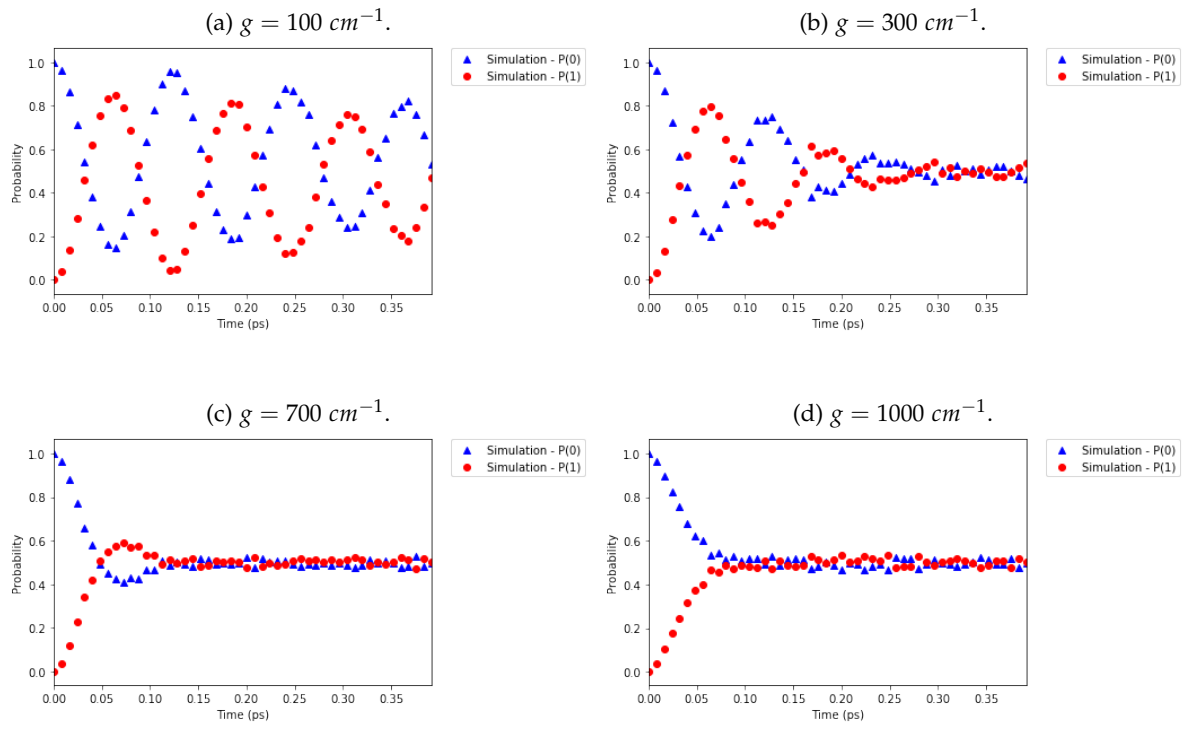


Figure 25: Time evolution simulation of the occupation probabilities for a near resonance system with decoherence for different values of fluctuation strengths.

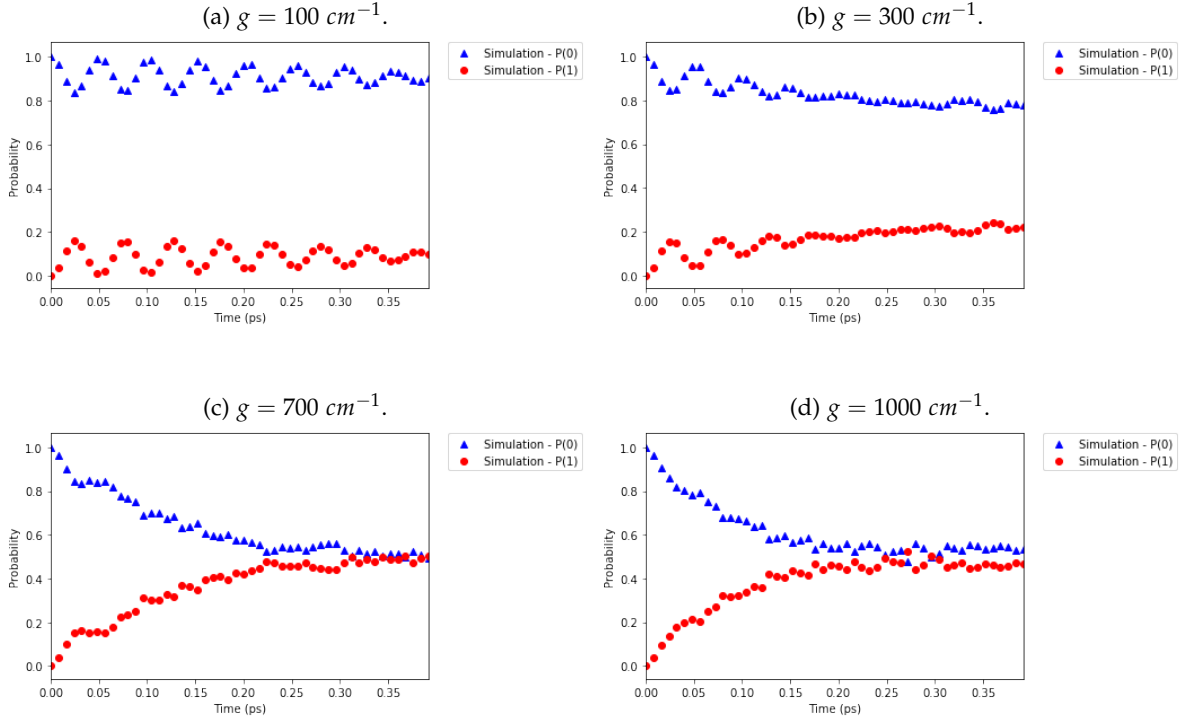


Figure 26: Time evolution simulation of the occupation probabilities for a off resonance system with decoherence for different values of fluctuation strengths.

It can be observed in Figures 25 and 26 that oscillation amplitudes decay over time, as expected, due to the loss of phase coherence between the molecule excited states, evidenced by the vanishing of quantum beating, which is associated with the irreversible evolution, where the system loses capacity of performing *coherent* transport. Additionally, it is also observable that, as correlated probabilities are eliminated along with quantum beating, the system is led to a classical distribution of the populations in the *site eigenbasis*.

In the regime under the study, where the environment is assumed to be at thermal equilibrium, the final probability distribution is calculated as the limit of the classical *Boltzmann* distribution $\langle m | \rho_S(t \rightarrow \infty) | m \rangle = \text{const} \times e^{-\frac{\epsilon_m}{k_B T}}$, where k_B is the Boltzmann constant, T is the temperature of the bath and const is a normalization constant [13]. Taking the limit at very high temperatures, the population terms approach the Boltzmann distribution $\langle 0 | \rho_S(t \rightarrow \infty) | 0 \rangle \approx \langle 1 | \rho_S(t \rightarrow \infty) | 1 \rangle \approx \frac{1}{2}$, which is compatible with the results obtained.

The switching rate must be high enough to observe the dephasing effects. For this, it has been employed a value about ≈ 33 times larger than the transport rate J (that is, the fluctuator waiting time is shorter than the inverse of the J^{-1}). As observed in the simulations, it was a suitable value to observe the relevant effects of the random fluctuations applied

to the system. At very low rates, it leads the system's evolution to a very similar behaviour as the previously observed in the no-decoherence regime, figs. 21 and 22.

In figures 25a, 26a and 26b the relaxation can not be fully observed because an high number of iterations would be required.

In a recent experiment, the quantum beating has been observed for a timescale higher than 660 fs [16], a timescale which can be modeled by the present simulation by changing the fluctuation strength.

Switching rates

In figures 27 and 28, the simulations results for different values of switching rates are presented, for the near resonant and non resonant systems, respectively. The fluctuation strength was chosen to be $g = 300 \text{ cm}^{-1}$. Some of the previously presented results are also used in the following figures for comparison.

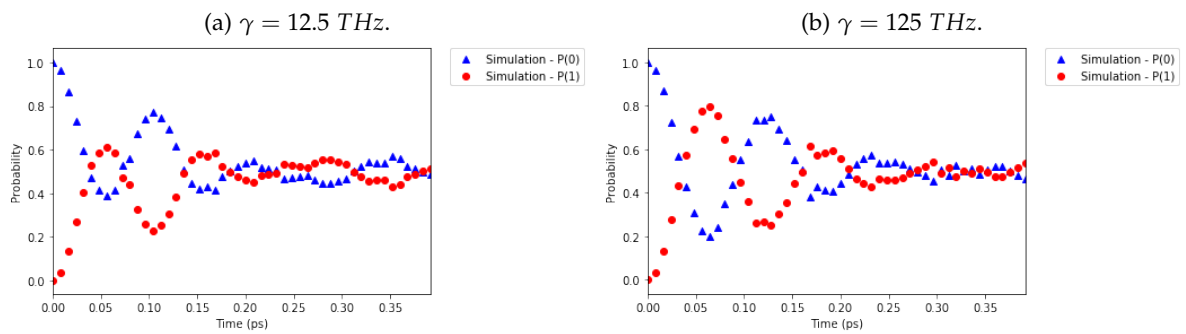


Figure 27: Time evolution simulation of the occupation probabilities for a near resonance system with decoherence for different values of switching rates.

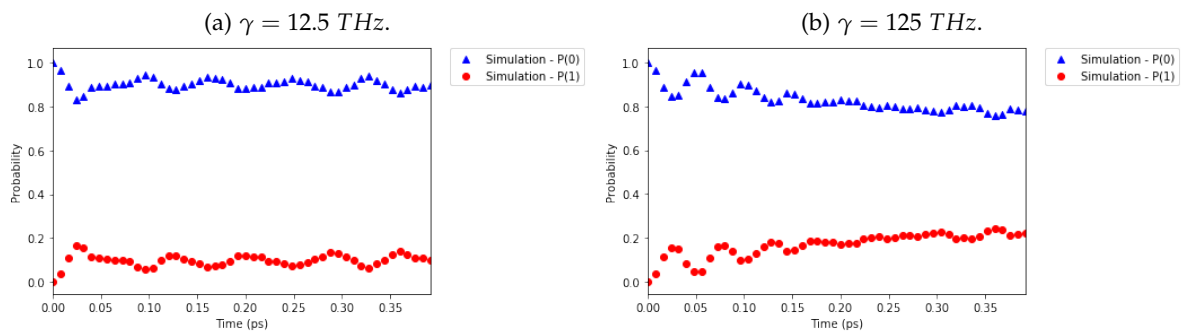


Figure 28: Time evolution simulation of the occupation probabilities for a off resonance system with decoherence for different values of switching rates.

The switching rate dictates how long the quantum beating lasts, for a fixed fluctuation strength. However, note that the effect of the former is not quite the same as that of the latter. While the fluctuation strength controls the degree of fluctuations, the switching rate controls the rate at which they appear. A balance between both is required to observe the desired dephasing effects. Note that very high switching rates have not been employed because many iterations would be required to watch the system's evolution in relevant timescales.

In figures 27a and 28a, the evolution of the population terms is not so smooth as in figures 27b and 28b, because at every 10 iterations the system is affected by the switching act while in figures 27b and 28b, the act is performed at every iteration. The *action* of the fluctuator is a sudden *jump* in the molecule excited state energies, which makes the system to evolve in two different transport regimes for a time Δt (iteration time-step). On the one hand the system has a free transport evolution, when there is no environment interaction, while on the other hand, the system evolves in a competition between the environmental interaction and the free energy transport, when the switching act is performed. The combination of these evolutions causes the non uniform evolution of the population terms observed in figures 27a and 28a. By employing the act at every iteration (figs. 27b and 28b), the system does not evolve in a combination of two types of evolution, but always in a competition between the environmental action and the free evolution, which allows for more uniform dynamics at the chosen observable timescale Δt .

Several fluctuators

In figures 29a and 29b, the simulation results for two fluctuators in each set of the environment are presented, for the near resonant and non resonant systems, respectively. The switching rate was chosen to be 125 THz for all the fluctuators and the fluctuation strengths $g_1 = 300 \text{ cm}^{-1}$ and $g_2 = 700 \text{ cm}^{-1}$.

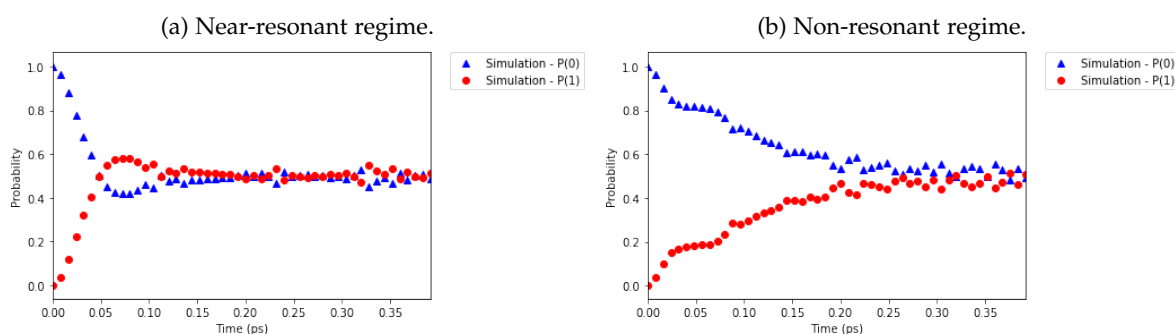


Figure 29: Evolution dynamics of the system with decoherence. The environment is modelled as two fluctuators in each set with different fluctuation strengths.

These results show that the effect of the highest fluctuator coupling strength in the system dominates its evolution. Oscillations are suppressed as in the simulation with only one fluctuator at $g = 700 \text{ cm}^{-1}$, figures 25c and 26c. This means that, in the presence of a fluctuator which induces high fluctuations (high g), adding another fluctuator to the same set, with a lower fluctuation strength, does not significantly change the dynamics of the system.

4.2.3 Comparisons of the classical algorithms and the quantum algorithm

In this subsection, comparisons between the Haken-Strobl model, introduced in the subsection 2.3.5 by equation (54) (in the Lindblad form), the Bloch-Redfield equation (22) and the quantum algorithm developed in this work will be discussed.

The classical algorithms (Lindblad and Bloch-Redfield equations) were solved using an open quantum systems framework, *Qutip* [45]. The solving methods for the Bloch-Redfield equation and the Lindblad equation are presented in the *Qutip User Guide*, in the following URL: <http://qutip.org/documentation.html>.

The Bloch-Redfield equation has been implemented with an identical environment to the one used in the quantum algorithm, i.e. with the spectral density given by equation (82), which was directly inputted to the time differential equation solver, as demonstrated in the *Qutip User Guide*. The derivation of the Bloch-Redfield equation in the subsection 2.2.3 is similar to the one presented in *Qutip User Guide*, where the main differences lie in choosing two interaction operators $S_l = |l\rangle\langle l|$, $l = 0, 1$ which are the projection operators in the site basis and the function $\text{Re}[\tilde{C}(w)] = F(w)$ (the imaginary part was neglected as suggested in *Qutip User Guide*), where $F(w)$ denotes the fluctuator spectral density in equation (82).

The Lindblad equation has been solved with the only environmental parameter being the dephasing rate. Therefore, for each quantum simulation performed, a fitting process is employed by adjusting the dephasing rate, so that the system's evolution in both classical and quantum simulations have similar behaviours. This enables one to perform a direct comparison between both theories and to find the actual dephasing rate of the modeled environment over the various regimes implemented in this work.

The following results, figs. 30 and 31, compare the results from the classical algorithms previously introduced and the quantum algorithm developed in this work, by varying the fluctuation strength, for the near-resonant and non-resonant systems, respectively. Each set of the environment contains only one fluctuator with switching rate $\gamma = 125 \text{ THz}$. The dephasing rate γ_{deph} in the Lindblad equation is adjusted by observing the behaviour of the system under the influence of a specific fluctuation strength g .

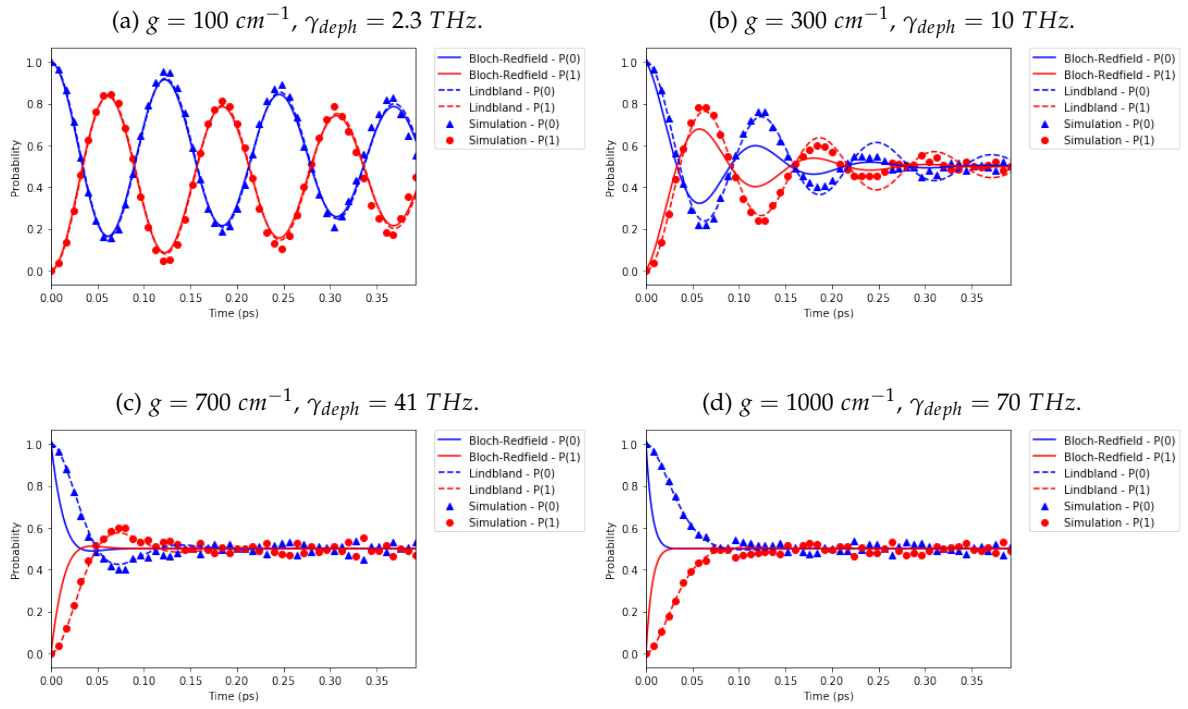


Figure 30: Comparison of the evolution dynamics obtained by employing the quantum and classical algorithms for the near-resonant system.

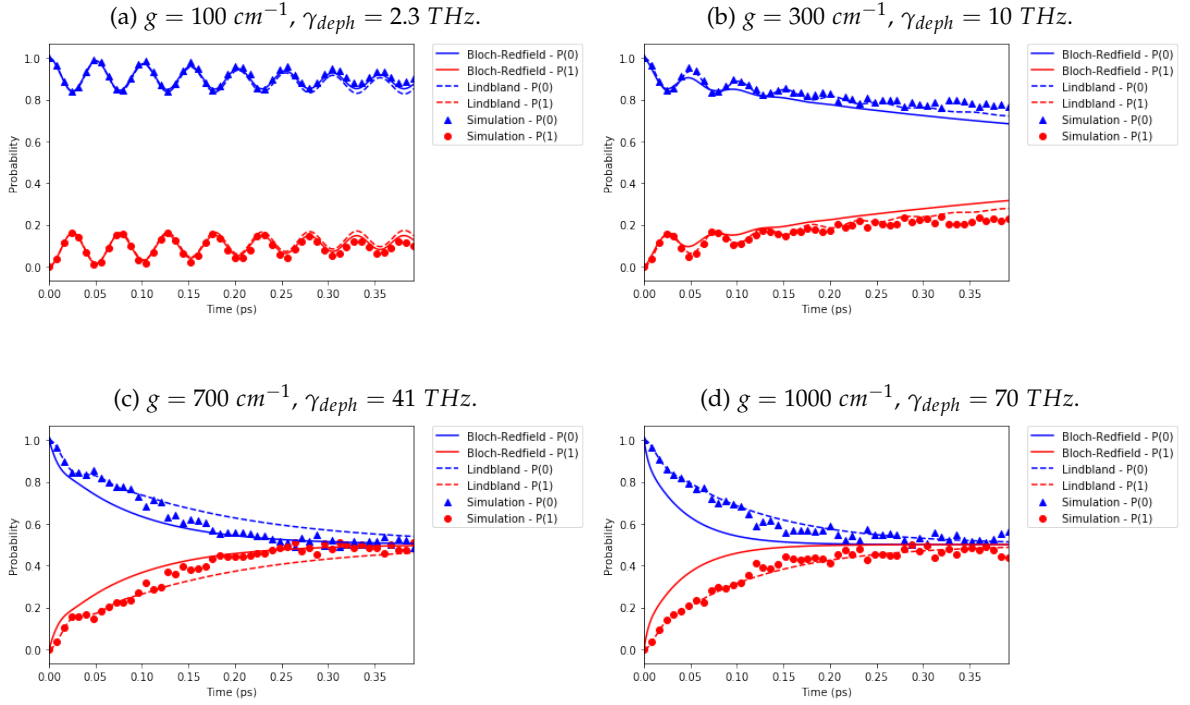


Figure 31: Comparison of the evolution dynamics obtained by employing the quantum and classical algorithms for the non-resonant system.

Overall, the classical algorithms show evolution behaviours similar to the quantum algorithm. However it can be observed, in figures 30 and 31, that by increasing g , the Bloch-Redfield equation shows a stronger quantum beating suppression than the quantum algorithm. This can be related to the mathematical formalism employed to produce the Bloch-Redfield equation, which is different from the quantum algorithm formalism. However, some formal similarities still hold in the quantum algorithm, such as the approximation of a constant environment (at thermal equilibrium) throughout time, i.e. $\rho_E(t) \approx \rho_E$, [12]. The quantum algorithm not only neglects dissipation in the system just as the Redfield equation does, but the environment's density matrix variation is also neglected, i.e. it does not change over time, which is the same approximation used to derive the Redfield equations [12]. Thus, the quantum algorithm used here is valid only in the no dissipation regime, i.e. in the weak system-environment interaction regime (weak with respect to the reorganization energy, where its dynamics were neglected). Therefore, using the Markovian approximation and implementing a pure-dephasing model, the simulation does not capture any dissipative process, i.e. any reorganization dynamics. Förster theory implicitly involves energy dissipation hence, the Förster regime *could not be simulated* in this work.

The Lindblad equation shows results more similar to the quantum algorithm than the Bloch-Redfield equation. In fact, increasing the dephasing rate in the Lindblad formalism, corresponds to an increasing fluctuation strength in the quantum algorithm, which by its own corresponds to an higher suppression of the quantum beating, as theoretically predicted [29]. For a range of fluctuation strengths, in the quantum algorithm, of $[100, 1000] \text{ cm}^{-1}$, the corresponding dephasing rate range in the Haken-Ströbl model lies in the $\sim [2.3, 70] \text{ THz}$ range.

The comparison between the classical and quantum algorithms by varying the switching rate presents some challenges. The Lindblad equation lacks environmental parameters to perform a direct comparison when it comes to switching rates, because by varying the dephasing rate, the non-uniformity of the populations dynamics, seen in the quantum algorithm results (figures 27 and 28), would not be observed in this classical algorithm. The Bloch-Redfield algorithm shows the behaviour opposite to that predicted by the quantum algorithm, when one increases or decreases γ . Decreasing γ , it is expected the quantum beating (oscillations) to last for more time, as supported by the quantum algorithm results. In fact, when the rate decreases, the Bloch-Redfield equation suppresses the oscillations. Increasing the rate, the Bloch-Redfield equation holds the quantum beating for longer. However, when $\gamma \sim 125 \text{ THz}$, both quantum and Bloch-Redfield algorithms show a similar behaviour. This is a strange and probably nonphysical behaviour of the classical algorithm. Decreasing the switching rate should allow the system to keep its coherence for longer times and in the limit of $\gamma = 0$, the system should not feel any *dephasing action* from outer systems. This is not verified in the Bloch-Redfield equation results. In fact, at $\gamma = 0$, the Bloch-Redfield algorithm does not provide a valid system's density matrix. It is known that the Bloch-Redfield equation, sometimes, does not give a correct system's density matrix [13], therefore it is hypothesized this classical algorithm only gives a valid system's evolution in the $\sim 125 \text{ THz}$ switching rate regime. In a recent paper [18], some issues with the Bloch-Redfield equation have been addressed, such as the non-validity of the system's density matrix in some physical models. In particular, a non-Markovian spectral density can be related to the fluctuator spectral density at small switching rates in this work, which can yield an invalid system's density matrix using the Bloch-Redfield equation.

Changing the number of fluctuators in the Bloch-Redfield equation, i.e. adding Lorentzian terms to the spectral density (82) with different fluctuation strengths and equal switching rate $\gamma = 125 \text{ THz}$, gives similar results to the quantum algorithm simulations, fig. 29.

Information on the classical complexity of the Bloch-Redfield and Lindblad equation solvers in *Qutip* has not been found, thus a comparison of the computational complexity between the classical and the quantum algorithms could not be made.

4.2.4 Final considerations

As discussed above, the quantum algorithm created in this work, is only valid in the weak system-environment interaction regime, with respect to the reorganization energy λ . This coupling is not the same as the fluctuation strength (or the fluctuator-molecule coupling strength) g . While g determines only the fluctuation magnitude of dephasing, λ contains information about the reorganization dynamics of the molecule excited state, i.e. dissipation, as well as the dephasing effect. Furthermore, by neglecting the reorganization dynamics (as previous approaches also did [28, 29]), it is being considered that the reorganization of the nucleus timescale is very high relatively to the free energy transport evolution timescale, i.e. $\tau_B \gg J^{-1}$ as discussed in subsection 2.3.3. This essentially means, once again, that this is the *non-dissipative, coherent* regime.

It is also worth noticing that the switching rate is not the same as the dephasing rate. The latter is the rate at which the system and the environment interact, while the switching rate gives the rate at which the fluctuator changes its fluctuation value. In the developed model, the fluctuators are always in interaction with the system and the switching rate only controls the *randomness rate*. The fluctuator strength plus the switching rate define the dephase, which, after all, is not so simple as the Haken-Ströbl model shows (which uses the Lindblad equation, with only the dephasing rate as an environmental parameter). All in all, the decoherence in the quantum algorithm is modelled as dephasing, which is applied to the system as Gaussian energy fluctuations. From the quantum information point of view, the fluctuations relate to classical random walks applied to each molecule's excited state.

The results provided for the quantum algorithm are very similar to those presented in a recent paper [39], where a quantum analog simulation using Nuclear Magnetic Resonance (NMR) is reported. The timescale of the energy transfer in these paper results, is not the same as in the quantum algorithm results, because the authors of the paper scaled down the energies.

The quantum gate complexity of this algorithm increases approximately in a polynomial way with the number of molecules and the qubit resources increase logarithmical with the number of molecules in the system. The complexity of the rotation decomposition matrices is the most costly operation in the algorithm, which is one of the main disadvantages of this algorithm. Another disadvantage of using this algorithm is that it requires a specific number of runs to correctly average the results, although this number is *not dependent on the number of molecules*. The re-run process is a consequence of implementing dephasing directly at the system's qubits. These two disadvantages, together with the use of the iterated Trotter product formula, only allows the system to be simulated with a few molecules in the current quantum computers, or even quantum simulators.

The advantages of using the quantum algorithm consist of providing a direct implementation of the evolution operators in the system. This does not require great calculations and it is an intuitive method to be employed. Furthermore, the implementation of dephasing in this algorithm, as fluctuations, is very focused in the actual environment interactions on the system, such as performing classical random walks in the energy spectrums. As a comparison, in the paper [46], a classical algorithm was developed to calculate random walks in the energies of the molecules which is not as intuitive as the quantum algorithm developed in this work.

As a final note, the quantum algorithm results on the near-resonance regime, show how coherent energy transport can, indeed, be more efficient than incoherent energy transport (diffusive dynamics), as affirmed by others [4, 25, 16]. The quantum beating, provides the acceptor molecule to have, momentarily, a high probability of being excited. This probability can be higher than the final thermal equilibrium state occupation, which in this work, at very high temperatures, is $\frac{1}{2}$ (50%). Therefore, in a few oscillations, the acceptor molecule can trap the energy in it (the trapping efficiency depends on the trapping rate of the molecule [29]). In diffusive dynamics, i.e. incoherent regime (high g), however, the highest probability of having the excitation in the acceptor molecule is the thermal equilibrium state probability (50%) which is smaller than the 90% achieved in the *full-coherent* regime (no decoherence). Thus, it can be observed how coherence can enhance the energy transport in near-resonant systems. In non-resonant systems, quantum beating does not significantly enhance the energy transfer, because the momentarily high probability induced by the oscillations is lower than the thermal equilibrium state probability. Therefore, in this scenario, a fast thermal relaxation is desired (diffusive dynamics), so that the acceptor molecule reaches the 50% probability of being excited, the fast as possible. Concluding, in photosystems, near-resonant and non-resonant subsystems are present, therefore a balance between quantum beating and diffusive dynamics, i.e. coherent and incoherent regimes, is necessary to have the most efficient energy transport. This can be translated to the requirement of a balanced proportion of dephase injected in the system, so that coherent and incoherent transport regimes can be present as stated in the subsection 2.3.5 .

4.3 SUMMARY

In this chapter, the computational setup of the quantum circuits used in the simulations was presented. The results were gathered under various resonance regimes, as well as several environmental regimes. The discussion of the results was given, followed by a comparison between the developed quantum algorithm and some existent classical algorithms. Finally, some remarks about the proposed quantum algorithm were presented.

CONCLUSION

5.1 CONCLUSIONS

The quantum simulation of photosynthesis, focused on the energy transport in photosystems, has been implemented in a quantum computer as an isolated system. Coherence has been observed to be present, in the form of *quantum beating*. Aiming to produce a simulation of real photosystems, *decoherence*, in the form of pure-dephasing, was artificially introduced in the system. This provided answers about how coherence can last for timescales which can significantly affect energy transfer over molecules. These questions are much debated within the scientific community [4] due to the fact that biological environments are too noisy so that quantum effects can hardly play any role [3]. In fact, coherence can enhance the energy transfer if present in the right proportion [4]. This was demonstrated in this work, by implementing a very high temperature environment composed by *fluctuators*. Such environments can indeed simulate real photosystems, in the limit of a *coherent* regime. This scenario is suitable to simulate in a quantum computer, where dephasing, the ultimate frontier between the quantum and classical world, limits the time quantum effects last in the system. Unfortunately, the algorithm proposed and implemented in this work required some heavy computational resources to be implemented in current real quantum computers. Therefore a quantum simulator was used to demonstrate the results. Classical algorithms were compared with the proposed quantum algorithm for verification of the results. The quantum algorithm, formulated in the form of a quantum circuit, provided a way to simulate quantum systems in a direct approach to the Hamiltonians without the need to use advanced and complicated calculations as classical algorithms require. Furthermore, the environment derived in this dissertation, provided a clear understanding of the interactions between the system and the biological environment, using energy fluctuations, in the energy transport regime where quantum phenomena are relevant.

The state-of-art approaches on photosynthesis are currently in an advanced stage, where various quantum models explain their properties and dynamics. The algorithm proposed in this dissertation opened up some possibilities for quantum computation in the field. However, quantum simulation is still at an underdeveloped stage, where open quantum

systems simulation still requires a breakthrough to be widely applied to more general transport regimes or biological systems.

5.2 FUTURE WORK

The current knowledge about quantum effects in photosynthesis, already goes beyond the regime simulated in this work, where non-Markovian dynamics are currently simulated in classical computers as well as real environments, which induce dissipation and dephasing in the system. These processes, are not currently possible to be simulated in real quantum computers where more knowledge about quantum software, specifically, open quantum systems simulation, is required. To this end, research on the creation of new quantum algorithms for simulating open systems should be, in the future, addressed and possibly applied to the photosynthesis.

Quantum effects in photosynthesis, particularly in the energy transport, are of extreme importance, where solar energy harvesting can be a main application of discoveries in this field. For instance, artificial biological systems have started to be investigated [47] and a clear understanding of the microscopic biological structures and dynamics in photosynthesis is fundamental to create biomimetic light-harvesting devices. Therefore, in a future work, it could be further investigated how quantum effects may play a role in such artificial devices.

Quantum simulation and quantum effects in biology seem to be as emergent fields with plenty of challenges as well as quantum phenomena still not fully understood. Therefore, both offer several open problems which make them very attractive for future research.

BIBLIOGRAPHY

- [1] Mark Lundstrom. "Moore's law forever?" In: *Science* 299.5604 (2003), pp. 210–211.
- [2] Richard P Feynman. "Quantum mechanical computers." In: *Found. Phys.* 16.6 (1986), pp. 507–532.
- [3] Masoud Mohseni et al. *Quantum effects in biology*. Cambridge University Press, 2014.
- [4] Aurélia Chenu and Gregory D Scholes. "Coherence in energy transfer and photosynthesis". In: *Annual review of physical chemistry* 66 (2015), pp. 69–96.
- [5] Khan Academy. *Photosynthesis*. URL: <https://www.khanacademy.org/science/biology/photosynthesis-in-plants>.
- [6] David G. Nicholls and Stuart J. Ferguson. *Bioenergetics* 2. Academic Press, 1992.
- [7] Melih Şener et al. "Photosynthetic vesicle architecture and constraints on efficient energy harvesting". In: *Biophysical journal* 99.1 (2010), pp. 67–75.
- [8] R Van Grondelle. "Excitation energy transfer, trapping and annihilation in photosynthetic systems". In: *Biochimica et Biophysica Acta (BBA)-Reviews on Bioenergetics* 811.2 (1985), pp. 147–195.
- [9] V Sundström et al. "Excitation-energy transport in the bacteriochlorophyll antenna systems of *Rhodospirillum rubrum* and *Rhodobacter sphaeroides*, studied by low-intensity picosecond absorption spectroscopy". In: *Biochimica et Biophysica Acta (BBA)-Bioenergetics* 851.3 (1986), pp. 431–446.
- [10] OpenStax. *The Light-Dependent Reactions of Photosynthesis: Figure 8*. Copyright Holders: Rice University, License: Creative Commons Attribution License (by 4.0). 2012.
- [11] Michael A Nielsen and Isaac Chuang. *Quantum computation and quantum information*. 2002.
- [12] 22.51 Course Notes, Chapter 8: Open Quantum Systems. MIT OpenCourseWare. Massachusetts Institute of Technology, 2012. URL: https://ocw.mit.edu/courses/nuclear-engineering/22-51-quantum-theory-of-radiation-interactions-fall-2012/lecture-notes/MIT22_51F12_Ch8.pdf.
- [13] Heinz-Peter Breuer, Francesco Petruccione, et al. *The theory of open quantum systems*. Oxford University Press on Demand, 2002.
- [14] Hida Nakazato et al. "Solution of the Lindblad equation in the Kraus representation". In: *Physical Review A* 74.6 (2006), p. 062113.

- [15] Gregory S Engel et al. "Evidence for wavelike energy transfer through quantum coherence in photosynthetic systems". In: *Nature* 446.7137 (2007), p. 782.
- [16] Gitt Panitchayangkoon et al. "Long-lived quantum coherence in photosynthetic complexes at physiological temperature". In: *Proceedings of the National Academy of Sciences* 107.29 (2010), pp. 12766–12770.
- [17] Elisabetta Collini et al. "Coherently wired light-harvesting in photosynthetic marine algae at ambient temperature". In: *Nature* 463.7281 (2010), pp. 644–647.
- [18] Jan Jeske et al. "Bloch-Redfield equations for modeling light-harvesting complexes". In: *The Journal of chemical physics* 142.6 (2015), p. 064104.
- [19] Derek Abbott, Paul CW Davies, and Arun K Pati. *Quantum aspects of life*. World Scientific, 2008.
- [20] Gert-Ludwig Ingold. "Dissipative quantum systems". In: (1998).
- [21] Klaus Hornberger. "Introduction to decoherence theory". In: *Entanglement and decoherence*. Springer, 2009, pp. 221–276.
- [22] Th Förster. "10th Spiers Memorial Lecture. Transfer mechanisms of electronic excitation". In: *Discussions of the Faraday Society* 27 (1959), pp. 7–17.
- [23] David L Dexter. "A theory of sensitized luminescence in solids". In: *The Journal of Chemical Physics* 21.5 (1953), pp. 836–850.
- [24] Sarah Mostame et al. "Quantum simulator of an open quantum system using superconducting qubits: exciton transport in photosynthetic complexes". In: *New Journal of Physics* 14.10 (2012), p. 105013.
- [25] Yuan-Chung Cheng, Gregory S Engel, and Graham R Fleming. "Elucidation of population and coherence dynamics using cross-peaks in two-dimensional electronic spectroscopy". In: *Chemical Physics* 341.1-3 (2007), pp. 285–295.
- [26] Dara PS McCutcheon and Ahsan Nazir. "Consistent treatment of coherent and incoherent energy transfer dynamics using a variational master equation". In: *The Journal of chemical physics* 135.11 (2011), p. 114501.
- [27] Ming-Jie Tao et al. "Coherent and incoherent theories for photosynthetic energy transfer". In: *arXiv preprint arXiv:1907.06528* (2019).
- [28] Hermann Haken and Gert Strobl. "An exactly solvable model for coherent and incoherent exciton motion". In: *Zeitschrift für Physik A Hadrons and nuclei* 262.2 (1973), pp. 135–148.
- [29] Patrick Rebentrost et al. "Environment-assisted quantum transport". In: *New Journal of Physics* 11.3 (2009), p. 033003.

- [30] Nathan Wiebe et al. "Higher order decompositions of ordered operator exponentials". In: *Journal of Physics A: Mathematical and Theoretical* 43.6 (2010), p. 065203.
- [31] Benjamin DM Jones et al. "Optimising trotter-suzuki decompositions for quantum simulation using evolutionary strategies". In: *Proceedings of the Genetic and Evolutionary Computation Conference*. 2019, pp. 1223–1231.
- [32] Dominic W Berry et al. "Simulating Hamiltonian dynamics with a truncated Taylor series". In: *Physical review letters* 114.9 (2015), p. 090502.
- [33] Guang Hao Low and Isaac L Chuang. "Hamiltonian simulation by qubitization". In: *Quantum* 3 (2019), p. 163.
- [34] Andrew M Childs et al. "Toward the first quantum simulation with quantum speedup". In: *Proceedings of the National Academy of Sciences* 115.38 (2018), pp. 9456–9461.
- [35] Zixuan Hu, Rongxin Xia, and Sabre Kais. "A quantum algorithm for evolving open quantum dynamics on quantum computing devices". In: *Scientific Reports* 10.1 (2020), pp. 1–9.
- [36] Hefeng Wang, Sahel Ashhab, and Franco Nori. "Quantum algorithm for simulating the dynamics of an open quantum system". In: *Physical Review A* 83.6 (2011), p. 062317.
- [37] Chi-Kwong Li, Rebecca Roberts, and Xiaoyan Yin. "Decomposition of unitary matrices and quantum gates". In: *International Journal of Quantum Information* 11.01 (2013), p. 1350015.
- [38] Brett Giles and Peter Selinger. "Exact synthesis of multiqubit Clifford+ T circuits". In: *Physical Review A* 87.3 (2013), p. 032332.
- [39] Bi-Xue Wang et al. "Quantum simulation of photosynthetic energy transfer". In: *arXiv preprint arXiv:1801.09475* (2018).
- [40] Jan A Leegwater. "Coherent versus incoherent energy transfer and trapping in photosynthetic antenna complexes". In: *The Journal of Physical Chemistry* 100.34 (1996), pp. 14403–14409.
- [41] Julia Adolphs and Thomas Renger. "How proteins trigger excitation energy transfer in the FMO complex of green sulfur bacteria". In: *Biophysical journal* 91.8 (2006), pp. 2778–2797.
- [42] Carsten Olbrich et al. "Quest for spatially correlated fluctuations in the FMO light-harvesting complex". In: *The Journal of Physical Chemistry B* 115.4 (2011), pp. 758–764.
- [43] Siddhartha Sinha and Peter Russer. "Quantum computing algorithm for electromagnetic field simulation". In: *Quantum Information Processing* 9.3 (2010), pp. 385–404.

- [44] Andrew Cross. “The IBM Q experience and QISKit open-source quantum computing software”. In: *Bulletin of the American Physical Society* 63 (2018).
- [45] J Robert Johansson, PD Nation, and Franco Nori. “QuTiP: An open-source Python framework for the dynamics of open quantum systems”. In: *Computer Physics Communications* 183.8 (2012), pp. 1760–1772.
- [46] Masoud Mohseni et al. “Environment-assisted quantum walks in photosynthetic energy transfer”. In: *The Journal of chemical physics* 129.17 (2008), 11B603.
- [47] Lin Liu and Seokheun Choi. “Self-sustainable, high-power-density bio-solar cells for lab-on-a-chip applications”. In: *Lab on a Chip* 17.22 (2017), pp. 3817–3825.
- [48] Artur K Ekert et al. “Direct estimations of linear and nonlinear functionals of a quantum state”. In: *Physical review letters* 88.21 (2002), p. 217901.
- [49] Rodney Doyle Van Meter III. “Architecture of a quantum multicomputer optimized for Shor’s factoring algorithm”. In: *arXiv preprint quant-ph/0607065* (2006).



ROTATION DECOMPOSITION OF THE BASIS TRANSFORMATION MATRICES

The notion of two-level unitary matrix is primarily introduced following [11]. Such type of matrix consists of a $d \times d$ unitary matrix where only the element in the j column and k row, the element in the k row and j column, the element in the j column and j row and the element in the k column and k row can have a value different from 0 or 1. The remaining diagonal terms of the matrix must be 1 and all the other off-diagonal elements must be 0. Note that the matrix must be unitary. Examples of a 3×3 two-level matrix are

$$U = \begin{pmatrix} a & 0 & b \\ 0 & 1 & 0 \\ c & 0 & d \end{pmatrix} \quad (113)$$

or

$$U = \begin{pmatrix} 1 & a & b \\ 0 & c & d \\ 0 & 0 & 1 \end{pmatrix} \quad (114)$$

The rotation decomposition algorithm [11] is now introduced. It will be given an example of a decomposition and then the generalization to other matrices will be explained. Consider a 3×3 unitary matrix U given as

$$U = \begin{pmatrix} a & d & g \\ b & e & h \\ c & f & j \end{pmatrix} \quad (115)$$

to be decomposed in products of two-level unitary matrices, such that

$$U_3 U_2 U_1 U = I \quad (116)$$

or, equivalently

$$U = U_1^\dagger U_2^\dagger U_3^\dagger \quad (117)$$

U_n is an unitary two-level matrix, thus its transconjugate is also an unitary two-level matrix. The procedure to find these matrices is the following: create and multiply a matrix U_1 by U that sets b equal to 0. If b is already 0, then choose $U_1 = I$. If one multiplies U_1U , then

$$U_1U = \begin{pmatrix} a' & d' & g' \\ 0 & e' & h' \\ c' & f' & j' \end{pmatrix} \quad (118)$$

Next, change c' in U_1U to 0 by multiplying U_2 by U_1U . If c' is already 0, then choose

$$U_2 = \begin{pmatrix} a'^* & 0 & 0 \\ 0 & 1 & 0 \\ 0 & 0 & 1 \end{pmatrix} \quad (119)$$

where the superscript $*$ denotes the conjugate value. The resulting matrix is

$$U_2U_1U = \begin{pmatrix} 1 & d'' & g'' \\ 0 & e'' & h'' \\ 0 & f'' & j'' \end{pmatrix} \quad (120)$$

Since U_2 , U_1 and U are unitary, then U_2U_1U is also unitary so $d'' = 0$ and $g'' = 0$ since the first row of U_2U_1U must have norm 1. Finally the next step is to choose

$$U_3 = \begin{pmatrix} 1 & 0 & 0 \\ 0 & e''^* & h''^* \\ 0 & f''^* & j''^* \end{pmatrix} \quad (121)$$

and multiply this matrix by U_2U_1U so that $U_3U_2U_1U = I$ or, equivalently, $U = U_1^\dagger U_2^\dagger U_3^\dagger$.

This process can be generalized for a $d \times d$ unitary matrix U . Matrices U_1, \dots, U_{d-1} are multiplied such that $U_{d-1} \dots U_1U$ has a 1 in the top left corner element and all zeros in the respective column and row. Then, this process is repeated for the $[d-1] \times [d-1]$ unitary matrix in the lower right hand corner of $U_{d-1} \dots U_1U$. This way, every two-level unitary matrix U_i will be found. The final result for a $d \times d$ matrix is $U = U_1^\dagger \dots U_k^\dagger$ where U_i^\dagger is a two-level unitary matrix and $k \leq (d-1) + (d-2) + \dots + 1 = d(d-1)/2$. In a system with n qubits, U can be decomposed at most in $2^{n-1}(2^n - 1)$ two-level unitary matrices [11].

The previous described decomposition algorithm is available in Quipper (*newsynth* library). It decomposes the matrix U in a multiplication of two-level matrices R_{Z-X} and one-level matrices $e^{i\theta}$. The unitary square R_{Z-X} matrix is given as

$$R_{Z-X}(\delta, \gamma) = \begin{pmatrix} I & \vdots & \mathbf{o} & \vdots & \mathbf{o} \\ \dots & e^{-i\delta/2}\cos(\gamma/2) & \dots & -ie^{-i\delta/2}\sin(\gamma/2) & \dots \\ \mathbf{o} & \vdots & I & \vdots & \mathbf{o} \\ \dots & -ie^{i\delta/2}\sin(\gamma/2) & \dots & e^{i\delta/2}\cos(\gamma/2) & \dots \\ \mathbf{o} & \vdots & \mathbf{o} & \vdots & I \end{pmatrix} \quad (122)$$

Where bold \mathbf{o} are square 0-matrices, the dots denote 0 columns or rows and I is the identity matrix. The unitary square one-level matrix $e^{i\theta}$ is

$$\begin{pmatrix} I & \vdots & \mathbf{o} \\ \dots & e^{i\theta} & \dots \\ \mathbf{o} & \vdots & I \end{pmatrix} \quad (123)$$

A basis transformation matrix T with dimensions $2^n \times 2^n$, where n is the number of system qubits, is decomposed, using Quipper, into two-level unitary matrices R_{Z-X} and one-level unitary matrices $e^{i\theta}$. The input of the program is the basis transformation matrix and it outputs the order of application of the $R_{Z-X}(\delta, \gamma)$ and $e^{i\theta}$ matrices, each matrix angles γ , δ and θ , and for each two-level matrix, the program outputs the j and k numbers (where the values which can be different from 0 and 1 in the matrices (122) and (123) are located). These numbers are important so that, using Gray code, each two-level matrix R_{Z-X} can be decomposed in a sequence of gates composed by X-Pauli, $C^{n-1}NOT$'s and the gate, defined below, $C^{n-1}U(\delta, \gamma)$. For the one-level matrices, only the number j is outputted. These matrices can be decomposed in a multiplication of X-Pauli and $C^n R_Z(\theta)$ gates.

$C^{n-1}U$ gates must be in the form

$$C^{n-1}U(\delta, \gamma) = |\Psi\rangle \langle \Psi|_c \otimes I_t + |11..1\rangle \langle 11..1|_c \otimes U_t(\delta, \gamma) \quad (124)$$

where $|11..1\rangle_c$ is the state of all control qubits at $|1\rangle$ and $|\Psi\rangle_c$ represent all the other control qubit states. The control qubits are the $n - 1$ system's qubits and the target is the remaining system's qubit. U is defined as

$$U(\delta, \gamma) = \begin{pmatrix} e^{-i\delta/2}\cos(\gamma/2) & -ie^{-i\delta/2}\sin(\gamma/2) \\ -ie^{i\delta/2}\sin(\gamma/2) & e^{i\delta/2}\cos(\gamma/2) \end{pmatrix} \quad (125)$$

$C^{n-1}U(\delta, \gamma)$ can be found by the product $C^{n-1}R_Z(\delta)C^{n-1}R_X(\gamma)$ where $R_X(\gamma) = U_3(\gamma, -\pi/2, \pi/2)$ in Qiskit. Gray code can be now introduced [11, 37].

After performing the previous rotation decomposition for an unitary matrix T with dimensions 4×4 , the basis transformation matrix is decomposed in two-level unitary matrices and one-level unitary matrices, both with dimensions 4×4 for a system with four molecules. The goal is to decompose the two-level unitary matrices into matrices 2×2 as the gates in matrix form (124) with $n = 2$ as well as X-Pauli and CNOT gates. In view of that, numbers j and k of each matrix, which the program outputs, are used. These numbers can be seen as system's states. For instance, the first column, i.e. $j = 0$, is the state $|00\rangle$. The second column, i.e. $j = 1$, is the state $|01\rangle$ and so on up to the column $j = 3$ which is the state $|11\rangle$. This process is also applied to rows. Therefore, when the program outputs numbers j and k , they will be equal to some state $|j\rangle$ and some state $|k\rangle$, respectively. The procedure is the following: consider as if the initial state of the system is $|j\rangle$ and perform a sequence of quantum gates so that the initial state is changed to a final state $|k\rangle$. The last change, i.e. the last step which changes some state $|\Phi\rangle$ to the state $|k\rangle$, is performed by applying a CU gate (because for a system with four molecules, entails $n = 2$ in the matrix (124)). Then the process is reversed by applying all the changes corresponding to $|\Phi\rangle \rightarrow |j\rangle$. Consider a R_{Z-X} matrix which outputs the number $j = 0$ and $k = 3$. This is equal to states $|00\rangle$ and $|11\rangle$, respectively, where the notation $|q_0\rangle \otimes |q_1\rangle$ is used from now on, so that q_0 is the qubit 0 and q_1 is the qubit 1. Therefore, the global change that needs to be performed is $|00\rangle \rightarrow |11\rangle$. First, do the change $|00\rangle \rightarrow |01\rangle$ in the quantum circuit. This is done by applying a X-Pauli gate in the qubit 0, followed by a CNOT with control at qubit 0 and target at qubit 1 followed by another X-Pauli gate applied to qubit 0. The system's state can be thought to be now $|01\rangle$. Then, the second step is to do the change $|01\rangle \rightarrow |11\rangle$, but because it is the last step to be done, one uses a CU gate with control at the qubit 1 and target at qubit 0. Then, the process is reversed by applying again, the step $|00\rangle \rightarrow |01\rangle$. In figure 33, it is demonstrated the implementation of this example.

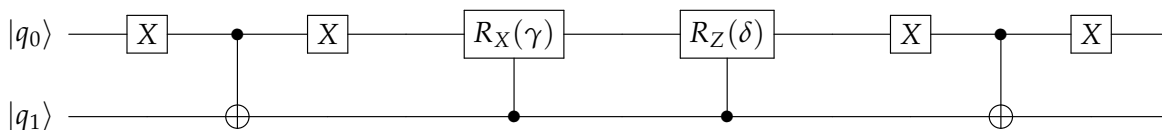


Figure 32: Implementation of the two-level unitary matrix decomposition example. The gate $CU(\delta, \gamma)$ is performed as $CR_Z(\delta)CR_X(\gamma)$.

To the one-level unitary matrices, the Quipper program outputs only one number j and the angle θ . This number j corresponds to the j column and the j row of the matrix (123), where the element $e^{i\theta}$ is, i.e. some state $|j\rangle$ in which the phase is applied. This matrix is easily converted to a quantum circuit by having an ancilla qubit initialized at $|1\rangle$. The procedure is the following: apply the change $|j\rangle \rightarrow |11..1\rangle$ to the system's qubits using

X-Pauli gates, where the state $|11..1\rangle$ denotes all the qubit states at $|1\rangle$. Then a $C^n R_Z$ with controls at the n system qubits and target at an ancilla qubit, initialized at $|1\rangle$, is applied. The process is reversed by implementing the same previous applied X-Pauli gates. Consider as an example, an one-level unitary matrix with dimensions 4×4 where the term $e^{i\theta}$ is in the $j = 2$ column and row. Then this column and row represent state $|10\rangle$, where the used notation is $|q_0\rangle \otimes |q_1\rangle$. The following circuit is implemented to represent this gate: apply a X-Pauli gate to the qubit 1, so the change $|10\rangle \rightarrow |11\rangle$ is employed. Then, a decomposition of the gate $C^2 R_Z$ is implemented. A Toffoli gate with controls at qubits 0 and 1 and target at an ancilla qubit, which was initialized at state $|0\rangle$, is applied. Then, a $CR_Z(2\theta)$ is applied with control at the ancilla qubit initialized at $|0\rangle$ and target at the other ancilla which was initialized at $|1\rangle$. As explained before, the coefficient 2 comes from the implementation of the gate $R_Z(\theta)$ in Qiskit, which is $e^{-i\frac{\theta Z}{2}}$. Finally, the circuit is reversed, by applying the Toffoli gate followed by the X-Pauli gate at the qubit 1 again. In figure 33, the implementation of this example can be visualized.

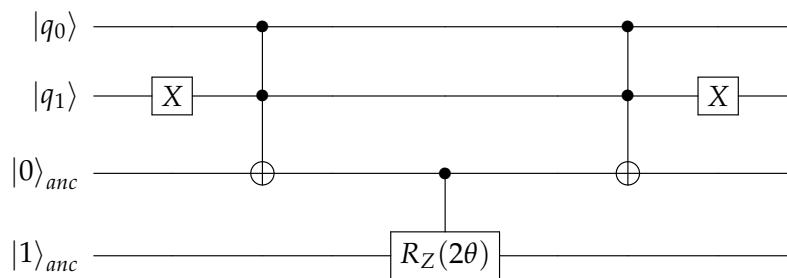


Figure 33: Implementation of the one-level unitary matrix example. The Toffoli gates plus the CR_Z gate denote the decomposition of the $C^2 R_Z$ gate.

The ancilla initialized at $|1\rangle$ should be the same used in the implementation of the system Hamiltonian evolution operator, as illustrated in figure 7, so that the minimum number of qubits are utilized.

B

A DIFFERENT APPROACH TO THE ARTIFICIAL DECOHERENCE INJECTION

This appendix discusses an algorithm which considers the system as an open system interacting with a bath. Some comments have been written about the wrong physical assumptions which were made, unwary, in the development of this algorithm.

The open quantum system (molecule system) is assumed to interact with a bath. Therefore, the Hilbert space of the overall system will be $\mathcal{H} = \mathcal{H}_S \otimes \mathcal{H}_B$. Assume that at the initial time $t = 0$, the density matrix is defined by $\rho(0) = \rho_S(0) \otimes \rho_B(0)$ so that somehow there are no correlations between the system and the bath at the initial time. The qubit model of the system is the one introduced in subsection 3.1.3.

B.1 QUBIT MODEL OF THE BATH

The bath is defined as a set of harmonic oscillators in thermal equilibrium. The initialization of the bath state is given following [36]. Each molecule is considered to have its own bath, with no correlations with any other baths [42]. The baths are considered identical. The absence of interactions between the normal modes of each bath allows each qubit to represent a normal mode state $|w_{k,m}\rangle$ of a bath m , i.e. the energy eigenvalue of each bath can be decomposed as

$$E(\rho_B^{th}) = \sum_k E_k |w_k\rangle \langle w_k| \quad (126)$$

The m subscript was dropped because every bath m has the same structure. The bath density matrix is then given as

$$\rho_B^{th} = \otimes_{k=1}^N \rho_k^{th} \quad (127)$$

where N is the number of qubits in a bath representing its N normal modes. Each normal mode qubit is initialized with the following density matrix

$$\rho_k^{th} = (1 - p_k) |0\rangle \langle 0| + p_k |1\rangle \langle 1| \quad (128)$$

where p_k is the probability of the normal mode qubit being in thermal equilibrium, i.e. the state $|1\rangle$ denotes a thermal equilibrium state and the state $|0\rangle$ denotes a non-thermal equilibrium state. This probability depends on the type of bath considered, i.e. a bosonic bath or a spin bath. Paper [36] employs a spin bath, however a bosonic bath (harmonic oscillator bath) is implemented in this work (in accordance with the *coherent EET* formalism introduced in subsection 2.3.2). For a bosonic bath, the probability of a phonon being found in the state $|w_k\rangle$ can be given as the mean occupation number of phonons in a single particle state ($\hbar = 1$) as $p_k = \frac{1}{e^{\beta w_k} - 1}$. The probability can only have values between 0 and 1 so the asymptotic behaviour of this probability distribution can be limited to 1 at low frequencies where the mean occupation number exceeds 1. This bath initialization can easily be applied with a $R_Y(\theta)$ gate where each bath qubit represents a normal mode of the bath w_k and

$$\sin(\theta/2) = \sqrt{\frac{1}{e^{\beta w_k} - 1}} \quad (129)$$

with an upper bound of 1 for lower frequencies, i.e. limited when $w_k \ll k_B T$, at the classical regime.

Comments:

- The initialization of the bath assumes that the thermal non-equilibrium phonons and the thermal equilibrium phonons have orthogonal states, relatively to each other. This can be a false assumption because, in a bath, there are always thermodynamic fluctuations, where the phonons can deviate from their mean energy eigenvalue.
- The mean occupation number of phonons in each state is not the probability of finding a phonon in the respective state.

B.2 THE MODEL

The system, the bath and their interaction have an unitary temporal evolution so one can implement an unitary evolution operator e^{-iHt} acting in the Hilbert space $\mathcal{H}_S \otimes \mathcal{H}_B$. Therefore, the Hamiltonian H is defined as

$$H = H_S + H_B + H_{SB} \quad (130)$$

where H_S is the system Hamiltonian, as implemented in the no-decoherence model, equation (53). H_B is the bath Hamiltonian defined as ($\hbar = 1$)

$$H_B = \sum_{m,k} w_k^{th} (a_k^\dagger a_k + \frac{1}{2}) \left| m, w_k^{th} \right\rangle \left\langle m, w_k^{th} \right|_B = \sum_k w_k^{th} (n_k^{th} + \frac{1}{2}) \left| m, w_k^{th} \right\rangle \left\langle m, w_k^{th} \right|_B \quad (131)$$

where k is the subscript for a normal mode and m the subscript for the molecule bath m . The bath Hamiltonian is considered as being applied to a normal mode in thermal equilibrium, thus

$$n_k^{th} = \frac{1}{e^{\beta \omega_k^{th}} - 1} \quad (132)$$

Comment:

- The non-equilibrium phonons must also evolve in time. Their evolution can not be employed by an operator acting in the state $|m, \omega_k^{n-th}\rangle$ (state $|0\rangle$ in the bath qubit model), because one can not know how many non-equilibrium phonons (n_k^{n-th}) exist in this state.

The system-bath interaction Hamiltonian H_{SB} is defined as

$$H_{SB} = \sum_m |m\rangle \langle m| \sum_k g_{m,k} |w_{k,m}^{th}\rangle \langle w_{k,m}^{th}|_B \quad (133)$$

There are two main reasons this interaction Hamiltonian was chosen in this form. The first is the simplicity of employing its evolution operator, which can be implemented by a simple quantum gate $C^x R_Z$. However, this requires one to admit the weak system-bath interaction approximation, because the projection operators in the Hamiltonian, applied to the bath Hilbert space do not change the normal mode qubit state up to a phase.

Comments:

- The creation and annihilation phonon operator terms, $(a_{m,k}^\dagger + a_{m,k})$, in the interaction Hamiltonian defined in Redfield equations (16), can not be simply neglected. At very high temperatures they can be substituted by a value, however they can not be removed. The implemented operator $|w_{k,m}^{th}\rangle \langle w_{k,m}^{th}|_B$, which acts in the bath Hilbert space, is an *ad-hoc* implementation. This operator can not substitute the creation and annihilation phonon operators.
- The non-equilibrium phonons can also have an interaction with the system which is not simply the application of the identity operator to the system's Hilbert space, i.e. $|w_{k,m}^{n-th}\rangle \langle w_{k,m}^{n-th}|_B \otimes I_S$.

B.3 QUANTUM CIRCUIT IMPLEMENTATION

The Hamiltonian H_{SB} does not commute with H_S (in general) thus Trotter product formula (59) must be performed so that the evolution operators of the Hamiltonians can be applied in series. The bath Hamiltonian commutes with the interaction Hamiltonian (they share

the same bath basis) and also commutes with the system Hamiltonian (commutes with the identity operator, applied in the bath Hilbert space, of $H_S \otimes I_B$), so the bath evolution operator can be applied in both basis. Thus, the following unitary evolution is applied in the quantum circuit, where Δt is the iteration time-step and N is the number of iterations

$$U(N\Delta t) = \prod_{n=1}^N \left(e^{-iH_{SB}\Delta t} e^{-iH_B\Delta t} T^\dagger e^{-iH_S\Delta t} T \right) \quad (134)$$

where T is the basis transformation matrix. This is the same transformation basis matrix implemented in the no decoherence algorithm.

The evolution operator of the bath Hamiltonian, using Trotter product formula, for one iteration is

$$e^{-iH_B\Delta t} = \prod_m \prod_k e^{-i w_{k,m}^{th} (n_k^{th} + \frac{1}{2}) \Delta t} \left| w_{k,m}^{th} \right\rangle \left\langle w_{k,m}^{th} \right| \quad (135)$$

This evolution operator can be implemented with a gate $R_Z(\theta)$ applied at each qubit representing a normal mode w_k , where $\theta = -w_k(n_k^{th} + 1/2)\Delta t$.

The evolution operator of the interaction Hamiltonian becomes, for one interaction only,

$$e^{-iH_{SB}\Delta t} = \prod_m \prod_k e^{-i g_{m,k} \Delta t} |m\rangle \langle m|_S \otimes \left| w_{k,m}^{th} \right\rangle \left\langle w_{k,m}^{th} \right|_B \quad (136)$$

The generalized implementation of $e^{-iH_{SB}\Delta t}$ is described in the following sequence:

Step 1: Select a system's state $|m\rangle$ and use X-Pauli gates to change it to $|11\dots 1\rangle$, i.e. each system's qubit state at $|1\rangle$.

Step 2: Apply a $C^{n+1}R_Z(\theta_k)$ where n is the number of system's qubits and the $+1$ comes from choosing a normal mode qubit w_k from the bath m . $\theta_k = -2g_k\Delta t$ and the target qubit is the same target ancilla used in the system Hamiltonian evolution operator.

Step 3: Once all the normal modes of the bath m have interacted, in this iteration, with the molecule m , reverse the process of step 1 by applying the same X-Pauli gates, so that $|11\dots 1\rangle \rightarrow |m\rangle$. Then proceed to step 4. If they have not all interacted, go back to step 2 and repeat the process but choose a different qubit k from the bath m for the control of the $C^{n+1}R_Z(\theta_k)$. Choose each normal mode to interact with the system only once per molecule.

Step 4: If all the molecules have interacted with the corresponding baths then the evolution operator implementation of the interaction Hamiltonian is over for this iteration, otherwise go back to the step 1 and pick another system's state $|m\rangle$ different from the ones previously picked and its corresponding bath m .

The process for the conversion of units in the exponent of the bath and interaction evolution operators is the same of the system's evolution operator. H_{SB} and H_B must have units *rad.THz*.

Coupling strengths

For a discrete distribution of frequencies one can formulate the spectral density of each bath as [36]

$$F(\omega) = \pi \sum_k g_k^2 \delta(\omega - \omega_k) \tag{137}$$

If the spectral density is a smooth continuous function over ω , the coupling strengths can be found by discretizing the function [36] as

$$\int_{\omega_k - \Delta\omega/2}^{\omega_k + \Delta\omega/2} d\omega F(\omega) \approx F(\omega) \Delta\omega = \pi g_k^2 \tag{138}$$

where the interval $\Delta\omega$ must be small enough for a precise definition of the bath. This requires a high number of qubits representing the normal modes ω_k in each bath.

B.4 MEASUREMENT

The third stage of the implementation is the measurement of the population terms in the system's density matrix (at the site basis). A quantum estimator can be used, as defined in [36] where it is illustrated in figure 34. It is required an ancilla qubit, where the measurement is performed, a set of qubits in the initialized state $|\varphi\rangle$ and, obviously, the qubits defining the system.

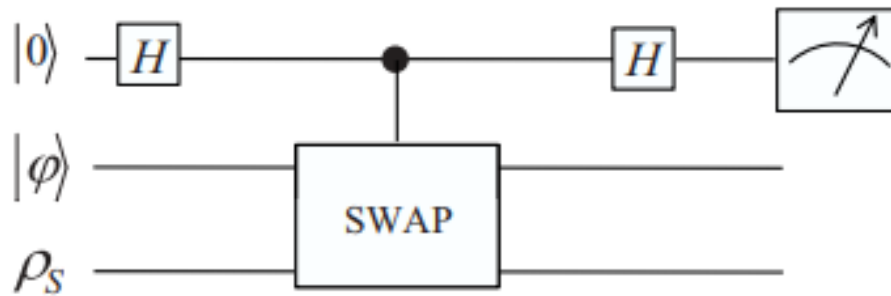


Figure 34: Quantum estimator used to measure the elements of the system density matrix. Image taken from [36].

After some mathematical derivation [48] one obtains,

$$P(0) = \frac{1}{2}(1 + \langle \varphi | \psi \rangle^2) \tag{139}$$

where $P(0)$ is the probability of measuring the state $|0\rangle$ in the ancilla qubit. If ρ_S is in a mixed state then

$$P(0) = \frac{1}{2}(1 + \langle \varphi | \rho_S | \varphi \rangle) \quad (140)$$

If one prepares the second set of qubits φ in the eigenstate $|n\rangle$ of an arbitrary operator eigenbasis $\{|n\rangle\}$, then $\rho_{nn}^S = \langle n | \rho_S | n \rangle$. This way the population terms can be found. If the real part of the coherence terms are needed, the second set of qubits φ is prepared in a state $|\varphi\rangle = (|m\rangle + |n\rangle)/\sqrt{2}$, thus $\rho_{mn}^S = \langle m | \rho_S | n \rangle$, where $|m\rangle$ is also an eigenstate of the arbitrary operator eigenbasis $\{|n\rangle\}$. The imaginary part of the coherence terms is found by setting $|\varphi\rangle = (|m\rangle + i|n\rangle)/\sqrt{2}$.

A controlled-SWAP gate or Fredkin gate can be decomposed as in figure 35. In a four molecule system, a controlled SWAP gate is performed with target qubit at the first qubit of the φ set of qubits and at the first qubit of ρ_S . Then another controlled SWAP gate is performed, in sequence, with target qubit at the second qubit of the φ set of qubits and at the second qubit of ρ_S .

In a four molecule system, four implementations of this algorithm with different φ states must be performed, so all the population terms of the system's density matrix can be known. The code can be parallelized in four different processes in the quantum simulator using *Python multiprocessing* library to faster simulation executions. Concurrency control can also be implemented with the use of a *lock* to agglomerate the results, so they can be printed, and to read the input parameters in each process. The first algorithm is sent to one process with the state $|\varphi\rangle = |00\rangle$, then at the second process another algorithm is executed with the state $|\varphi\rangle = |01\rangle$, at the third process the state $|\varphi\rangle$ is set to $|10\rangle$ and in the fourth process the state $|\varphi\rangle = |11\rangle$ is used. Therefore, the measurements in the ancilla qubit read:

$$\rho_S = \begin{pmatrix} 2P_1(0) - 1 & \rho_{12} & \rho_{1,3} & \rho_{1,4} \\ \rho_{2,1} & 2P_2(0) - 1 & \rho_{2,3} & \rho_{2,4} \\ \rho_{3,1} & \rho_{3,2} & 2P_3(0) - 1 & \rho_{3,4} \\ \rho_{4,1} & \rho_{4,2} & \rho_{4,3} & 2P_4(0) - 1 \end{pmatrix} \quad (141)$$

where $P_k(0)$ is the probability of measuring the state $|0\rangle$ in the ancilla qubit at the process k . The trace of the density matrix sometimes may not be equal to 1 because, N runs of the algorithm are executed for the corresponding N different diagonal terms of the system's density matrix. The non-deterministic nature of quantum mechanics causes the measurement results to conform to a probability distribution, thus the sum of the different diagonal system's density matrix elements measured in different runs of the algorithm, i.e. its trace, can give a value lower or higher than 1. To normalize the trace of the system's density matrix to 1, each population term is divided by $Tr[\rho_S(t)]$.

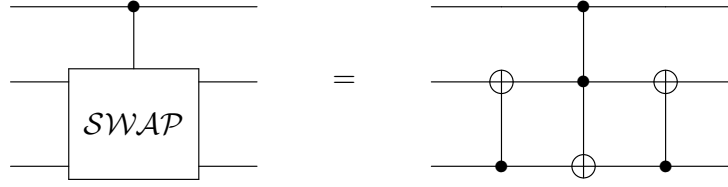


Figure 35: Controlled-SWAP gate or Fredkin gate decomposition [49].

B.5 COMPUTATIONAL RESOURCES

B.5.1 Qubit resources

The qubits required for the implementation are $3\log_2(N_{mol}) + N_{mol}M + 1$ where N_{mol} is the number of molecules in the system and M is the number of normal modes a bath has. N_{mol} baths must be implemented and each bath has M normal modes which are represented each one by a qubit. Therefore, $N_{mol}M$ qubits to define all baths are required. The number of ancilla qubits can be reduced to $\log_2(N_{mol}) + 1$ qubits, where $\log_2(N_{mol})$ ancillas are required for the $C^{n+1}R_Z$ decomposition in the interaction evolution operator, where $n = \log_2(N_{mol})$ is the number of system qubits. One more ancilla qubit is required, which is the target qubit of $C^{n+1}R_Z$. The measurement procedure needs another $\log_2(N_{mol})$ qubits to define the set of qubits φ , therefore a total of $3\log_2(N_{mol}) + N_{mol}M + 1$ qubits must be used.

B.5.2 Quantum gate resources

The evolution operator of the bath Hamiltonian can be applied with $\mathcal{O}(N_{mol}M)$ R_Z gates for each iteration.

The evolution operator of the interaction Hamiltonian can be applied with $\mathcal{O}(N_{mol}M\log_2[N_{mol}])$ single qubit and CNOT gates. The bath m interacts with the molecule m , where $m \in \{1, 2, \dots, N_{mol}\}$, and each bath has M normal modes, so $\mathcal{O}(N_{mol}M)$ $C^{n+1}R_Z$ gates are required to implement all the interactions in a single iteration. Decomposing $C^{n+1}R_Z$ requires an additional $\mathcal{O}(\log_2[N_{mol}])$ single qubit and CNOT gates thus the quantum gate complexity of the interaction evolution operator is $\mathcal{O}(N_{mol}M\log_2[N_{mol}])$.

The bath initialization needs $\mathcal{O}(N_{mol}M)$ R_Y gates.

The measurement procedure needs $\mathcal{O}(\log_2[N_{mol}])$ CNOT gates to implement the controlled SWAP gate.

The total algorithm quantum gate complexity in single qubit and CNOT gates, for a number I of iterations, considering the basis transformation matrix decomposition algorithm is

$$\mathcal{O}(I[N_{mol}^2\log_2^2(N_{mol}) + N_{mol}M\log_2(N_{mol})]) \quad (142)$$

Note however that to know all the population terms of the system's density matrix, $\mathcal{O}(N_{mol})$ runs of the algorithm must be performed.

 THEORETICAL EVOLUTION OF THE TWO MOLECULE SYSTEM

Making use of the Schrödinger equation ($\hbar = 1$)

$$i \frac{\delta}{\delta t} |\Psi\rangle = H |\Psi\rangle \quad (143)$$

and writing the state $|\Psi\rangle$ in the site basis as

$$|\Psi\rangle = \alpha |0\rangle + \beta |1\rangle \quad (144)$$

where $|\alpha|^2 + |\beta|^2 = 1$, one gets the following, by applying the Schrödinger equation to the state $|\Psi\rangle$ and multiplying it by $\langle 0|$ and $\langle 1|$

$$i\dot{\alpha} = \epsilon_0\alpha + J\beta \quad (145)$$

$$i\dot{\beta} = \epsilon_1\beta + J\alpha \quad (146)$$

By making the substitutions $\alpha = ae^{-i\epsilon_0 t}$ and $\beta = be^{-i\epsilon_1 t}$ so that

$$\dot{\alpha} = \dot{a}e^{-i\epsilon_0 t} - i\epsilon_0\alpha \quad (147)$$

$$\dot{\beta} = \dot{b}e^{-i\epsilon_1 t} - i\epsilon_1\beta \quad (148)$$

one has, taking into account the substitutions and the equations (145) and (146),

$$i\dot{a} = J e^{-i\omega t} b \quad (149)$$

$$i\dot{b} = J e^{i\omega t} a \quad (150)$$

where $w = \epsilon_1 - \epsilon_0$. Then the variable c is introduced as $c = ae^{iwt}$. One can observe through equation (149) that $\dot{a} = (\dot{c} - iwc)e^{-iwt}$ so that $i(\dot{c} - iwc) = Jb$. Differentiating with respect to time and using equation (150), one has

$$\ddot{c} - iwc + J^2c = 0 \quad (151)$$

By seeking solutions as $c = e^{i\lambda t}$,

$$-\lambda^2 + w\lambda + J^2 = 0 \quad (152)$$

one gets

$$\lambda_{0,1} = \frac{w}{2} \pm \sqrt{\frac{w^2}{4} + J^2} = \frac{1}{2}(w \pm \Omega) \quad (153)$$

where $\Omega = \sqrt{w^2 + 4J^2}$. The solution of equation (151) is

$$c = Ae^{i\lambda_0 t} + Be^{i\lambda_1 t} \quad (154)$$

then,

$$a(t) = Ae^{i\frac{\Omega-w}{2}t} + Be^{-i\frac{\Omega+w}{2}t} \quad (155)$$

and $b(t)$ is found by using equation (150),

$$b(t) = \frac{\Omega + w}{2J} Be^{i\frac{w-\Omega}{2}t} - \frac{\Omega - w}{2J} Ae^{i\frac{w+\Omega}{2}t} \quad (156)$$

The constants A and B depend on the initial conditions. If the donor molecule is the only one excited ($|0\rangle$) at the initial time $t = 0$, then $\alpha(0) = 1$ and $\beta(0) = 0$. Thus, $a(0) = 1$ and $b(0) = 0$ and one gets $A = \frac{\Omega+w}{2\Omega}$ and $B = \frac{\Omega-w}{2\Omega}$. The solutions are

$$a(t) = \frac{\lambda_0}{\Omega} e^{-i\lambda_0 t} - \frac{\lambda_1}{\Omega} e^{-i\lambda_1 t} \quad (157)$$

$$b(t) = \frac{J}{\Omega} [e^{i\lambda_0 t} - e^{i\lambda_1 t}] \quad (158)$$

and the system's density matrix becomes

$$\rho = |\Psi\rangle\langle\Psi| = \begin{pmatrix} |\alpha|^2 & \alpha\beta^\dagger \\ \alpha^\dagger\beta & |\beta|^2 \end{pmatrix} = \begin{pmatrix} |a(t)|^2 & a(t)b^\dagger(t)e^{iwt} \\ a^\dagger(t)b(t)e^{-iwt} & |b(t)|^2 \end{pmatrix} \quad (159)$$

D

OPTIMIZED QUANTUM CIRCUITS (TWO MOLECULE SYSTEM)

This annex contains the optimized circuits used to build the quantum simulations of the one qubit system in the no decoherence regime for the near resonance (figure 36) and off resonance (figure 37) regimes.

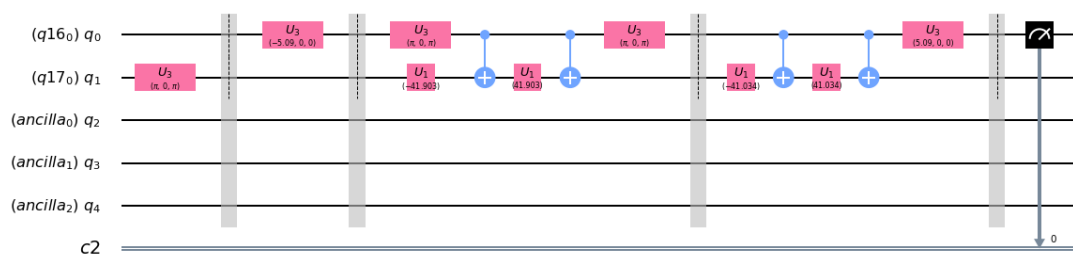


Figure 36: Optimized quantum circuit for the near-resonance system simulation.

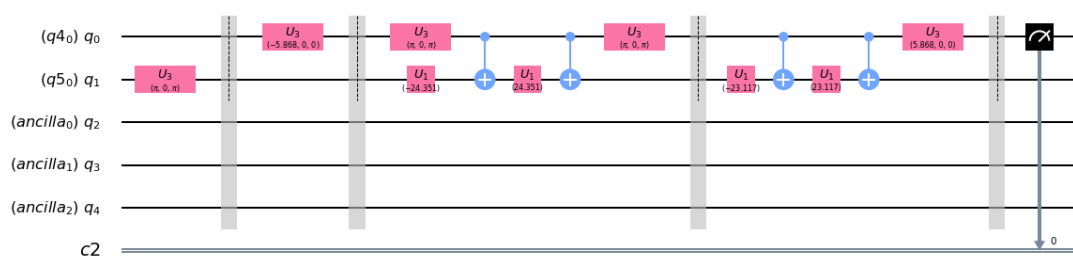


Figure 37: Optimized quantum circuit for the off resonance system simulation.

CALCULATION OF THE QUANTUM BEATING FREQUENCY

For a two molecule system, in the energy transport of photosynthesis, the energy eigenvalues E_0 and E_1 become, after diagonalizing the system Hamiltonian in equation (53),

$$E_0 = \frac{1}{2} \left[\epsilon_0 + \epsilon_1 + \sqrt{(\epsilon_0 - \epsilon_1)^2 + 4J^2} \right] \quad (160)$$

and

$$E_1 = \frac{1}{2} \left[\epsilon_0 + \epsilon_1 - \sqrt{(\epsilon_0 - \epsilon_1)^2 + 4J^2} \right] \quad (161)$$

Following the quantum beating derivation in subsection 2.2.5 and resorting to the equation (27), the coherence terms in the system's density matrix in the energy eigenbasis evolve as

$$\rho_{kj}(t) = e^{-i\Omega t} \rho_{kj}(0) \quad (162)$$

where the frequency of the quantum beating is given by $\Omega = \sqrt{(\epsilon_0 - \epsilon_1)^2 + 4J^2}$. The period of the oscillations is $\frac{2\pi}{\Omega}$.

Notice that the density matrix in Appendix C, equation (159), is presented in the site basis. In such a representation, both diagonal and non-diagonal terms oscillate with time, while the populations are constant in the energy eigenbasis.

